

Importance of Molecular Symmetry for Enantiomeric Excess Recognition by NMR

Karolis Norvaiša,^[a] John E. O'Brien,^[b] Irina Osadchuk,^[c] Brendan Twamley,^[b] Victor Borovkov^[c] and Mathias O. Senge^{*[a,d]}

Abstract: Recently prochiral solvating agents (*pro*-CSA) became a spotlight for the detection of enantiopurity by NMR. Chemical shift non-equivalency in achiral hosts introduced by the presence of chiral guest yields observable resonance signal splitting ($\Delta\delta$) correlating to the enantiomeric excess (e.e.). In this work, symmetry is our lens to explain porphyrin-based supramolecular receptors' activity in a chiral environment. Based on extensive NMR analyses of the atropisomeric receptors, host symmetry is shown to be affected by porphyrin nonplanarity and further desymmetrized in the presence of a chiral guest. We have formulated a simple, symmetry-based protocol that can be used to identify *pro*-CSA candidates. As such, the exposed porphyrin inner core (N–H), with its strong hydrogen bond abilities, for the first time, has been exploited in enantiomeric composition analysis. Our approach in e.e. detection by N–H signals appearing in a previously underutilized region of the spectrum (below 0 ppm.), shows chemical shifts (the e.e. dependent splitting $\Delta\delta$) three times more sensitive to enantiomeric compositions than previously reported systems. The findings are complemented by extensive 2D NMR studies, including the first reporting of e.e. dependent $\Delta\delta$ in non-hydrogen NMR, and supporting by density functional theory (DFT) calculations.

Among the numerous stereodiscrimination methods, nuclear magnetic resonance (NMR) spectroscopy continues to be one of the leading tools for determining the enantiomeric purity of chiral molecules.^[1] However, enantiomers cannot be distinguished in an achiral environment as NMR active nuclei are isochronous. Usually, some external source of chirality^[1d] is

introduced in the form of a covalently bonding chiral derivatization agent (CDA), a non-covalently interacting solvating agent (CSA), or even self-induced recognition of enantiomers (SIRE)^[1a] to convert the enantiomeric systems into diastereomeric ones. Recently, a new type of NMR spectroscopic detection of enantiomeric excess (e.e.) using prochiral solvating agents (*pro*-CSA) was introduced by Hill and co-workers.^[2] In principle, in the event of attractive noncovalent physicochemical interactions, the chiral information of a guest can be transferred to an achiral host and detected as the splitting of the NMR signals. The key example of *pro*-CSA, *N,N'*-disubstituted oxoporphyrinogen (**Bz₂oxP**) exhibits a linear response between the e.e. value and the magnitude of β -proton splitting ($\Delta\delta$) in ¹H NMR (Figure 1a).^[3] Due to *N*-alkylation of the **Bz₂oxP** core, the system cannot be protonated and hence suffers serious sensitivity issues compared to unmodified **oxP**. However, the inevitable prototropic tautomerism and macrocyclic inversions obstruct the potential applications of **oxP** as a *pro*-CSA.^[2a,4] Porphyrins, as prospective *pro*-CSA candidates for e.e. detection, have also been investigated.^[5] While 5,10,15,20-tetraphenylporphyrin (**TPP**) is not affected by the disadvantageous tautomeric processes, as opposed to **oxP**, the necessary use of depressed temperatures for the e.e. detection limits the analysis to explicit solvents with a low freezing point (e.g. CDCl₃) and analyte solubility during the screening (e.g. precipitation).

Frequently, the use of *pro*-CSA's ¹H NMR spectra for chiral analysis is severely hampered due to the numerous scalar couplings and overlapping signals that lead to analytical difficulties.^[6] As the majority of organic molecule resonances appear between 0–14 ppm in the ¹H NMR scale,^[7] it is desirable that the e.e. monitoring with *pro*-CSA would be in a distinct, well-separated region. One of the most unique characteristics of porphyrins is the closed-loop of electrons (ring current) exhibiting large magnetic anisotropy under an applied magnetic field. While peripheral macrocycle signals relate to the typical organic resonances, the nuclei positioned within the loop experience a strong shielding effect when subjected to an external magnetic field and resonate below 0 ppm in the ¹H NMR scale.^[8] Once the highly conjugated system is disrupted (e.g., in oxoporphyrinogens, calix[4]pyrroles), the anisotropic shielding effect of the inner core system is lost, resulting in downfield shifting of the corresponding inner core signals.

The attractive features of the metal-free (free base) porphyrin inner core has lately drawn attention in the fields of catalysis^[9], sensing^[10], supramolecular assemblies^[11], and absolute configuration determination.^[12] Typically, the imine and amine units of porphyrins are not involved in intermolecular interactions due to the planar nature of the macrocycle. However, the existing methods of ring puckering by steric strain^[13] can cause a degree of outwards orientation of the inner pyrrolic entities, making these positions more basic^[14] and accessible to

- [a] K. Norvaiša, Prof. Dr. M. O. Senge
School of Chemistry, Chair of Organic Chemistry
Trinity Biomedical Sciences Institute,
152–160 Pearse Street,
Trinity College Dublin,
The University of Dublin, Dublin 2 (Ireland)
- [b] Dr. B. Twamley, Dr. J. E. O'Brien
School of Chemistry,
Trinity College Dublin,
The University of Dublin, Dublin 2 (Ireland)
- [c] Dr. I. Osadchuk, Prof. Dr. V. Borovkov
Department of Chemistry and Biotechnology, Tallinn University of Technology, Akadeemia tee 15, Tallinn 12618, (Estonia)
- [d] Prof. Dr. M. O. Senge
Institute for Advanced Study (TUM-IAS)
Technical University of Munich
Focus Group – Molecular and Interfacial Engineering of Organic Nanosystems
Lichtenbergstrasse 2a, D-85748 Garching (Germany)
E-mail: mathias.senge@tum.de
twitter: @mathiassenge
www: <http://www.sengegroup.eu/>

Supporting information for this article is given via a link at the end of the document.

substrates.^[10] Even though porphyrins adopt a saddle-shaped 3D conformation^[15] creating an ‘active center’ in the core, only the saddle-deformation alongside chiral guest interactions is not enough to drive the inner N–H signal to split during the ¹H NMR e.e. analysis. For example, **Bz₂oxP** has a saddle shape and belongs to the *C_{2v}* point-group notation with two mirror planes diagonally dividing all pyrroles (Figure 1a). The symmetrical nature of **Bz₂oxP** does not permit the e.e. discrimination using the inner core. However, the N–H signal shifts to the lower field of the spectrum due to the non-covalent interactions nevertheless remain isochronous.^[3]

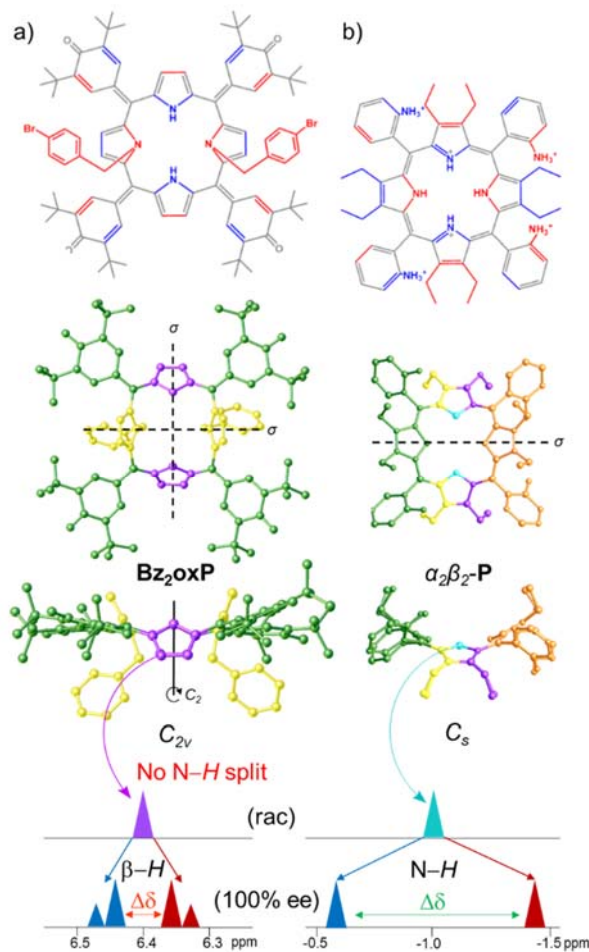


Figure 1. Top: representation of pro-CSA’s (blue above the plane, red — below); Middle: with symmetry elements (Mirror plane σ and rotation axis C_n); Bottom: the key units used for e.e. detection by ¹H NMR; a) **Bz₂oxP** highlighting β -H splitting;^[3] b) newly designed $\alpha_2\beta_2$ -P receptor system with chiral discrimination by N–H; c) All possible P atropisomers with corresponding point groups, N–H signals, and magnitude of splitting; see more detail in Figure S1.

Here we report the first example of e.e. detection using porphyrin inner core N–H resonances. We have designed P

[5,10,15,20-tetrakis(2-aminophenyl)-2,3,7,8,12,13,17,18-octaethylporphyrin] as a receptor system (Figure 2a) exploiting three main molecular engineering strategies: 1) steric overcrowding to obtain a saddle-shaped macrocycle while retaining the porphyrin conjugation^[13] and exposing the inner pyrrolic units for host-guest interactions; 2) peripheral donating groups creating a lock-and-key^[10c] comparable system to encapsulate chiral analytes in the porphyrin lattice and allow the detailed NMR analysis at room temperature.^[10d] 3) formation of atropisomers based on the orientation of peripheral groups^[16] to have the ultimate control of the symmetry elements in pro-CSA.^[17]

In our previous study, we have highlighted the selective nature of host P for guests containing sulfonate or phosphonate motifs.^[10d] The analyte interacts directly with the inner ring system and generates static and well-resolved NMR spectral lines. As previously mentioned, the depressed temperatures can also offer slow exchange rates for potential detection of e.e.^[5] However, the aim of the following studies is the development of a readily available and highly effective analytical tool for room-temperature measurements. Therefore, (\pm)-10-camphorsulfonic acid (**10CSA**) bearing the sulfonic moiety and stereogenic centers was selected as a chiral guest in the present study.

Operating with enantiopure **10CSA(S or R)** four distinct scenarios with four different P atropisomers were observed and subsequently rationalized by the symmetry operations found in P (Figure 1c).^[17] In the α_4 -P·**10CSA(S or R)** complex, the inner core remains isochronous, due to the *C_{2v}* point-group notation with a two-fold symmetry axis and two mirror planes passing through the pyrroles. The identical situation previously reported by Hill and co-workers in **Bz₂oxP** pinpoints the interactions with inner N–H, however, without the e.e. discrimination due to the *C_{2v}* symmetry (Figure 1a).^[3] The $\alpha_2\beta_2$ -P atropisomer with *C_s* symmetry features a single well-defined mirror plane dividing two pyrrolic units which preserve its achiral nature, hence allowing it to be classified as pro-CSA. The lack of other symmetry elements in $\alpha_2\beta_2$ -P allows the N–H protons to become anisochronous in a chiral environment, making chiral discrimination possible (with the highest magnitude of splitting ($\Delta\delta_{max}$) of 0.653 ppm at 100% e.e.) (Figure 1b). The $\alpha_3\beta$ -P atropisomer belongs to the *C₁* point-group, as it contains no symmetry elements, making the system chiral. Thus, eight signals are observed with enantiopure **10CSA** due to diastereomer formation (SS- and SR- or RR- and RS-) (Figure S1). While the e.e. detection is possible with $\alpha_3\beta$ -P (Figure S2), the practical use of such system falls short mainly due to three dominating factors: 1) the high number of inner core system signals hampers direct e.e. interpretation; 2) the magnitude of $\Delta\delta_{max}$ (~0.39 ppm) is lowest of the three atropisomers with inner core splitting making it the least sensitive system; 3) the concentration of $\alpha_3\beta$ -P is required to be significantly higher than that of other systems due to a large number of resonance signals and their comparatively lower intensities. On the other hand, $\alpha\beta\alpha\beta$ -P which belongs to the *S₄* point group has four equivalent protons located in the principal axis. While it has no mirror planes, the inversion center situated between the pyrrole units allows the inner core protons to split in equal proportions (above and below the plane) upon interaction with a chiral analyte. A single isochronous N–H signal of $\alpha\beta\alpha\beta$ -P-**10CSA(S or R)** becomes

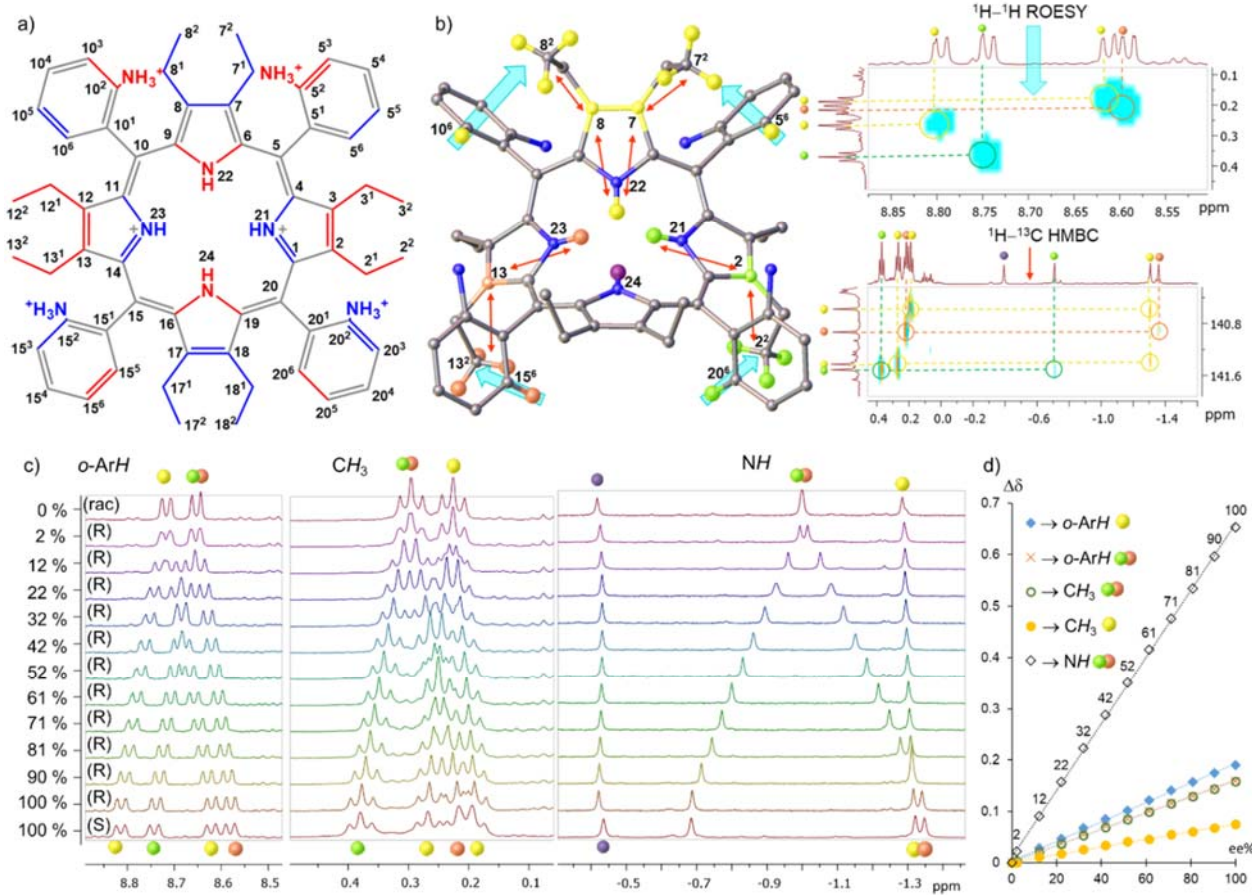


Figure 2. a) Illustration of the structure of $\alpha_2\beta_2$ -P (blue — above and red — below the plane) with corresponding positions; b) representation and color-coding reference of the ¹H splitting signals with blue arrows showing ¹H-¹H ROESY and red arrows ¹H-¹³C HMBC correlations of 20 eq. $\alpha_2\beta_2$ -P-**10CSA(R)**; c) Observable $\Delta\sigma$ of ¹H signals in o-ArH, CH₃, and inner core system (NH) regions; d) Graph of the $\Delta\sigma$ dependence on the e.e.% value. All spectra have been recorded in CD₃CN.

anisochronous, with $\Delta\sigma_{\max}$ (0.520 ppm) comparable to the $\alpha_2\beta_2$ -P-**10CSA(S or R)** system (0.653 ppm). While a singular inner core proton splitting is an attractive feature, the practicality of such a system in the e.e. detection is challenging, mainly due to the low atropisomeric rotational barrier, which leads to the formation of other atropisomers at room temperature^[10d] and low abundance (only 1/8 obtained from statistical mixtures) in comparison to other P rotamers. Since $\alpha_2\beta_2$ -P displayed the highest $\Delta\sigma_{\max}$ value compared to other P atropisomeric species (Figure 1c), in-depth chirality determination studies listed below were carried out with this receptor system.

Overall, three distinct and well-resolved regions (o-ArH, CH₃, and N-H) were identified for possible e.e. monitoring with $\alpha_2\beta_2$ -P (Figure 2c, S5). The correlation between the signals of interest was investigated by 2D NMR techniques with enantiopure **10CSA(R)** (20 eq.) and their corresponding locations are illustrated in Figure 2b. The gradual addition of **10CSA(R)** to $\alpha_2\beta_2$ -P and the influence of water on $\Delta\sigma_{\max}$ as a competitive agent is detailed in the SI (Figure S3-S9). While the $\Delta\sigma_{\max}$ values of o-ArH and CH₃ are comparable to known pro-CSAs^[2-5, 18] being 0.190 ppm (o-ArH yellow), 0.159 ppm (o-ArH red/green), 0.158 ppm (CH₃ red/green), and 0.075 ppm (CH₃ yellow), the $\Delta\sigma_{\max}$ values of

the inner system (N-H red/green) was found to be more than threefold greater than those of other regions (0.653 ppm).

The origin of the chemical shift non-equivalence lies deep within the concept of prochirality.^[19] The desymmetrization of $\alpha_2\beta_2$ -P atoms in a single step by weak interactions with a chiral guest proves to be particularly useful for the e.e. determination. To illustrate **10CSA** interactions with $\alpha_2\beta_2$ -P[SO₄²⁻]₄ structure for building starting geometries. Corresponding noncovalent interactions of the major conformer are illustrated in Figure S14. When racemic and non-racemic mixtures of **10CSA** were applied in the system at constant concentrations it was found that $\Delta\sigma$ of the o-ArH, CH₃, and N-H peaks rely on respective % of the e.e. value (Figure 2c). At the racemic point, the isochronous profile of $\alpha_2\beta_2$ -P is restored since the chiral information is transmitted in equal proportions from both the chiral components. Since the $\Delta\sigma_{\max}$ value of the inner core system is substantially higher than that of other regions, the resolution, of which e.e. can be detected, is considerably enhanced. Astonishingly, at as low as 2% e.e., two distinct N-H resonance singlets ($\Delta\sigma$ 0.022 ppm.) can clearly be identified, while the other regions show only a broadening of the signals. Plotting the differences in the chemical shifts of split

peaks against the % e.e. values revealed a linear dependency with the R^2 values being above 0.997 and the inner N–H fitting $R^2 = 0.9994$ (Figure 2d). The linear fit of the plots is a fundamental property in unlocking the easy calibration of the referenced systems for quick detection of the e.e. value (a detailed example shown in SI; Figure S10–S12). Moreover, spatially distant neighboring protons from N–H offer another important feature. Sharp and well-isolated singlets do not suffer from any vicinal scalar J -couplings or roofing effects underlining the simplicity in tracking chiral compositions. Overall, monitoring changes of this inner core system in a model chiral environment demonstrates a powerful tool for easy and sensitive detection of enantiomeric compositions.

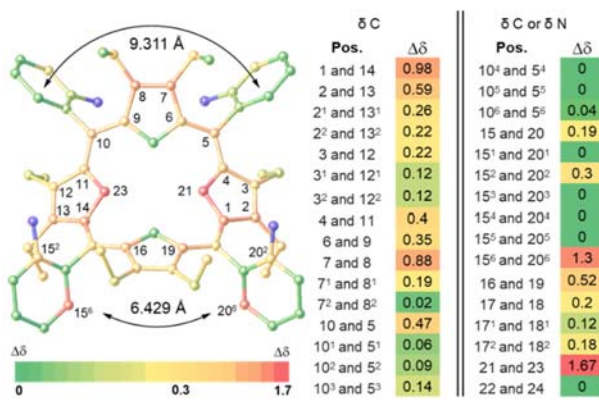


Figure 3. Illustration of $\Delta\sigma_{\text{max}}$ (ppm) of ^{13}C and ^{15}N NMR in 20 eq. $\alpha_2\beta_2\text{-P}\cdot\text{10CSA(S)}$ complex, determined in comparison to the corresponding racemate $\alpha_2\beta_2\text{-P}\cdot\text{10CSA(SR)}$ using 2D NMR techniques (CD_3CN) (Figure S16–S31). The highlighted positions in the illustration on the left side shows $\Delta\sigma \geq 0.3$ ppm. Atoms in blue are peripheral nitrogen atoms that did not resonate.

The magnitude of non-hydrogen $\Delta\sigma$ relies on the spatial positions, distances, and interactions with chiral guests.^[3] The further the stereogenic center of a chiral guest from the host molecule, the weaker the chirality transfer is. Interestingly, this principle was previously well-defined in the porphyrin-based host-guest chirogenic systems by using circular dichroism spectroscopy.^[20]

The dependence of the non-equivalency to the chiral guest location can be illustrated by ^{13}C and ^{15}N NMRs. (For detailed comparison of non-hydrogen resonances see Table S1). When $\alpha_2\beta_2\text{-P}\cdot\text{10CSA(S)}$ was compared to racemic $\alpha_2\beta_2\text{-P}\cdot\text{10CSA(SR)}$, most of the macrocyclic ring system exhibited $\Delta\sigma_{\text{max}} > 0.3$ ppm with the central two nitrogen atoms having $\Delta\sigma_{\text{max}} = 1.67$ ppm (Figure 3). Nevertheless, due to the greater distance from the active site, most of the phenyl ring resonance signals remained isochronous. Despite this, two particularly different scenarios were portrayed by the o-Ar- ^{13}C NMR signals. The $\Delta\sigma_{\text{max}}$ between 15^6 and 20^6 positions yielded excellent separation (~ 1.3 ppm), whereas the 5^6 and 10^6 imposed only marginal $\Delta\sigma_{\text{max}}$ (0.04 ppm). A closer examination of the crystal structure of $\alpha_2\beta_2\text{-P}[\text{SO}_4^{2-}][\text{HSO}_4^-]_4$ revealed a closer distance between C15⁶ and C20⁶ (~ 6.429 Å) than between C5⁶ and C10⁶ (~ 9.311 Å),

subsequently forming a narrow channel for the chiral guest to occupy (Figure 3). Moreover, the calculated chemical shifts of non-hydrogen atoms in $\alpha_2\beta_2\text{-P}\cdot\text{10CSA(R)}$ using the GIAO-B3LYP/6-311++G**//BP86-D3BJ/def-SVP method and SMD solvent model correlated well with the splitting patterns observed experimentally (for more information check SI, Table S8). Of note, in ^1H NMR the 15^6 and 20^6 positions had similar $\Delta\sigma_{\text{max}}$. Hence, while hydrogens of the o-Ar group were more likely to form weak interactions with the chiral compounds, the corresponding $\Delta\sigma_{\text{max}}$ value of carbon resonances hinges on the spatial arrangements and proximity to the guest. Comparison of the $\alpha_2\beta_2\text{-P}\cdot\text{10CSA(S)}$ and SR splitting resonance signals to other atropisomeric species is detailed in SI (Table S2–S3).

To conclude, the point groups were found to play a fundamental role in adjusting supramolecular receptor systems for e.e. determinations by the NMR method. Four atropisomers containing different point group notations were thoroughly investigated by NMR with (*S* and *R*) camphorsulphonic acid pinpointing the $\alpha_2\beta_2$ rotamer as the most sensitive receptor for chirality detection. It was found that the $\Delta\sigma_{\text{max}}$ value of N–H signals can reach 0.653 ppm, a three-fold greater splitting than any known *pro*-CSA. Such enhanced sensitivity towards the chiral components allows for readily available and exceptionally detailed enantiomeric excess detection at room temperature by NMR.

Deposition number 2143572 (for $\alpha_2\beta_2\text{-P}[\text{SO}_4^{2-}][\text{HSO}_4^-]_4$) contains the supplementary crystallographic data for this paper. These data are provided free of charge by the joint Cambridge Crystallographic Data Centre and Fachinformationszentrum Karlsruhe <http://www.ccdc.cam.ac.uk/structures> Structures service.

Acknowledgements

This work was prepared with the support of the Technical University of Munich – Institute for Advanced Study through a Hans Fischer Senior Fellowship and has received funding from the European Union's Horizon 2020 research and innovation program under the FET-OPEN grant agreement No.828779, the Irish Research Council (GOIPG 2017/1172), Science Foundation Ireland (IvP 13/IA/1894) and was supported by the Higher Education Authority and the Department of Further and Higher Education, Research, Innovation and Science (Ireland).

Conflict of Interest

The authors declare no conflict of interest.

Keywords: Enantiomeric Excess • Porphyrinoids • Atropisomers • NMR • Symmetry Elements

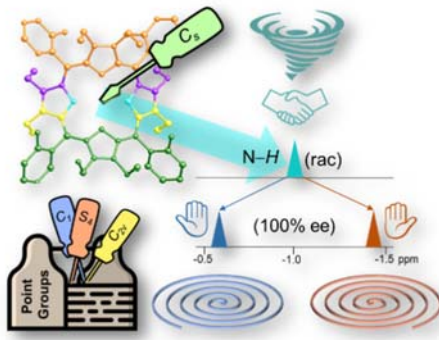
- [1] a) Z. Szakács, Z. Sánta, A. Lomoschitz, C. Szántay, *TrAC, Trends Anal. Chem.* **2018**, *109*, 180–197; b) M. S. Silva, *Molecules* **2017**, *22*, 247–268; c) J. S. Fossey, E. V. Anslyn, W. D. G. Brittain, S. D. Bull, B. M. Chapin, C. S. Le Duff, T. D. James, G. Lees, S. Lim, J. A. C. Lloyd, C. V.

-
- Manville, D. T. Payne, K. A. Roper, *J. Chem. Educ.* **2017**, *94*, 79–84; d) T. J. Wenzel, J. D. Wilcox, *Chirality* **2003**, *15*, 256–270.
- [2] a) J. Labuta, J. P. Hill, S. Ishihara, L. Hanyková, K. Ariga, *Acc. Chem. Res.* **2015**, *48*, 521–529; b) A. Shundo, J. Labuta, J. P. Hill, S. Ishihara, K. Ariga, *J. Am. Chem. Soc.* **2009**, *131*, 9494–9495.
- [3] J. Labuta, S. Ishihara, T. Šikorský, Z. Futera, A. Shundo, L. Hanyková, J. V. Burda, K. Ariga, J. P. Hill, *Nat. Commun.* **2013**, *4*, 2188–2196.
- [4] a) J. Labuta, S. Ishihara, K. Ariga, J. Hill, *Symmetry* **2014**, *6*, 345–367; b) J. Labuta, Z. Futera, S. Ishihara, H. Kourilova, Y. Tateyama, K. Ariga, J. P. Hill, *J. Am. Chem. Soc.* **2014**, *136*, 2112–2118.
- [5] a) J. Labuta, S. Ishihara, J. P. Hill, *J. Porphyr. Phthalocyanines* **2020**, *24*, 320–329; b) J. Labuta, S. Ishihara, A. Shundo, S. Arai, S. Takeoka, K. Ariga, J. P. Hill, *Chem. Eur. J.* **2011**, *17*, 3558–3561.
- [6] J. Labuta, S. Ishihara, D. T. Payne, K. Takimoto, H. Sato, L. Hanyková, K. Ariga, J. P. Hill, *Chemosensors* **2021**, *9*, 259–276.
- [7] a) G. R. Fulmer, A. J. M. Miller, N. H. Sherden, H. E. Gottlieb, A. Nudelman, B. M. Stoltz, J. E. Bercaw, K. I. Goldberg, *Organometallics* **2010**, *29*, 2176–2179; b) M. Balci, in *Basic 1H- and 13C-NMR Spectroscopy* (Ed.: M. Balci), Elsevier Science, Amsterdam, **2005**, pp. 25–85.
- [8] J. E. Falk, in *Porphyrins and Metalloporphyrins* (Ed.: K. M. Smith), Elsevier Scientific Pub. Co, Amsterdam **1975**, pp. 399–514.
- [9] a) M. Roucan, M. Kielmann, S. J. Connon, S. S. R. Bernhard, M. O. Senge, *Chem. Commun.* **2018**, *54*, 26–29; b) E. Aoki, W. Suzuki, H. Kotani, T. Ishizuka, H. Sakai, T. Hasobe, T. Kojima, *Chem. Commun.* **2019**, *55*, 4925–4928; c) T. A. Dar, B. Upadhyay, M. Sankar, M. R. Maurya, *Green Chem.* **2019**, *21*, 1757–1768; d) M. Kielmann, N. Grover, W. W. Kalisch, M. O. Senge, *Eur. J. Org. Chem.* **2019**, 2448–2452; e) W. Suzuki, H. Kotani, T. Ishizuka, T. Kojima, *J. Am. Chem. Soc.* **2019**, *141*, 5987–5994.
- [10] a) N. Chaudhri, M. Sankar, *RSC Adv.* **2015**, *5*, 3269–3275; b) R. Kumar, N. Chaudhri, M. Sankar, *Dalton Trans.* **2015**, *44*, 9149–9157; c) M. Kielmann, M. O. Senge, *Angew. Chem. Int. Ed.* **2019**, *58*, 418–441; d) K. Norvaiša, K. J. Flanagan, D. Gibbons, M. O. Senge, *Angew. Chem. Int. Ed.* **2019**, *58*, 16553–16557; e) K. Norvaiša, M. Kielmann, M. O. Senge, *ChemBioChem* **2020**, *21*, 1793–1807.
- [11] a) C. J. Kingsbury, K. J. Flanagan, H.-G. Eckhardt, M. Kielmann, M. O. Senge, *Molecules* **2020**, *25*, 3195–3218; b) K. Norvaiša, K. Yeow, B. Twamley, M. Roucan, M. O. Senge, *Eur. J. Org. Chem.* **2021**, 1871–1882.
- [12] P. Bhyrappa, V. V. Borovkov, Y. Inoue, *Org. Lett.* **2007**, *9*, 433–435.
- [13] a) M. O. Senge, in *The Porphyrin Handbook*, Vol. 1 (Eds.: K. M. Kadish, K. M. Smith, R. Guilard), Academic Press, **2000**, pp. 239–347; b) M. O. Senge, *Chem. Commun.* **2006**, 243–256.
- [14] O. S. Finikova, A. V. Cheprakov, P. J. Carroll, S. Dalosto, S. A. Vinogradov, *Inorg. Chem.* **2002**, *41*, 6944–6946.
- [15] C. J. Kingsbury, M. O. Senge, *Coord. Chem. Rev.* **2021**, *431*, 213760.
- [16] K. Norvaiša, S. Maguire, C. Donohoe, J. E. O'Brien, B. Twamley, L. C. Gomes-da-Silva, M. O. Senge, *Chem. Eur. J., Accepted Author Manuscript*, DOI: 10.1002/chem.202103879.
- [17] K. Norvaiša, J. E. O'Brien, D. J. Gibbons, M. O. Senge, *Chem. Eur. J.* **2020**, *27*, 331–339.
- [18] a) S. Ishihara, J. Labuta, Z. Futera, S. Mori, H. Sato, K. Ariga, J. P. Hill, *J. Phys. Chem. B* **2018**, *122*, 5114–5120; b) K. Takimoto, S. Ishihara, J. Labuta, V. Březina, D. T. Payne, J. P. Hill, K. Ariga, M. Sumita, S. Mori, H. Sato, *J. Phys. Chem. Lett.* **2020**, *11*, 8164–8169.
- [19] P. Lesot, C. Aroulanda, H. Zimmermann, Z. Luz, *Chem. Soc. Rev.* **2015**, *44*, 2330–2375.
- [20] V. V. Borovkov, J. M. Lintuluoto, Y. Inoue, *J. Am. Chem. Soc.* **2001**, *123*, 2979–2989.

Table of Contents

COMMUNICATION

Just like a screwdriver turning screws, symmetry elements can be adjusted by fine-tuning the orientation of rotationally restricted side-groups in supramolecular receptors. In this research we highlight the fundamental role of symmetry in chiral reporting by NMR. Newly designed porphyrins with exposed inner core N–H system can respond to a chiral guest with exceptionally sensitive enantiomeric excess detection.



Karolis Norvaiša, John E. O'Brien, Irina Osadchuk, Brendan Twamley, Victor Borovkov and Mathias O. Senge

Importance of Molecular Symmetry for Enantiomeric Excess Recognition by NMR

Supporting Information

SUPPORTING INFORMATION

Table of Contents

Experimental Procedures	3
General Methods.....	3
In Text Supplementary Material	4
<i>NMR Investigation of the P-10CSA Atropisomers</i>	4
10CSA Additions to $\alpha_2\beta_2\text{-P}$	5
<i>Influence of Water on the Complexation.</i>	8
<i>Detection of Enantiomeric Excess</i>	10
^{13}C and ^{15}N Investigations	12
<i>Structural Determination of $\alpha_2\beta_2\text{-P}[\text{SO}_4^{2-}][\text{HSO}_4^-]$</i>	16
Computational Analysis.....	18
<i>Geometry analysis</i>	18
<i>NMR calculations and analysis</i>	21
<i>NBO partial charges calculations and analysis</i>	25
Geometries.....	27
<i>Conformer A</i>	27
<i>Conformer B</i>	27
<i>Conformer C</i>	28
<i>Conformer D</i>	29
<i>Conformer E</i>	29
<i>Conformer F</i>	30
<i>Conformer G</i>	31
<i>Conformer H</i>	31
$[\alpha_2\beta_2\text{-P}]^{4+}$ conf. 1	32
$[\alpha_2\beta_2\text{-P}]^{4+}$ conf. 2	32
$[\alpha_2\beta_2\text{-P}]^{6+}$	33
$\alpha_2\beta_2\text{-P}[\text{H}_2\text{SO}_4 \cdot \text{H}_2\text{O}]_2^{4+}$	33
Experimental NMR Data.....	35
$\alpha_2\beta_2\text{-P-10CSA(S)}$	35
$\alpha_2\beta_2\text{-P-10CSA(SR)}$	44
$\alpha_4\text{-P-10CSA(S)}$	51
$\alpha_4\text{-P-10CSA(SR)}$	58
$\alpha\beta\alpha\beta\text{-P-10CSA(S)}$	65
$\alpha\beta\alpha\beta\text{-P-10CSA(SR)}$	72
$\alpha_3\beta\text{-P-10CSA(S)}$	78
$\alpha_3\beta\text{-P-10CSA(SR)}$	82
References	85

SUPPORTING INFORMATION

Experimental Procedures

General Methods

NMR spectra were recorded on a Bruker Advance III 400 MHz, a Bruker Advance HD 400 and an Agilent 400 spectrometer for ^1H (400.13 MHz) and ^{13}C (100.61 MHz) NMR spectra. A Bruker Ultrashield 600 spectrometer was employed for ^1H (600.13 MHz), ^{13}C (150.90 MHz) and ^{15}N NMR (61 MHz) spectra. All NMR experiments were performed at 25 °C. Resonances δ are given in ppm units and referenced to the deuterium signal in the NMR solvents, acetonitrile- d_3 ($\delta_{\text{H}} = 1.94$ ppm, $\delta_{\text{C}} = 1.32, 118.26$ ppm). Signal multiplicities are abbreviated as follows: singlet = s, doublet = d, triplet = t, dq = doublet of quartets, multiplet = m.

Normal-structural decomposition (NSD): The NSD method, as developed by Shelnutt and coworkers,^[1] was used to delineate, quantify, and illustrate the various distortions modes present in the tetrapyrrole macrocycles. Analysis was performed with the NSD online interface, available at <https://www.sengegroup.eu/nsd>.^[2]

Single crystal X-ray crystallography: Crystals were grown following the protocol developed by Hope, liquid-liquid diffusion of CHCl_3 and MeOH with H_2SO_4 .^[3] Diffraction data were collected on a Bruker APEX 2 DUO CCD diffractometer using Incoatec $1\mu\text{s Cu}-K_{\alpha}$ ($\lambda = 1.54178 \text{ \AA}$) radiation. Crystal was mounted on a MiTeGen MicroMount and collected at 100(2) K using an Oxford Cryosystems Cobra low-temperature device. Data were collected using omega and phi scans and were corrected for Lorentz and polarization effects using the APEX software suite.^[4] Data were corrected for absorption effects using the multi-scan method (SADABS).^[5] Using Olex2, the structure was solved with the XT structure solution program, using the intrinsic phasing solution method and refined against $|F^2|$ with XL using least-squares minimization.^[6] If electron density was not sufficient, the C and N bound H atoms were placed in their expected calculated positions and refined using a riding model: $\text{N-H} = 0.88 \text{ \AA}$, $\text{C-H} = 0.95-0.98 \text{ \AA}$, with U_{iso} (H) = $1.5U_{\text{eq}}$ (C) for methyl H atoms and $1.2U_{\text{eq}}$ (C, N). Details of data refinements can be found in Table S4. All images were prepared using Olex2.^[6a]

In the structure $\alpha_2\beta_2\text{-P}[\text{SO}_4^{2-}][\text{HSO}_4^-]_4$, two phenyl rings at C5 and C10 and one ethyl group are modelled over two locations using DFIX, SIMU, SADI restraints and EADP constraints. In terms of counter anion, only the SO_4^{2-} group is not disordered, while all other HSO_4^- groups were modelled disordered using rigid groups. Some hydrogen atoms were placed geometrically to compensate for close contacts, the remaining hydrogens could not be located on the disordered HSO_4^- moieties but were added to the formula to make the formula weight correct. Multiple disordered and partially occupied H_2O molecules are modelled in the structure using SIMU and ISOR restraints. The weighting scheme was manually adjusted to ensure the goodness of fit was reasonable.

Deposition number 2143572 contain the supplementary crystallographic data for this paper. These data are provided free of charge by the joint Cambridge Crystallographic Data Centre and Fachinformationszentrum Karlsruhe <http://www.ccdc.cam.ac.uk/structures>.

All calculations were done with Gaussian16 Rev. B.01.^[7] A conformational search for $\alpha_2\beta_2\text{-P}\cdot\textbf{10CSA(R)}$ was performed using a crystal structure of $\alpha_2\beta_2\text{-P}[\text{SO}_4^{2-}][\text{HSO}_4^-]_4$ supramolecules as a starting point for building porphyrin/camphorsulfonic acid supramolecules, followed by optimization in acetonitrile. The geometry optimization and frequencies calculations were performed using BP86^[8]-D3BJ^[9]/def2-SVP^[10] – the method which showed a good agreement with the experimental data reported in our previous works.^[11] To include acetonitrile effects the SMD^[12] continuum solvent model was used, where molecular surface was represented as Solvent Accessible Surface (SAS) and the Bondi atomic radii were used. A ground state was characterized by absence of imaginary frequencies and more accurate electronic energies were calculated using the BP86-D3BJ/def2-TZVPP^[10] and SMD model. During conformational search twenty start geometries converged into eight conformers corresponding to the ground state (Table S5) with one major conformer A making up 90%. The geometry were visualized using GaussView 6.1.^[13] and is illustrated in figure S14.

The NMR shielding tensors were calculated at the GIAO^[14]-B3LYP^[15]/6-311++G**^[14a, 16] level of theory using the SMD continuum solvent model to include acetonitrile effects. To calculate the ^{13}C chemical shifts, a scaling factor of 1.0228^[17] and a reference point TMS (180.7 ppm) were used, for calculation of the ^{15}N chemical shifts NH_3 was used as a reference point (253.70 ppm) (Table S6 – S8). Population analysis was done using the BP86-D3BJ/def2-TZVPP//BP86-D3BJ/def2-SVP level of theory in acetonitrile and NBO^[18] approach in acetonitrile. Non-covalent interactions were also analyzed using the SMD (acetonitrile), the BP86-D3BJ/def2-SVP level of theory and AIMAll program version 19.10.12^[19]

SUPPORTING INFORMATION

In Text Supplementary Material

NMR Investigation of the **P-10CSA** Atropisomers

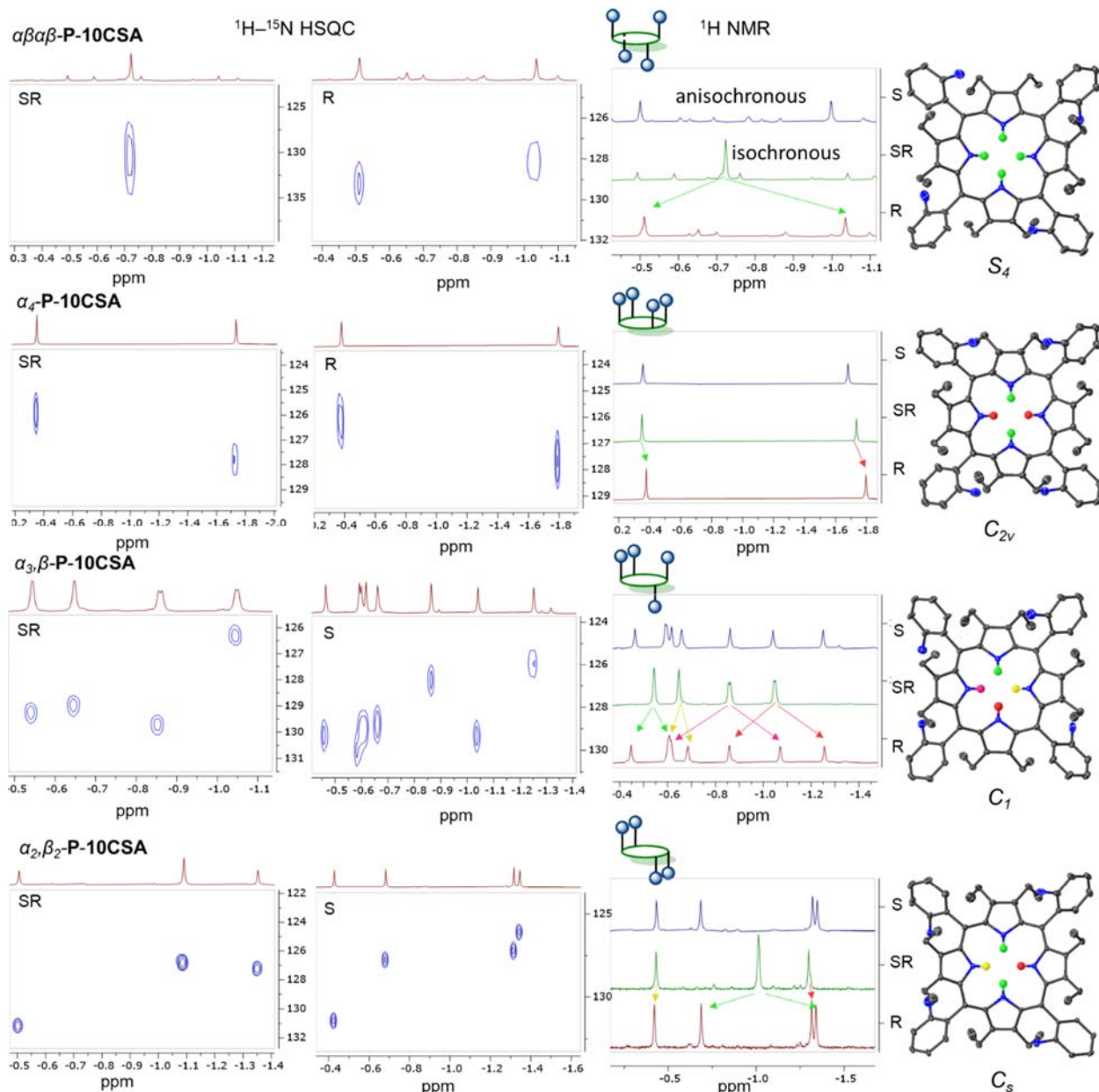


Figure S1. ^1H and $^1\text{H}-^{15}\text{N}$ HSQC NMR spectra obtained for 0% and 100% e.e. **P-10CSA** solutions (20 equivalents) in d_3 -acetonitrile. On the right side, a graphical illustration of **P-10CSA** atropisomers with corresponding point group notations, inner core system protons are highlighted in different colors correlating to the arrows marked in ^1H NMR spectra.

SUPPORTING INFORMATION

We performed ^1H NMR and $^1\text{H}-^{15}\text{N}$ HSQC analyses of all **P** atropisomers with racemic mixtures and enantiopure **10CSA(S or R)**. For the racemic **10CSA** solutions, as expected ^1H NMR spectra of **P** atropisomers remained isochronous (Figure S2). Due to the chiral information transmitted in equal proportions from both chiral components (**10CSA R** and **S**), the observed inner core signals resonate in an identical manner to achiral acids (**BSA** and **MSA**) previously reported by us.^[20] One singlet is observed for $\alpha\beta\alpha\beta\text{-P}\cdot\text{10CSA}$, two in $\alpha_4\text{-P}\cdot\text{10CSA}$, three signals of relative intensity 1:2:1 in $\alpha_2\beta_2\text{-P}\cdot\text{10CSA}$, and finally the spectrum for the unsymmetrical $\alpha_3\beta\text{-P}\cdot\text{10CSA}$ atropisomer has four differently shifted signals. The enantiopure solutions are described in the main text.

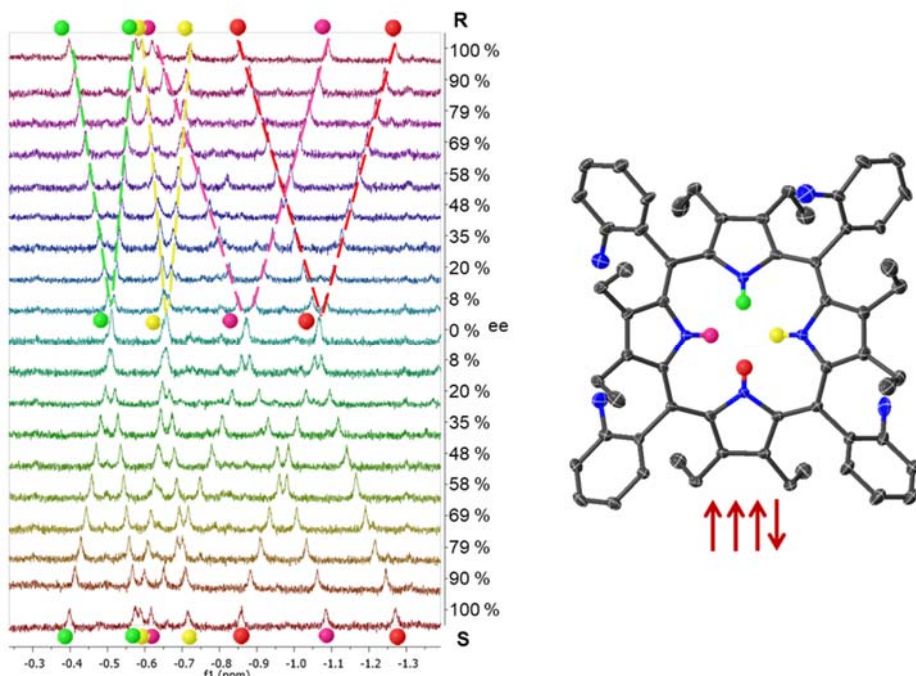


Figure S2. ^1H NMR titration studies of the $\alpha_3\beta\text{-P}$ inner core system using different ratios of chiral components (**10CSA(R** and **S**, 20 eq.). Spectra recorded in CD_3CN

10CSA Additions to $\alpha_2\beta_2\text{-P}$

The gradual addition of **10CSA(R)** into the CD_3CN solution of $\alpha_2\beta_2\text{-P}$ resulted in downfield shifts of the ^1H NMR aromatic region signals with the observable splitting pattern of the o-ArH (Figure S3), while the split pyrrolic N-H were upfield shifted upon emerging at ~3 eq. of **10CSA(R)** in the ^1H NMR spectra (Figures S4 and S5). The magnitude of chemical shifts of split peaks ($\Delta\sigma$) drastically increased over the first ~7 eq., while the later additions resulted in marginal changes to $\Delta\sigma$ (Figure S6).

SUPPORTING INFORMATION

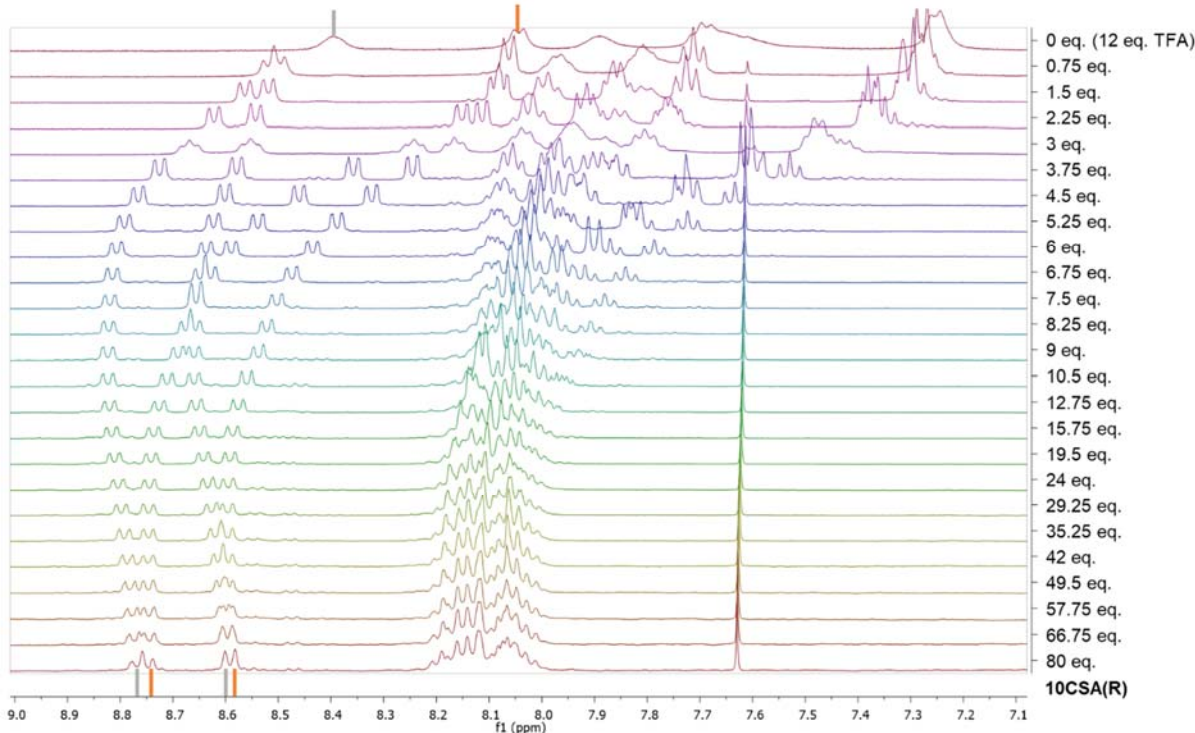


Figure S3. ¹H NMR of the $\alpha_2\beta_2\text{-P}$ aromatic region dependence to the **10CSA(R)** equivalents, recorded in CD₃CN. The addition of 12 eq. of TFA was to solubilize and protonate $\alpha_2\beta_2\text{-P}$. Highlighted in grey and orange is two different splitting o-Ar-H regions.

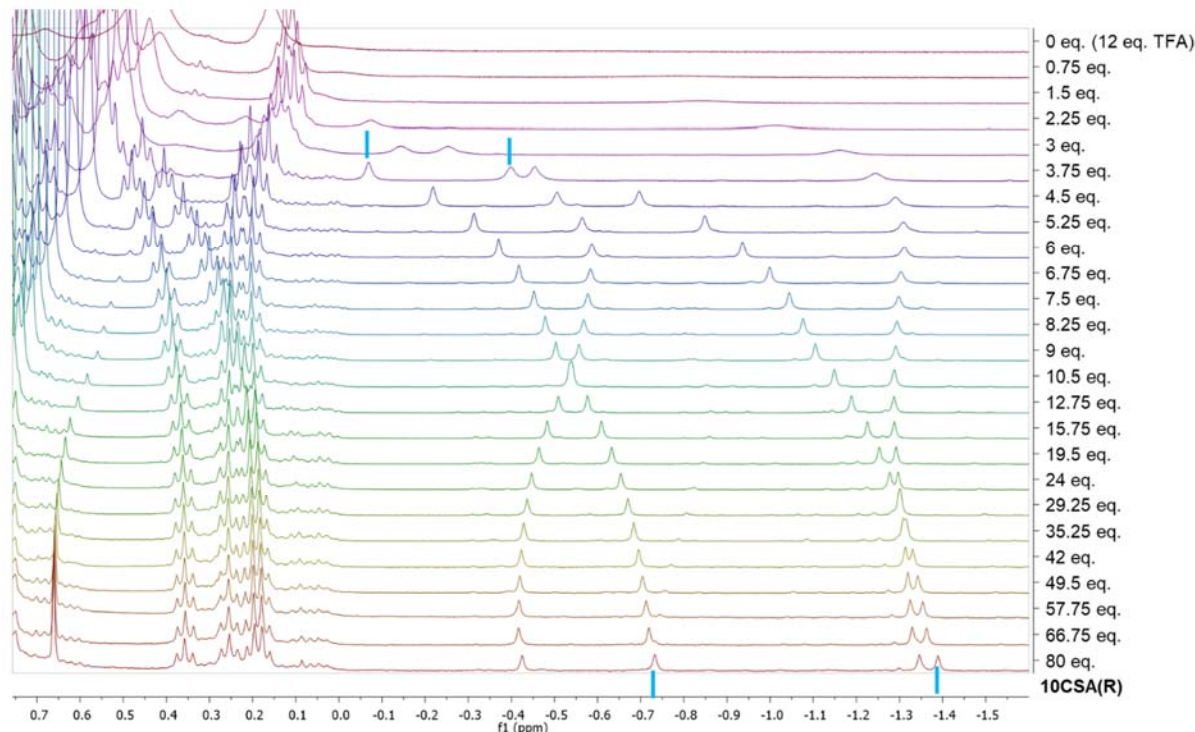


Figure S4. ¹H NMR of the $\alpha_2\beta_2\text{-P}$ N-H and CH₃ regions dependence to the **10CSA(R)** equivalents, recorded in CD₃CN. The addition of 12 eq. of TFA was to solubilize and protonate $\alpha_2\beta_2\text{-P}$. Highlighted in blue are two different splitting N-H resonance signals.

SUPPORTING INFORMATION

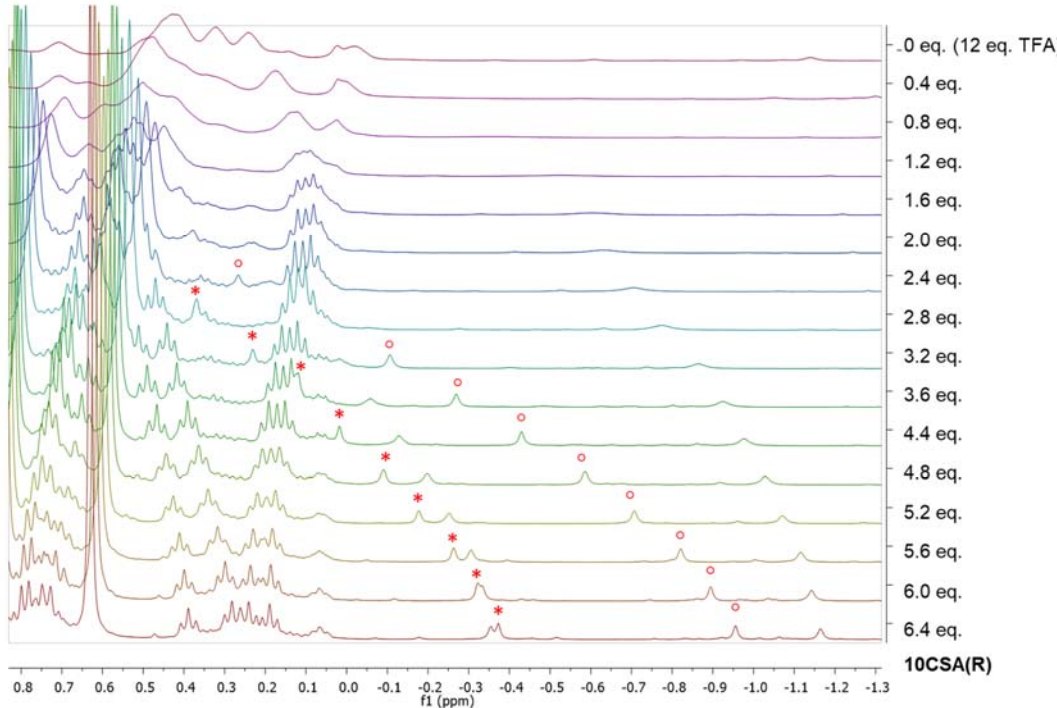


Figure S5. ¹H NMR of the $\alpha_2\beta_2\text{-P}$ N–H regions dependence to the **10CSA(R)** equivalents, recorded in CD₃CN. The addition of 12 eq. of TFA was to solubilize and protonate $\alpha_2\beta_2\text{-P}$. Highlighted with red dot and star is two different splitting N–H resonance signals. Note, these spectra were recorded with higher concentrations of $\alpha_2\beta_2\text{-P}$ expecting to get a better resolution of the inner N–H. From the obtained spectra it appears that the inner core system of interest originates downfield shifted and overlays with the aliphatic CH₃ region.

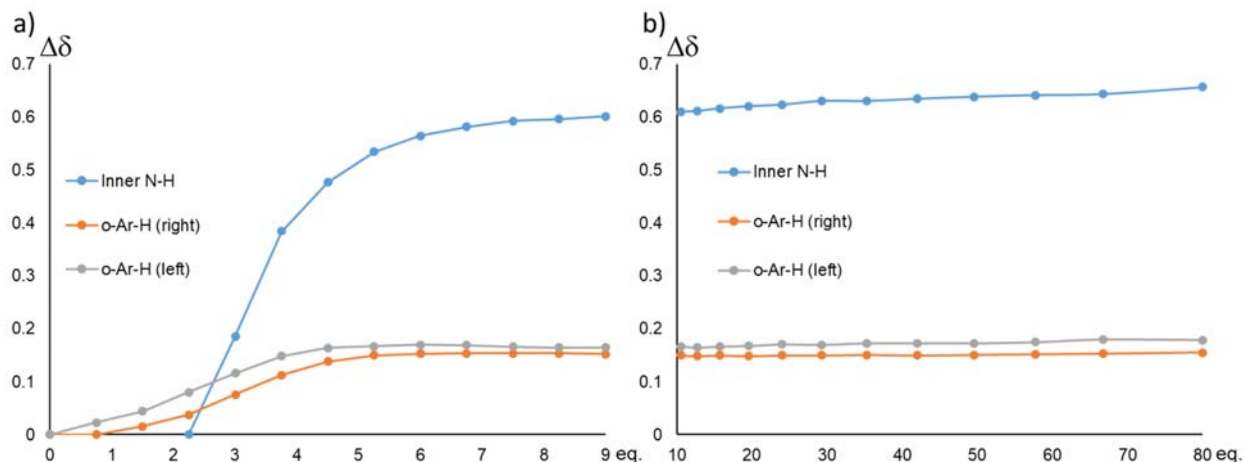


Figure S6. A graph showing the magnitude of the split chemical shifts $\Delta\delta$ in the inner N–H and o-Ar-H of the phenyl rings independence on the **10CSA(R)** equivalents, a) 0 to 9 eq., b) 10 to 80 eq. Recorded in CD₃CN with the addition of 12 eq. of TFA to solubilize and protonate $\alpha_2\beta_2\text{-P}$. The color coding corresponds to the highlighted signals in Figures S3 and S4.

SUPPORTING INFORMATION

Influence of Water on the Complexation

We have previously mentioned that one of the best-known *pro*-CSA (**Bz₂oxP**) suffers serious sensitivity issues due in part to *N*-alkylation.^[21] Additionally, the competitive binding of water molecules significantly contributes to the magnitude of splitting $\Delta\sigma$. Trace amounts of water in solutions or titrants results in the necessary use of high guest concentrations to obtain well-resolved spectra. The hypersensitivity towards water is a major limitation for functional *pro*-CSA, since water is ubiquitous, avoiding it is at least tedious if not almost impossible for most of the solvents and reagents, especially for the analytes bearing high polarity. Hence, investigation of water influence as a competitive agent to the enantio-pure $\alpha_2\beta_2\text{-P}\cdot\mathbf{10CSA(S)}$ complex in CD₃CN was carried out. From the first instance, the gradual addition of water has a considerable effect on $\Delta\sigma$. By the addition of 240 eq. of water, the $\Delta\sigma$ of N–H has contracted by 0.132 ppm. (Figure S9). Despite the competitive nature of water, the overall binding strength of **10CSA(S)** remains observable considering the ~12.5 fold higher water consistency in the solution. Even at substantially higher (>4000 eq.) quantity of water the signals remained anisochronous highlighting the strong relationship between the host and chiral guest (Figure S8-S9).

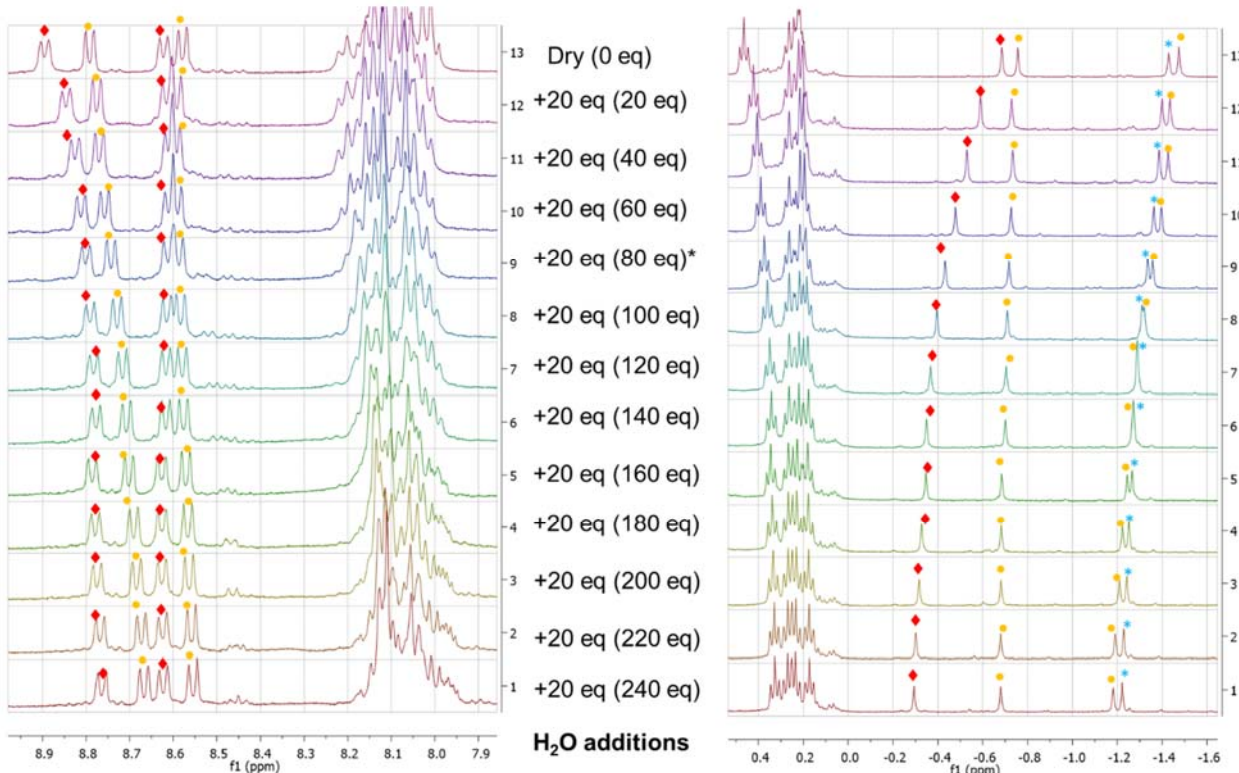


Figure S7. ^1H NMR titration with H₂O (0-240 eq) of $\alpha_2\beta_2\text{-P}\cdot\mathbf{10CSA(S)}$ (19 eq). The split inner N–H is highlighted with orange dots. In the aromatic region, the split o-ArH signals are highlighted with orange and red dots. Spectra recorded in CD₃CN

SUPPORTING INFORMATION

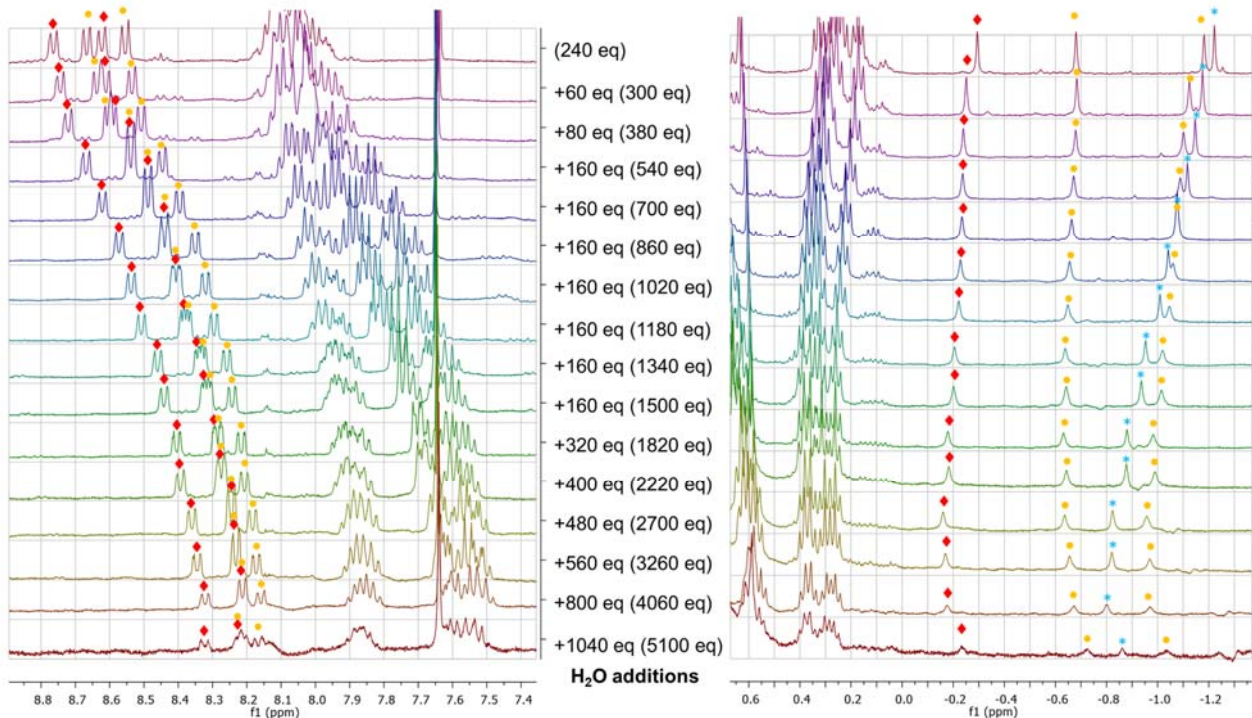


Figure S8. ^1H NMR titration with H_2O (240-5100 eq) of $\alpha_2\beta_2\text{-P}\cdot\text{10CSA(S)}$ (19 eq). The split inner N–H is highlighted with orange dots. In the aromatic region, the split o-ArH signals are highlighted with orange and red dots. Spectra recorded in CD_3CN .

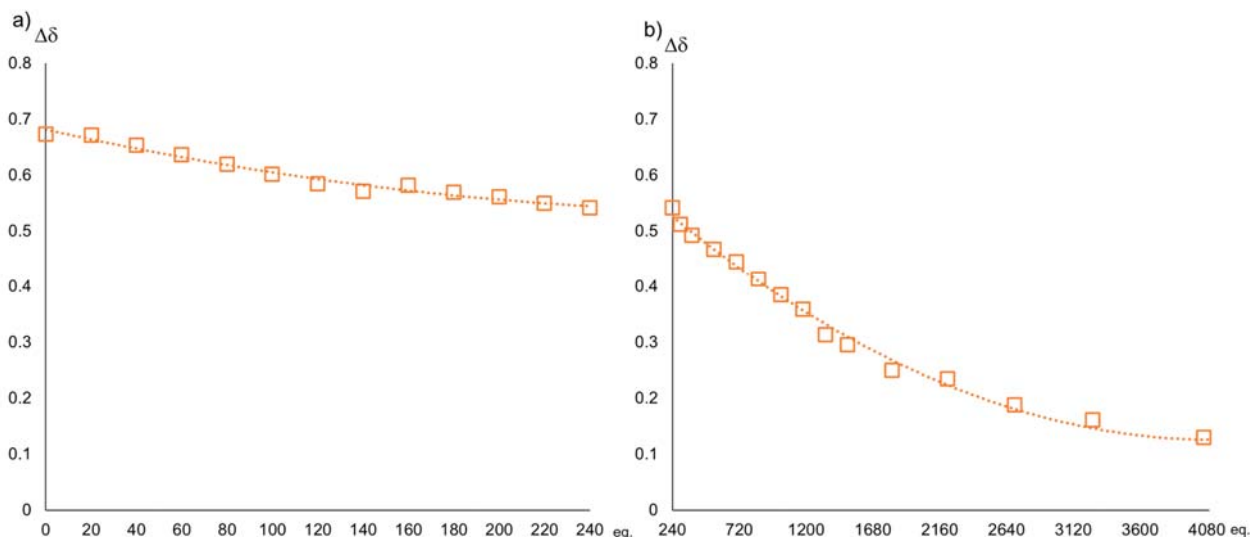


Figure S9. The graph of $\alpha_2\beta_2\text{-P}\cdot\text{10CSA(S)}$ (19 eq) representing N–H $\Delta\sigma$ dependence to the various additions of water a) 0-240 eq. b) 240-5100 eq.

SUPPORTING INFORMATION

Detection of Enantiomeric Excess

For example, 19 eq. of an unknown enantiomeric mixture of **10CSA** was complexed with $\alpha_2\beta_2\text{-P}$ (Figure S11). The inner core system shows clearly split resonance signals with $\Delta\sigma = 0.13$ ppm. A small addition of **10CSA(R)** decreased $\Delta\sigma$ (0.051 ppm), while a similar amount of **10CSA(S)** increased $\Delta\sigma$ (0.224 ppm) revealing the predominant enantiomeric identity ($S > R$). Next, a linear calibration plot with 7 data points ($e.e._{10CSA(S)} = 0, 48, 58, 69, 79, 90, 100 \%$) was constructed. It is worth noting that it is possible to generate a calibration curve from a single measured enantiopure point due to the linear dependency with the second point being $\Delta\sigma = 0$ ppm. where $e.e. = 0\%$. Lastly, the $\Delta\sigma$ can be fitted to the calibration plot and reveal the unknown e.e. (21%) based on the inner N–H chemical shift difference between the split peaks (for more information on this example see figure S12). The same principle can be applied to quickly test the purity of enantiomers, i.e. by equally pre-mixing stereoisomers of interest with opposite chirality, in the event of matching purity, the $\alpha_2\beta_2\text{-P}$ signals will remain isochronous. Overall, monitoring changes of this inner core system in a model chiral environment demonstrates a powerful tool for easy and sensitive detection of enantiomeric compositions.

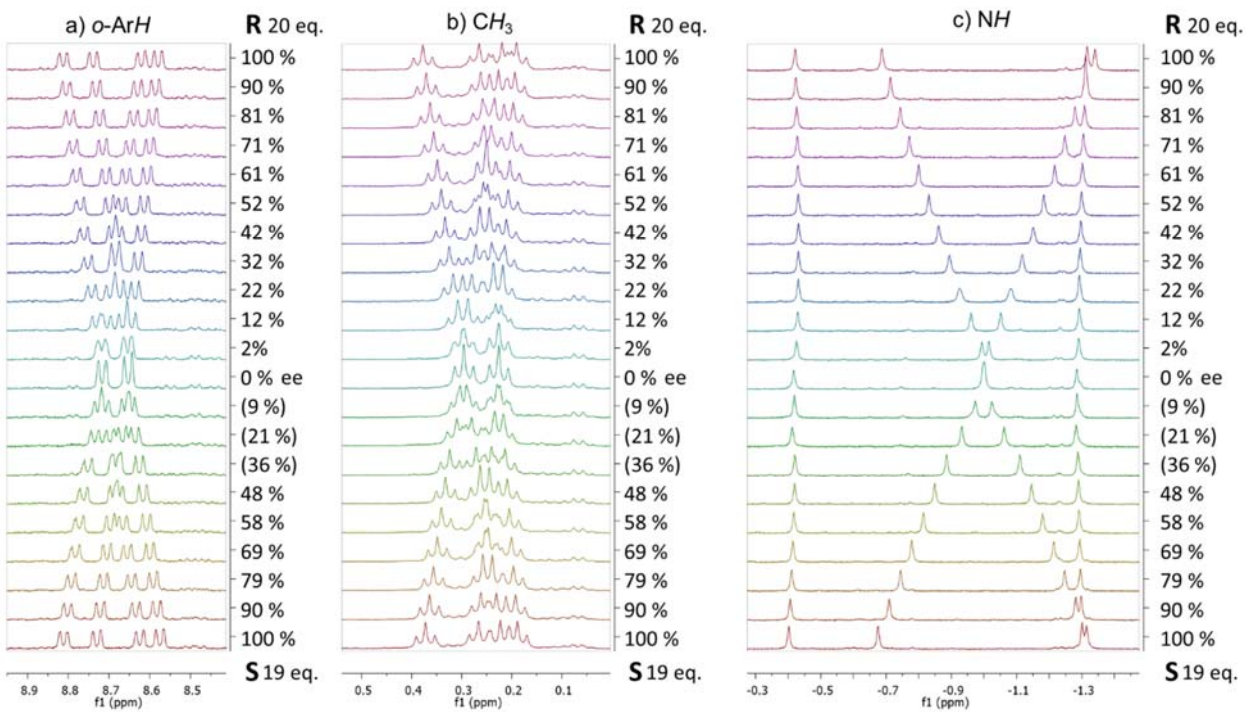


Figure S10. ^1H NMR representation of the three non-overlapping regions for the detection of e.e. (values in brackets calculated from the plot see Figure S8-S9: a) o-ArH, g) CH_3 , and h) inner core system N–H. Two different concentrations of analytes (20 eq. of **10CSA(R)** and 19 eq. of **10CSA(S)**) were used to highlight the diversity of the enantiomeric excess detection using $\alpha_2\beta_2\text{-P}$. Spectra recorded in CD_3CN .

SUPPORTING INFORMATION

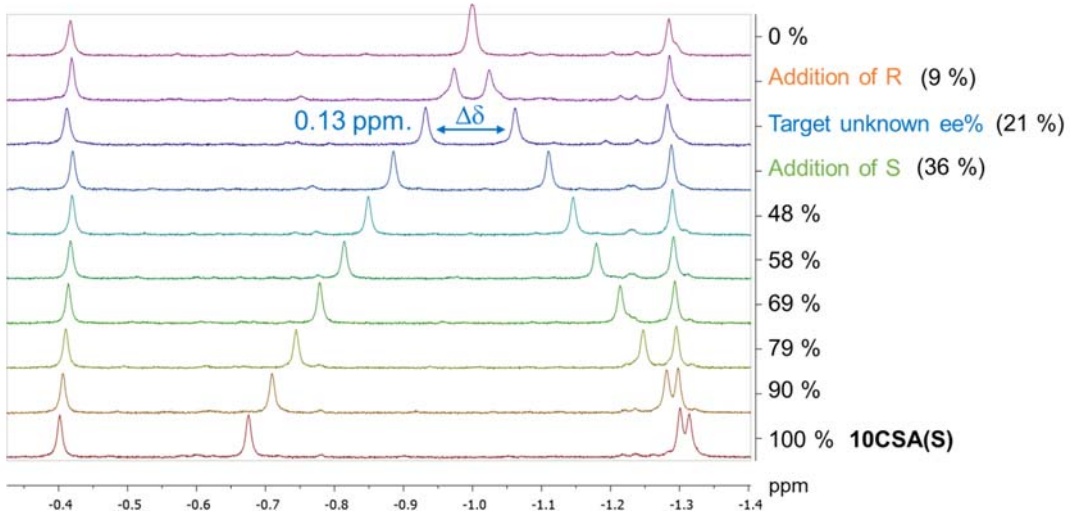


Figure S11. The ^1H NMR spectra of the inner core system N–H unknown e.e.% target compound (highlighted in blue), after small **10CSA(R)** (red) and **10CSA(S)** (green) additions, and the rest of the spectra for the construction of the calibration curve. Spectra recorded in CD_3CN .

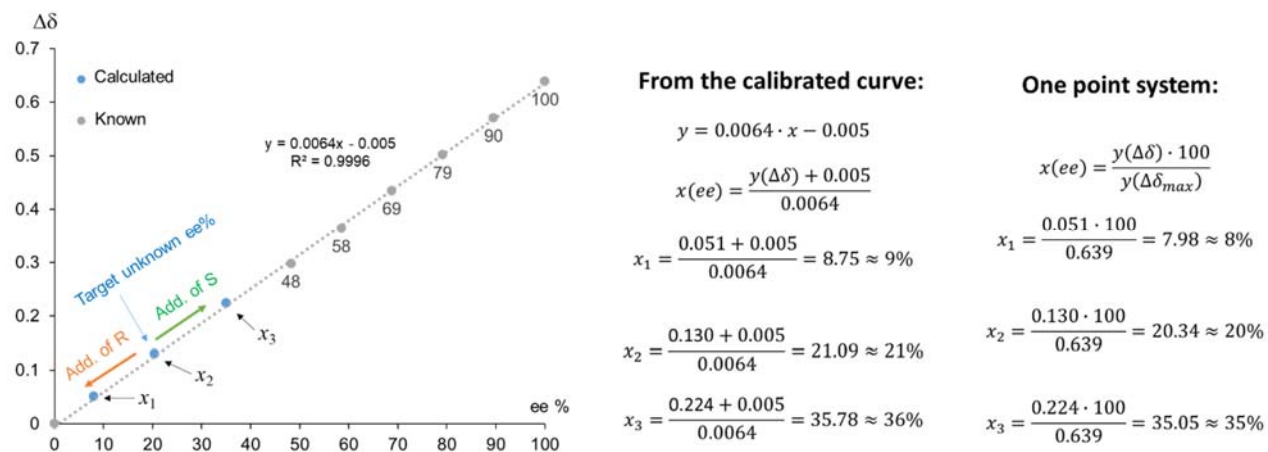


Figure S12. Graph of the $\Delta\sigma$ dependence on the ee% with 19 eq. of **10CSA**. Measured from the ^1H NMR split N–H signals recorded in CD_3CN (at 100 ee% — 19 eq. $\alpha_2\beta_2\text{-P}\cdot\text{10CSA(S)}$). On the right side: calculations of the unknown ee from the calibrated curve and using a one-point system. Note, calculations using a one-point system should only be used for quick, approximate determinations of the ee.

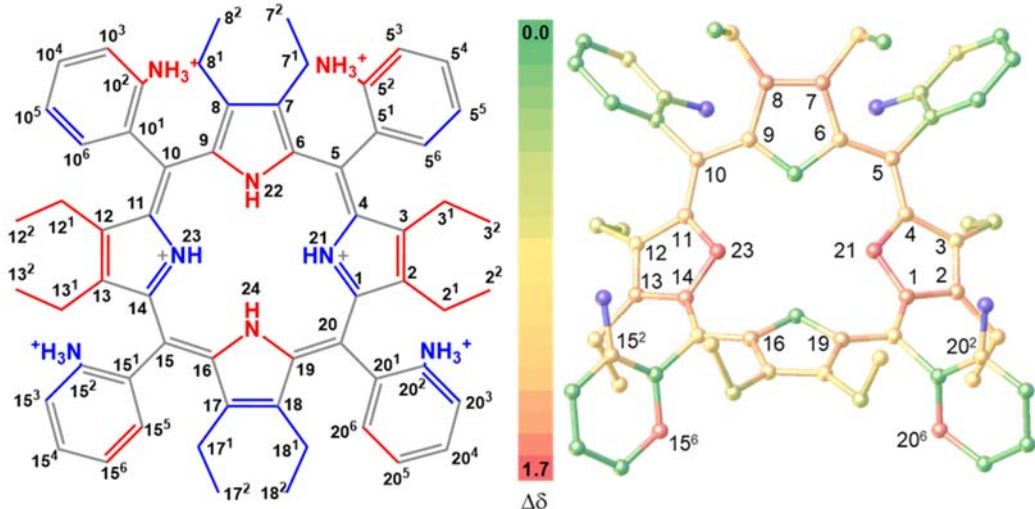
SUPPORTING INFORMATION

^{13}C and ^{15}N Investigations

To further understand the transfer of chirality to the atropisomeric receptor systems **P**, we have performed 2D NMR analyses with enantiopure **10CSA**. The ^{15}N resonance signals obtained from ^1H - ^{15}N HSQC varied from 125 to 135 ppm and correlated well with the corresponding inner core system protons. The $\Delta\sigma_{\max}$ of the ^{15}N were found to be $\alpha_2\beta_2\text{-P}$ (1.67 ppm) > $\alpha\beta\alpha\beta\text{-P}$ (1.03 ppm) > $\alpha_3\beta\text{-P}$ (0.77 ppm) > $\alpha_4\text{-P}$ (0 ppm) (Table S2). Full 2D NMR analyses to determine all of the resonance signals were done for $\alpha_2\beta_2\text{-P}$, $\alpha\beta\alpha\beta\text{-P}$ and $\alpha_4\text{-P}$ with **10CSA(S)**. Unfortunately, due to formation of diastereomers in $\alpha_3\beta\text{-P}\cdot\mathbf{10CSA(S)}$ the large number of signals hampered detailed NMR analysis (Figure S59-S64). While some of the ^1H resonance signals in $\alpha_4\text{-P}\cdot\mathbf{10CSA(S)}$ showed possible splitting patterns, the $\Delta\sigma_{\max}$ were found to not surpass 0.08 ppm. In $\alpha_2\beta_2\text{-P}\cdot\mathbf{10CSA(S)}$ and $\alpha\beta\alpha\beta\text{-P}\cdot\mathbf{10CSA(S)}$ other than inner core N-H the ^1H $\Delta\sigma_{\max}$ showed to be highest in o-Ar-H (0.16 – 0.2 ppm) and certain CH_3 groups (0.22 ppm in $\alpha\beta\alpha\beta\text{-P}$ 2² and 12², 7² and 17²; 0.16 ppm in $\alpha_2\beta_2\text{-P}$ 2² and 13² positions). Only particular ^{13}C in the $\alpha\beta\alpha\beta\text{-P}\cdot\mathbf{10CSA(S)}$ 24-atom macrocycle displayed $\Delta\sigma_{\max}$ with >0.11 ppm (0.47 ppm between 6 and 16, 1 and 11; 0.8 ppm between 8 and 18, 3 and 13 positions). Similarly, in $\alpha_4\text{-P}\cdot\mathbf{10CSA(S)}$ only between 1 and 4, 13 and 12 positions the ^{13}C $\Delta\sigma_{\max}$ (0.23 ppm) was observed to be >0.11 ppm. On the other hand, the majority of the $\alpha_2\beta_2\text{-P}\cdot\mathbf{10CSA(S)}$ pyrrolic ^{13}C displayed $\Delta\sigma_{\max}$ >0.2 ppm, reaching 0.98 ppm between 1 and 14 positions. In the phenyl rings, except for the previously discussed significant ^{13}C $\Delta\sigma_{\max}$ (1.3 ppm) between 15⁶ and 20⁶ in $\alpha_2\beta_2\text{-P}\cdot\mathbf{10CSA(S)}$, other phenyl positions and likewise in other atropisomeric species displayed $\Delta\sigma_{\max}$ <0.31 ppm.

SUPPORTING INFORMATION

Table S1. Comparison of ^{13}C and ^{15}N atom resonances $\alpha_2\beta_2\text{-P-BSA}$,^[20] $\alpha_2\beta_2\text{-P-10CSA(S)}$ and $\alpha_2\beta_2\text{-P-10CSA(SR)}$ complexes. The $\Delta\sigma_{\max}$ (ppm) in ^{13}C and ^{15}N atoms of $\alpha_2\beta_2\text{-P-10CSA(S)}$ recorded with 20 eq. of analyte. The signal positions were determined using various NMR techniques (CD_3CN). Top left side, illustration of the $\alpha_2\beta_2\text{-P}$ (blue — above and red — below the plane) with corresponding positions. The highlighted positions in the illustration on the top right side shows $\Delta\sigma \geq 0.3$ ppm (atoms in blue are peripheral nitrogen atoms that did not resonate).



Pos.	BSA	CSA-SR	CSA-S	Pos.	BSA	CSA-SR	CSA-S	δ C or δ N	$\Delta\delta$
	δ C or δ N	δ C or δ N	δ C or δ N		δ C or δ N	δ C or δ N	δ C or δ N		
1	144.1	144.1	143.7	12 ¹	20.5	20.6	20.6	1 and 14	0.98
2	142.0	142.1	142.3	12 ²	15.2	15.6	15.6	2 and 13	0.59
2 ¹	19.1	19.3	19.5	13	142.0	142.1	141.7	2 ¹ and 13 ¹	0.26
2 ²	15.9	16.0	16.0	13 ²	19.1	19.3	19.3	2 ² and 13 ²	0.22
3	143.9	143.4	143.2	14	144.1	144.1	144.7	3 and 12	0.22
3 ¹	20.5	20.6	20.5	15	112.0	112.6	112.5	3 ¹ and 12 ¹	0.12
3 ²	15.2	15.6	15.5	15 ¹	132.0	132.3	132.3	3 ² and 12 ²	0.12
4	143.9	144.3	144.5	15 ²	133.0	134.0	134.3	4 and 11	0.4
5	114.9	114.1	113.9	15 ³	130.5	129.9	129.7	6 and 9	0.35
5 ¹	132.1	132.0	132.0	15 ⁴	134.2	133.8	133.8	7 and 8	0.88
5 ²	133.1	133.1	133.1	15 ⁵	125.9	126.3	126.1	7 ¹ and 8 ¹	0.19
5 ³	130.6	130.5	130.6	15 ⁶	140.4	139.3	139.9	7 ² and 8 ²	0.02
5 ⁴	134.2	133.8	133.8	16	144.9	145.6	145.9	10 and 5	0.47
5 ⁵	126.4	125.9	125.9	17	145.6	144.4	144.4	10 ¹ and 5 ¹	0.06
5 ⁶	139.8	141.0	141.1	17 ¹	20.8	20.6	20.6	10 ² and 5 ²	0.09
6	142.8	143.0	142.8	17 ²	15.4	15.4	15.3	10 ³ and 5 ³	0.14
7	142.9	141.9	141.4	18	145.6	144.4	144.2	10 ⁴ and 5 ⁴	0
7 ¹	19.1	19.4	19.2	18 ¹	20.8	20.6	20.5	10 ⁵ and 5 ⁵	0
7 ²	15.9	16.4	16.3	18 ²	15.4	15.4	15.5	10 ⁶ and 5 ⁶	0.04
8	142.9	141.9	142.3	19	144.9	145.6	145.3	15 and 20	0.19
8 ¹	19.1	19.4	19.4	20	112.0	112.6	112.7	15 ¹ and 20 ¹	0
8 ²	15.9	16.4	16.3	20 ¹	132.0	132.3	132.3	15 ² and 20 ²	0.3
9	142.8	143.0	143.1	20 ²	133.0	134.0	134.6	15 ³ and 20 ³	0
10	114.9	114.1	114.3	20 ³	130.5	129.9	129.7	15 ⁴ and 20 ⁴	0
10 ¹	132.1	132.0	131.9	20 ⁴	134.2	133.8	133.8	15 ⁵ and 20 ⁵	0
10 ²	133.1	133.1	133.2	20 ⁵	125.9	126.3	126.1	15 ⁶ and 20 ⁶	1.3
10 ³	130.6	130.5	130.4	20 ⁶	140.4	139.3	138.6	16 and 19	0.52
10 ⁴	134.2	133.8	133.8	21	127.0	127.6	128.5	17 and 18	0.2
10 ⁵	126.4	125.9	125.9	22	126.9	128.0	128.0	17 ¹ and 18 ¹	0.12
10 ⁶	139.8	141.0	141.1	23	127.0	127.6	126.9	17 ² and 18 ²	0.18
11	143.9	144.3	144.1	24	125.9	131.9	132.2	21 and 23	1.67

SUPPORTING INFORMATION

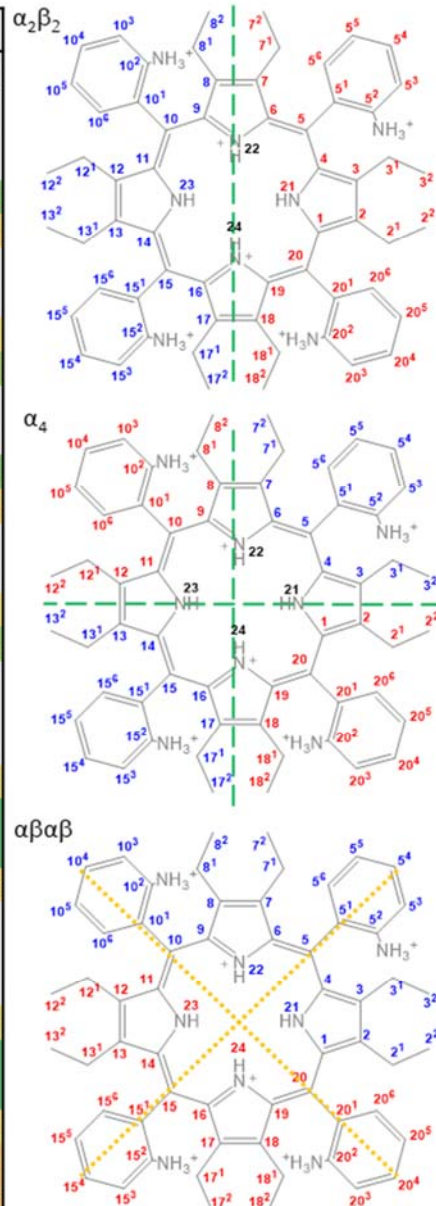
Table S2. Comparison of ^{13}C and ^{15}N atom resonances a) $\alpha_4\text{-P-BSA}$,^[20] $\alpha_4\text{-P-10CSA(S)}$, $\alpha_4\text{-P-10CSA(SR)}$ and, b) $\alpha\beta\alpha\beta\text{-P-BSA}$,^[20] $\alpha\beta\alpha\beta\text{-P-10CSA(S)}$, $\alpha\beta\alpha\beta\text{-P-10CSA(SR)}$ complexes. The signal positions were determined using various NMR techniques (CD_3CN) recorded with 20 eq. of analyte.

a)				$\alpha_4\text{-P}$				b)				$\alpha\beta\alpha\beta\text{-P}$			
Pos.	BSA	CSA-SR	CSA-S	Pos.	BSA	CSA-SR	CSA-S	Pos.	BSA	CSA-SR	CSA-S	Pos.	BSA	CSA-SR	CSA-S
	$\delta \text{C or } \delta \text{N}$	$\delta \text{C or } \delta \text{N}$	$\delta \text{C or } \delta \text{N}$		$\delta \text{C or } \delta \text{N}$	$\delta \text{C or } \delta \text{N}$	$\delta \text{C or } \delta \text{N}$		$\delta \text{C or } \delta \text{N}$	$\delta \text{C or } \delta \text{N}$	$\delta \text{C or } \delta \text{N}$		$\delta \text{C or } \delta \text{N}$	$\delta \text{C or } \delta \text{N}$	$\delta \text{C or } \delta \text{N}$
1	143.2	143.9	141.9	12 ¹	18.2	19.2	19.2	1	143.6	145.0	145.3	12 ¹	19.8	20.5	20.2
2	142.2	145.0	143.7	12 ²	16.2	16.1	16.2	2	143.8	142.7	142.7	12 ²	15.3	15.8	15.8
2 ¹	18.2	19.2	19.2	13	142.2	145.0	143.7	2 ¹	19.8	20.5	20.2	13	144.0	142.5	142.2
2 ²	16.2	16.1	16.2	13 ¹	18.2	19.2	19.2	2 ²	15.3	15.8	15.8	13 ¹	20.6	19.7	19.7
3	142.2	145.0	143.7	13 ²	16.2	16.1	16.1	3	144.0	142.5	143.0	13 ²	15.6	16.1	16.1
3 ¹	18.2	19.2	19.2	14	143.2	143.9	141.8	3 ¹	20.6	19.7	19.7	14	145.0	143.9	143.9
3 ²	16.2	16.1	16.1	15	114.1	113.8	113.8	3 ²	15.6	16.1	16.1	15	113.1	113.2	113.2
4	143.2	143.9	141.8	15 ¹	131.7	131.6	131.6	4	145.0	143.9	143.9	15 ¹	132.1	132.2	132.5
5	114.1	113.8	113.8	15 ²	133.0	133.5	133.4	5	113.1	113.2	113.1	15 ²	132.9	134.6	133.9
5 ¹	131.7	131.6	131.6	15 ³	126.2	126.3	126.2	5 ¹	132.1	132.2	132.2	15 ³	126.0	125.8	126.1
5 ²	133.0	133.5	133.4	15 ⁴	134.3	134.1	134.0	5 ²	132.9	134.6	133.9	15 ⁴	134.4	133.8	133.9
5 ³	126.2	126.3	126.2	15 ⁵	130.7	130.5	130.5	5 ³	126.0	125.8	125.9	15 ⁵	130.9	129.9	130.3
5 ⁴	134.3	134.1	134.0	15 ⁶	140.6	141.0	140.9	5 ⁴	134.4	133.8	133.9	15 ⁶	140.1	140.3	133.9
5 ⁵	130.7	130.5	130.5	16	144.9	143.8	144.9	5 ⁵	130.9	129.9	130.1	16	143.6	145.0	145.3
5 ⁶	140.6	141.0	140.9	17	144.8	141.9	143.9	5 ⁶	140.1	140.3	133.9	17	143.8	142.7	142.7
6	144.9	143.8	144.9	17 ¹	20.4	20.4	19.2	6	143.6	145.0	144.8	17 ¹	19.8	20.5	20.2
7	144.8	141.9	143.9	17 ²	15.0	15.7	15.7	7	143.8	142.7	142.8	17 ²	15.3	15.8	15.8
7 ¹	20.4	20.4	19.2	18	144.8	141.9	143.9	7 ¹	19.8	20.5	20.2	18	144.0	142.5	143.0
7 ²	15.0	15.7	15.7	18 ¹	20.4	20.4	19.2	7 ²	15.3	15.8	15.8	18 ¹	20.6	19.7	19.7
8	144.8	141.9	143.9	18 ²	15.0	15.7	15.6	8	144.0	142.5	142.2	18 ²	15.6	16.1	16.1
8 ¹	20.4	20.4	19.2	19	144.9	143.8	145.2	8 ¹	20.6	19.7	19.7	19	145.0	143.9	143.9
8 ²	15.0	15.7	15.6	20	114.1	113.8	113.8	8 ²	15.6	16.1	16.1	20	113.1	113.2	113.1
9	144.9	143.8	145.2	20 ¹	131.7	131.6	131.7	9	145.0	143.9	143.9	20 ¹	132.1	132.2	132.2
10	114.1	113.8	113.8	20 ²	133.0	133.5	133.5	10	113.1	113.2	113.2	20 ²	132.9	134.6	133.9
10 ¹	131.7	131.6	131.7	20 ³	126.2	126.3	126.3	10 ¹	132.1	132.2	132.5	20 ³	126.0	125.8	125.9
10 ²	133.0	133.5	133.5	20 ⁴	134.3	134.1	134.1	10 ²	132.9	134.6	133.9	20 ⁴	134.4	133.8	133.9
10 ³	126.2	126.3	126.3	20 ⁵	130.7	130.5	130.5	10 ³	126.0	125.8	126.1	20 ⁵	130.9	129.9	130.1
10 ⁴	134.3	134.1	134.1	20 ⁶	140.6	141.0	141.1	10 ⁴	134.4	133.8	133.9	20 ⁶	140.1	140.3	133.9
10 ⁵	130.7	130.5	130.5	21	125.8	127.9	127.7	10 ⁵	130.9	129.9	130.3	21	126.5	129.0	129.2
10 ⁶	140.6	141.0	141.1	22	125.1	125.8	126.1	10 ⁶	140.1	140.3	133.9	22	126.5	129.0	128.2
11	143.2	143.9	141.9	23	125.8	127.9	127.7	11	143.6	145.0	144.8	23	126.5	129.0	128.2
12	142.2	145.0	143.7	24	125.1	125.8	126.1	12	143.8	142.7	142.8	24	126.5	129.0	129.2

SUPPORTING INFORMATION

Table S3. Comparison of the $\Delta\sigma_{\max}$ (ppm) in ^{13}C , ^{15}N and ^1H atoms of $\alpha_2\beta_2\text{-P}\cdot\text{10CSA(S)}$, $\alpha_4\text{-P}\cdot\text{10CSA(S)}$, and $\alpha\beta\alpha\beta\text{-P}\cdot\text{10CSA(S)}$ recorded with 20 eq. of analyte. The signal positions were determined using 2D NMR techniques (CD_3CN). On the right side, illustration of the $\alpha_2\beta_2\text{-P}$, $\alpha_4\text{-P}$, and $\alpha\beta\alpha\beta\text{-P}$ with highlighted positions (blue and red represents the splitting signals between them), dashed green line — mirror planes, yellow dotted lines — inversion points.

$\alpha_2\beta_2\text{-P}\cdot\text{10CSA(S)}$			$\alpha_4\text{-P}\cdot\text{10CSA(S)}$			$\alpha\beta\alpha\beta\text{-P}\cdot\text{10CSA(S)}$		
Pos.	$\Delta\delta \text{ C or } \Delta\delta \text{ N}$	$\Delta\delta \text{ H}$	Pos.	$\Delta\delta \text{ C or } \Delta\delta \text{ N}$	$\Delta\delta \text{ H}$	Pos.	$\Delta\delta \text{ C or } \Delta\delta \text{ N}$	$\Delta\delta \text{ H}$
1 and 14	0.98		1 and 4	0.23		1 and 11	0.47	
2 and 13	0.59		2 and 3	0.01		2 and 12	0.09	
2 ¹ and 13 ¹	0.26	0.03	2 ¹ and 3 ¹	0	0	2 ¹ and 12 ¹	0	0.02
2 ² and 13 ²	0.22	0.16	2 ² and 3 ²	0.11	0.08	2 ² and 12 ²	0	0.22
3 and 12	0.22		6 and 9	0.1		4 and 14	0	
3 ¹ and 12 ¹	0.12	0.09	7 and 8	0.08		3 and 13	0.8	
3 ² and 12 ²	0.12	0.03	7 ¹ and 8 ¹	0	0	3 ¹ and 13 ¹	0	0.1
4 and 11	0.4		7 ² and 8 ²	0.03	0	3 ² and 13 ²	0.03	0.03
6 and 9	0.35		10 and 5	0.06		6 and 16	0.47	
7 and 8	0.88		10 ¹ and 5 ¹	0.05		7 and 17	0.09	
7 ¹ and 8 ¹	0.19	0.03	10 ² and 5 ²	0.18		7 ¹ and 17 ¹	0	0.02
7 ² and 8 ²	0.02	0.07	10 ³ and 5 ³	0.07	0.07	7 ² and 17 ²	0	0.22
10 and 5	0.47		10 ⁴ and 5 ⁴	0.06	0.01	9 and 19	0	
10 ¹ and 5 ¹	0.06		10 ⁵ and 5 ⁵	0	0	8 and 18	0.8	
10 ² and 5 ²	0.09		10 ⁶ and 5 ⁶	0.19	0.01	8 ¹ and 18 ¹	0	0.1
10 ³ and 5 ³	0.14		13 and 12	0.23		8 ² and 18 ²	0.03	0.03
10 ⁴ and 5 ⁴	0		13 ¹ and 12 ¹	0.01		15 and 5	0.1	
10 ⁵ and 5 ⁵	0		13 ² and 12 ²	0	0	15 ¹ and 5 ¹	0.31	
10 ⁶ and 5 ⁶	0.04	0.2	11 and 14	0.11	0.08	15 ² and 5 ²	0	
15 and 20	0.19		16 and 19	0.1		15 ³ and 5 ³	0.16	0.05
15 ¹ and 20 ¹	0		17 and 18	0.08		15 ⁴ and 5 ⁴	0	0
15 ² and 20 ²	0.3		17 ¹ and 18 ¹	0	0	15 ⁵ and 5 ⁵	0.22	0
15 ³ and 20 ³	0		17 ² and 18 ²	0.03	0	15 ⁶ and 5 ⁶	0	0.16
15 ⁴ and 20 ⁴	0		15 and 20	0.06		10 and 20	0.1	
15 ⁵ and 20 ⁵	0		15 ¹ and 20 ¹	0.05		10 ¹ and 20 ¹	0.31	
15 ⁶ and 20 ⁶	1.3	0.17	15 ² and 20 ²	0.18		10 ² and 20 ²	0	
16 and 19	0.52		15 ³ and 20 ³	0.07	0.07	10 ³ and 20 ³	0.16	0.05
17 and 18	0.2		15 ⁴ and 20 ⁴	0.06	0.01	10 ⁴ and 20 ⁴	0	0
17 ¹ and 18 ¹	0.12	0.09	15 ⁵ and 20 ⁵	0	0	10 ⁵ and 20 ⁵	0.22	0
17 ² and 18 ²	0.18	0.03	15 ⁶ and 20 ⁶	0.19	0.01	10 ⁶ and 20 ⁶	0	0.16
21 and 23	1.67	0.66	21 and 23	0	0	21 and 23	1.03	0.52
22 and 24	0	0	22 and 24	0	0	22 and 24	1.03	0.52



SUPPORTING INFORMATION

Structural Determination of $\alpha_2\beta_2\text{-P}[\text{SO}_4^{2-}][\text{HSO}_4^-]_4$

Table S4: Details of XRD data refinement of $\alpha_2\beta_2\text{-P}[\text{SO}_4^{2-}][\text{HSO}_4^-]_4$

Compound	$\alpha_2\beta_2\text{-P}[\text{SO}_4^{2-}][\text{HSO}_4^-]_4$
<i>Internal code</i>	KN007
<i>CCDC #</i>	2143572
<i>Empirical formula</i>	C ₆₀ H _{84.38} N ₈ O _{23.95} S ₅
<i>Formula weight</i>	1461.23
<i>Temperature/K</i>	100(2)
<i>Crystal system</i>	Monoclinic
<i>Space group</i>	P2 ₁ /n
<i>a/Å</i>	18.7594(9)
<i>b/Å</i>	16.0888(8)
<i>c/Å</i>	24.9988(12)
<i>$\alpha/^\circ$</i>	90
<i>$\beta/^\circ$</i>	90.962(2)
<i>$\gamma/^\circ$</i>	90
<i>Volume/Å³</i>	7544.0(6)
<i>Z</i>	4
<i>D_{calc} g/cm³</i>	1.287
<i>μ/mm^{-1}</i>	2.066
<i>F(000)</i>	3088.0
<i>Crystal size/mm³</i>	0.15 × 0.1 × 0.07
<i>Radiation</i>	CuKα
<i>Wavelength/Å</i>	1.54178
<i>2θ/°</i>	5.844 to 140.326
<i>Reflections collected</i>	94031
<i>Independent reflections</i>	14243
<i>R_{int}</i>	0.0578
<i>R_{sigma}</i>	0.0345
<i>Restraints</i>	3307
<i>Parameters</i>	1354
<i>GooF</i>	1.104
<i>R₁ [I > 2σ (I)]</i>	0.1354
<i>wR₂ [I > 2σ (I)]</i>	0.3912
<i>R₁ [all data]</i>	0.1537
<i>wR₂ [all data]</i>	0.4253
<i>Largest peak/e Å⁻³</i>	1.73
<i>Deepest hole/e Å⁻³</i>	-0.99

SUPPORTING INFORMATION

basis	Δ_{ip}	δ_{ip}	B_{2g}	B_{1g}	$E_u(x)$	$E_u(y)$	A_{1g}	A_{2g}
min.	0.75	0.18	-0.02	0.11	-0.02	0.00	-0.74	0.01
ext.	0.88	0.13	-0.02	0.11	-0.02	0.00	-0.74	0.01
			0.01	0.01	-0.03	0.01	-0.46	0.01
total	1.11	0.00	-0.02	0.11	-0.02	0.00	-0.71	0.01
	0.01	0.01	-0.03	0.01	-0.45	0.01		
	0.01	-0.01	-0.01	-0.01	0.71	0.00		
	0.00	0.00	-0.02	0.02	0.00	0.00		
	0.01	0.01	0.01	-0.01	-0.07	0.00		
	0.00	0.00	0.01	-0.01	-0.07			
			-0.01	0.02				
			0.00	0.00				
			0.00	-0.02				
			0.00	0.00				
			0.00	0.01				
comp.	1.11	0.00	0.02	0.11	0.04	0.04	1.10	0.02
basis	Δ_{oop}	δ_{oop}	B_{2u}	B_{1u}	A_{2u}	$E_g(x)$	$E_g(y)$	A_{1u}
min.	3.88	0.11	-3.88	-0.02	0.02	0.02	-0.01	0.02
ext.	3.92	0.00	-3.87	-0.02	0.02	0.02	-0.01	0.02
	0.65	-0.01	-0.02	-0.04	0.00	0.00		
total	3.92	0.00	-3.87	-0.02	0.02	0.02	-0.01	0.02
	0.65	-0.01	-0.02	-0.04	0.00	0.00		
	0.07	-0.01	0.00	0.01	-0.03			
			-0.01	0.00				
			-0.01	0.00				
comp.	3.92	0.00	3.92	0.02	0.03	0.04	0.03	0.02

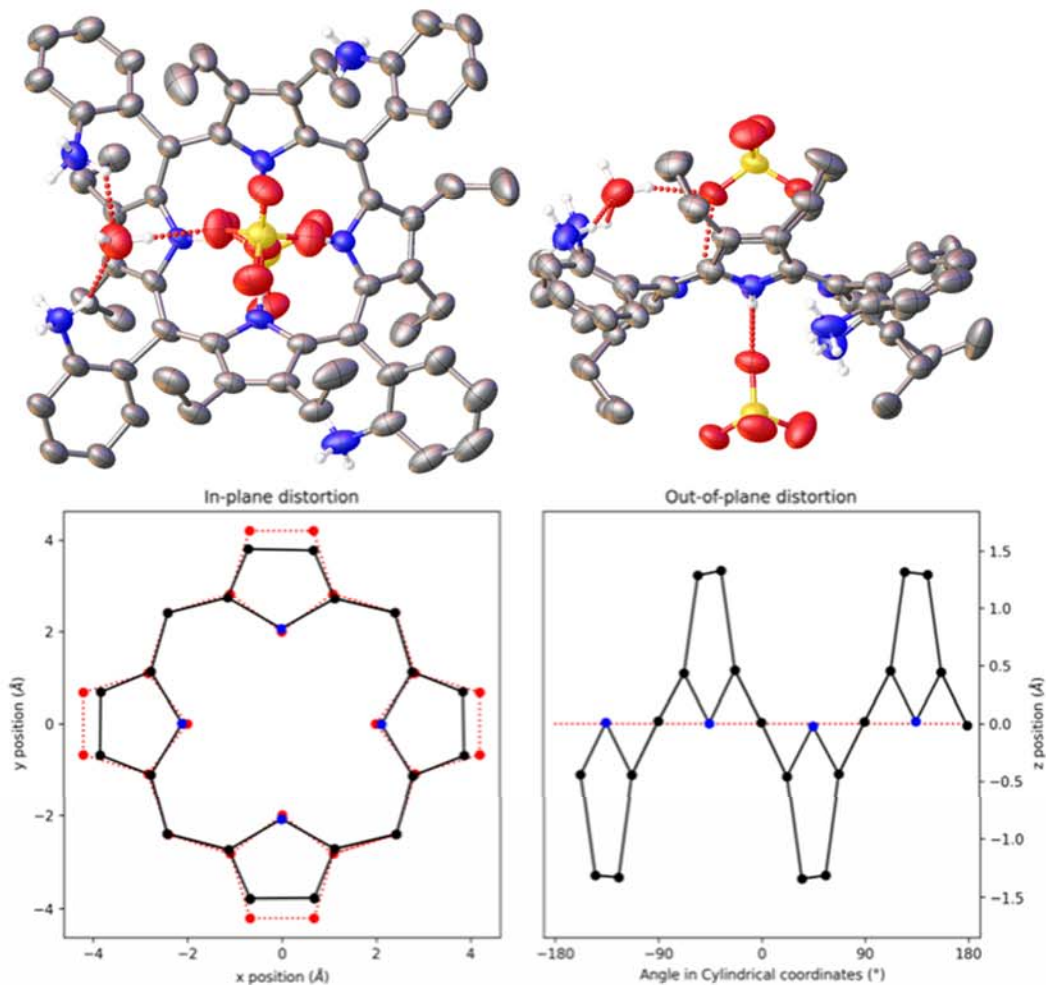


Figure S13. Left: in-plane (ip) and out-of-plane (oop) NSD results of $\alpha_2\beta_2\text{-P}[\text{SO}_4^{2-}]_4$; Right bottom: out-of-plane and in-plane skeletal plots of the porphyrin $\alpha_2\beta_2\text{-P}[\text{SO}_4^{2-}]_4$ core. Porphyrin $\alpha_2\beta_2\text{-P}$ is represented in black(C) and blue(N), with the reference structure (CuTPP) in red dotted lines.^[2] Right top: top view and sideview of $\alpha_2\beta_2\text{-P-SO}_4$ structure. Non-essential hydrogens, majority of counter anions and solvent molecules omitted for clarity, thermal ellipsoids shown at 50% probability.

SUPPORTING INFORMATION

Computational Analysis

Geometry analysis

Based on the crystallographic data we concluded that one porphyrin cation binds two camphorsulfonic acid molecules. Using this ratio and the $\alpha_2\beta_2\text{-P}[\text{SO}_4^{2-}][\text{HSO}_4^-]_4$ crystal data the corresponding host-guest complexes were built with subsequent conformation search. According to the Boltzmann distribution, in acetonitrile one major conformer **A** (90%) and one minor conformer **B** (up to 10%) being higher in energy by 1.30 kcal/mol are presented (Table S5).

In all host-guest complexes, the porphyrin plane is significantly distorted (the $\text{C}_\beta\text{-C}_\beta\text{-C}_{\beta\text{opp}}\text{-C}_{\beta\text{opp}}$ angles varying in the range of 0° - 25° and $\text{N-C}_\alpha\text{-C}_\alpha\text{-N}$ angles varying in the range of 37° - 48°) because of a steric hindrance between the peripheral substituents (for NSD profile check Figure S13). This deformation results in appearance of two cavities on both sides of the porphyrin macrocycle, which differ by the position of NH_3^+ groups. In one cavity the ammonia groups are placed on the same side of the cavity and in another – on the opposite sides (Figure S14a), and the distance between two nitrogen atoms increases from 4.899 \AA to 8.7174 \AA , respectively. The difference in the position of NH_3^+ groups results in a non-identical mode of the binding of two camphorsulfonic acids (“standing” and “lying”). Both the NBO and AIMALL analysis showed that the guest molecules interact with the porphyrin cation through the formation of four H-bonds, which cause significant elongation of the N-H bonds by 0.08-0.03 \AA in the case of NH_3^+ groups and by 0.03 \AA in the case of inner core protons for the major conformer **A** (Figure S14b, Tables S6 and S7).

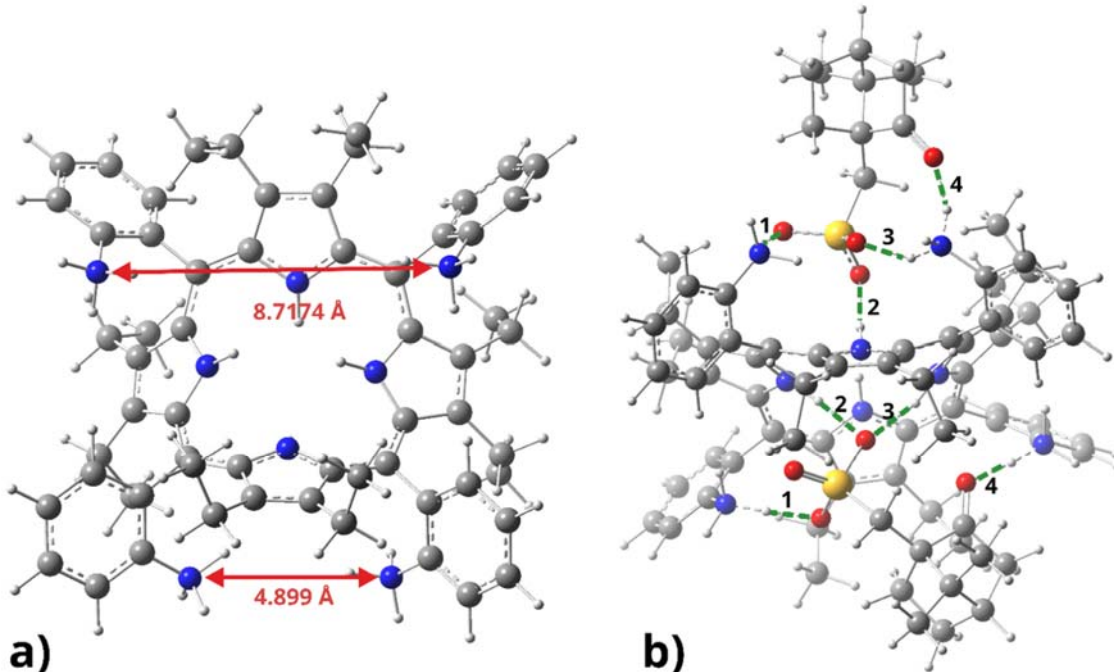


Figure S14. a) Position of NH_3^+ groups in porphyrin cation; b) major conformer **A** of the $\alpha_2\beta_2\text{-P}\cdot10\text{CSA(R)}$ complex, where hydrogen bonds formed between porphyrin and two guest molecules are shown by the green dashed lines and numbered.

SUPPORTING INFORMATION

Table S5. Relative energies and Boltzmann distribution of $\alpha_2\beta_2\text{-P}\cdot\text{10CSA(R)}$ conformers.

Conf.	El. energy, Hartree (def2-SVP)	El. energy, Hartree (def2-SVP)	Gibbs Free energy correction, Hartree	Relative Gibbs Free energy, kcal/mol	Boltzmann distribution, %
A	-4942,80946	-4947,6688	1,534213	0	90
B	-4942,80783	-4947,66664	1,534117	1,3	10
C	-4942,79772	-4947,65773	1,533141	6,28	0
D	-4942,79733	-4947,6544	1,534908	9,48	0
E	-4942,79347	-4947,65221	1,532854	9,56	0
F	-4942,79077	-4947,64779	1,536709	14,75	0
G	-4942,77487	-4947,63394	1,532741	20,96	0
H	-4942,7644	-4947,6243	1,532105	26,6	0

Table S6. Perturbation theory energy analysis of A conformer of $\alpha_2\beta_2\text{-P}\cdot\text{10CSA(R)}$ complex.

Num. of H- bond	“standing” guest			“lying” guest		
	Donor NBO	Acceptor NBO	E(2), kcal/ mol	Donor NBO (l)	Acceptor NBO (j)	E(2), kcal/ mol
1	BD (1) O 138 - S 165	RY*(2) H 103	0.12	BD (1) N 127 - H 130	RY*(3) O81	0.06
	BD (1) O 138 - S 165	RY*(3) H 103	0.1	BD (1) N 127 - H 130	RY*(9) O81	0.06
	BD (1) O 138 - S 165	RY*(4) H 103	0.1	BD (1) N 127 - H 130	BD*(1) O81 - S 169	0.52
	BD (1) O 138 - S 165	RY*(5) H 103	0.07	BD (1) N 127 - H 130	RY*(3) O81	1.42
	BD (1) O 138 - S 165	BD*(1) N 100 - H 103	0.31	BD (1) O81 - S 169	RY*(2) H 130	0.09
	CR (1) O 138	BD*(1) N 100 - H 103	0.84	BD (1) O81 - S 169	RY*(3) H 130	0.09
	LP (1) O 138	RY*(1) H 103	0.29	BD (1) O81 - S 169	RY*(4) H 130	0.18
	LP (1) O 138	RY*(3) H 103	0.14	BD (1) O81 - S 169	BD*(1) N 127 - H 130	0.48
	LP (1) O 138	BD*(1) N 100 - H 103	10.53	CR (1) O81	RY*(1) H 130	0.06
	LP (2) O 138	RY*(6) H 103	0.15	CR (1) O81	RY*(2) H 130	0.06
	LP (3) O 138	RY*(1) H 103	1.08	CR (1) O81	BD*(1) N 127 - H 130	1.24
	LP (3) O 138	RY*(2) H 103	1.28	CR (1) O81	RY*(1) H 130	0.34
	LP (3) O 138	RY*(3) H 103	0.31	CR (1) O81	RY*(2) H 130	0.06
	LP (3) O 138	RY*(4) H 103	0.25	CR (1) O81	RY*(3) H 130	0.06
	LP (3) O 138	RY*(5) H 103	0.08	CR (1) O81	BD*(1) N 127 - H 130	11.71
	LP (3) O 138	RY*(8) H 103	0.07	LP (2) O81	RY*(3) H 130	0.1
	LP (3) O 138	BD*(1) N 100 - H 103	33.97	LP (2) O81	RY*(6) H 130	0.07
	BD*(1) O 138 - S 165	BD*(1) N 100 - H 103	4.38	LP (2) O81	RY*(7) H 130	0.05
	BD (1) N 100 - H 103	RY*(2) O 138	0.07	LP (2) O81	BD*(1) N 127 - H 130	0.32
	BD (1) N 100 - H 103	BD*(1) O 138 - S 165	0.4	LP (3) O81	RY*(1) H 130	0.65
				LP (3) O81	RY*(2) H 130	2.32
				LP (3) O81	RY*(3) H 130	0.13
				LP (3) O81	RY*(4) H 130	0.23
				LP (3) O81	RY*(5) H 130	0.16
				LP (3) O81	RY*(8) H 130	0.06
				LP (3) O81	BD*(1) N 127 - H 130	43.13
				LP (3) O81	BD*(1) N 127 - H 130	5.51
	Total		54.54	Total		69.16
2	BD (1) S 165 - O 167	RY*(2) H53	0.07	BD (1) N50 - H51	RY*(2) O87	0.11

SUPPORTING INFORMATION

	BD (1) S 165 - O 167	RY*(4) H53	0.05	BD (1) N50 - H51	RY*(3) O87	0.09
	BD (1) S 165 - O 167	BD*(1) N52 - H53	0.35	BD (1) N50 - H51	BD*(1) O87 - S 169	0.18
	CR (1) O 167	BD*(1) N52 - H53	0.56	BD (1) O87 - S 169	RY*(3) H51	0.16
	LP (1) O 167	RY*(1) H53	0.12	BD (1) O87 - S 169	RY*(6) H51	0.11
	LP (1) O 167	RY*(2) H53	0.33	BD (1) O87 - S 169	BD*(1) N50 - H51	0.69
	LP (1) O 167	RY*(3) H53	0.09	CR (1) O87	BD*(1) N50 - H51	0.71
	LP (1) O 167	BD*(1) N52 - H53	8.72	LP (1) O87	RY*(1) H51	0.12
	LP (2) O 167	RY*(2) H53	0.13	LP (1) O87	RY*(2) H51	0.26
	LP (2) O 167	BD*(1) N52 - H53	0.88	LP (1) O87	BD*(1) N50 - H51	8.05
	LP (3) O 167	RY*(1) H53	0.05	LP (2) O87	RY*(7) H51	0.07
	LP (3) O 167	RY*(2) H53	2.3	LP (3) O87	RY*(1) H51	2.29
	LP (3) O 167	RY*(3) H53	0.61	LP (3) O87	RY*(2) H51	0.45
	LP (3) O 167	RY*(4) H53	0.09	LP (3) O87	RY*(3) H51	0.08
	LP (3) O 167	RY*(5) H53	0.46	LP (3) O87	RY*(4) H51	0.14
	LP (3) O 167	BD*(1) N52 - H53	16.92	LP (3) O87	RY*(5) H51	0.59
	BD*(1) S 165 - O 167	BD*(1) N52 - H53	1.36	LP (3) O87	BD*(1) N50 - H51	18.95
	BD (1) N52 - H53	RY*(1) O 167	0.15	BD*(1) O87 - S 169	BD*(1) N50 - H51	0.8
	BD (1) N52 - H53	RY*(2) O 167	0.06			
	BD (1) N52 - H53	BD*(1) S 165 - O 167	0.18			
	Total		33.48	Total		33.85
3	BD (1) S 165 - O 166	RY*(1) H91	0.36	BD (1) N54 - H55	RY*(1) O87	0.16
	BD (1) S 165 - O 166	RY*(3) H91	0.24	BD (1) N54 - H55	RY*(4) O87	0.06
	BD (1) S 165 - O 166	RY*(4) H91	0.06	BD (1) N54 - H55	BD*(1) O87 - S 169	1.3
	BD (1) S 165 - O 166	BD*(1) N90 - H91	0.08	BD (1) O87 - S 169	RY*(1) H55	1.57
	CR (1) O 166	BD*(1) N90 - H91	0.48	BD (1) O87 - S 169	RY*(2) H55	0.22
	LP (1) O 166	RY*(1) H91	0.52	BD (1) O87 - S 169	RY*(3) H55	0.63
	LP (1) O 166	RY*(2) H91	0.21	BD (1) O87 - S 169	BD*(1) N54 - H55	0.06
	LP (1) O 166	RY*(5) H91	0.06	CR (1) O87	BD*(1) N54 - H55	0.48
	LP (1) O 166	BD*(1) N90 - H91	9.85	LP (1) O87	RY*(1) H55	1.93
	LP (2) O 166	BD*(1) N90 - H91	0.46	LP (1) O87	RY*(2) H55	0.14
	LP (3) O 166	RY*(1) H91	2.14	LP (1) O87	RY*(3) H55	0.06
	LP (3) O 166	RY*(3) H91	0.21	LP (1) O87	BD*(1) N54 - H55	15.73
	LP (3) O 166	RY*(5) H91	0.12	LP (2) O87	RY*(1) H55	0.08
	LP (3) O 166	BD*(1) N90 - H91	13.33	LP (2) O87	RY*(4) H55	0.08
	BD*(1) S 165 - O 166	BD*(1) N90 - H91	3.44	LP (2) O87	BD*(1) N54 - H55	0.4
	BD (1) N90 - H91	RY*(1) O 166	0.27	LP (3) O87	RY*(1) H55	0.55
	BD (1) N90 - H91	BD*(1) S 165 - O 166	0.84	LP (3) O87	RY*(6) H55	0.08
				LP (3) O87	BD*(1) N54 - H55	1.08
				BD*(1) O87 - S 169	RY*(3) H55	2.82
				BD*(1) O87 - S 169	BD*(1) N54 - H55	5.06
	Total		32.07	Total		32.49
4	BD (1) C1 - O25	RY*(1) H 147	0.49	BD (1) N66 - H67	BD*(1) C 170 - O 195	0.63
	BD (1) C1 - O25	RY*(2) H 147	0.14	BD*(1) N66 - H67	BD*(1) C 170 - O 195	1.11
	BD (1) C1 - O25	RY*(3) H 147	0.21	BD (1) C 170 - O 195	RY*(5) H67	0.07
	BD (1) C1 - O25	BD*(1) N90 - H 147	0.53	BD (1) C 170 - O 195	BD*(1) N66 - H67	0.59
	BD (2) C1 - O25	RY*(1) H 147	0.1	BD (1) C 170 - O 195	RY*(6) H67	0.08
	BD (2) C1 - O25	RY*(2) H 147	0.16	CR (1) O 195	BD*(1) N66 - H67	0.48

SUPPORTING INFORMATION

	BD (2) C1 - O25	RY*(3) H 147	0.37	LP (1) O 195	RY*(1) H67	0.21
	BD (2) C1 - O25	RY*(4) H 147	0.07	LP (1) O 195	RY*(4) H67	0.12
	BD (2) C1 - O25	BD*(1) N90 - H 147	0.77	LP (1) O 195	BD*(1) N66 - H67	6.81
	CR (1) O25	BD*(1) N90 - H 147	0.3	LP (2) O 195	RY*(2) H67	1.46
	LP (1) O25	RY*(2) H 147	0.96	LP (2) O 195	RY*(4) H67	0.35
	LP (1) O25	RY*(3) H 147	0.08	LP (2) O 195	RY*(7) H67	0.05
	LP (1) O25	BD*(1) N90 - H 147	17.28	LP (2) O 195	RY*(8) H67	0.06
	LP (2) O25	RY*(2) H 147	0.44	LP (2) O 195	BD*(1) N66 - H67	31.56
	LP (2) O25	BD*(1) N90 - H 147	5.58	BD*(2) C 170 - O 195	BD*(1) N66 - H67	0.09
	BD*(2) C1 - O25	BD*(1) N90 - H 147	0.73			
	BD (1) N90 - H 147	RY*(2) O25	0.23			
	BD (1) N90 - H 147	RY*(4) O25	0.1			
	BD (1) N90 - H 147	BD*(1) C1 - O25	1.01			
	BD (1) N90 - H 147	BD*(2) C1 - O25	0.72			
	Total		30.27	Total		43.67

Table S7. Topological analysis of the electron density of A conformer of $\alpha_2\beta_2\text{-P}\cdot\text{10CSA(R)}$ complex.

Guest	Atoms	Electron delocalization index	Electron Dnsity ($\rho(r)$), a.u.	Laplacian of Rho
“Standing”	O ₁₃₈ & H ₁₀₃	3.934	0.06974	0.15993
	O ₁₆₇ & H ₅₃	4.277	0.04978	0.16467
	O ₁₆₆ & H ₉₁	3.915	0.04906	0.15993
	O ₂₅ & H ₁₄₇	4.013	0.05257	0.17475
“Lying”	O ₈₁ & H ₁₃₀	3.888	0.07823	0.14315
	O ₈₇ & H ₅₁	4.225	0.04127	0.15588
	O ₈₇ & H ₅₅	4.062	0.04127	0.15757
	O ₁₉₅ & H ₆₇	3.938	0.04127	0.14724

NMR calculations and analysis

In addition, the ^{13}C and ^{15}N NMR shielding tensors and chemical shifts, as well as $\Delta\sigma_{\max}$ between the corresponding chemical shifts of the main dominant conformer **A** of $\alpha_2\beta_2\text{-P}\cdot\text{10CSA(R)}$ were calculated (Tables S8-S10). The calculated ^{13}C and ^{15}N NMR chemical shifts were found to deviate from the experimentally measured data, while the calculated and experimental $\Delta\sigma_{\max}$ values are in good agreement (Table S8), except the $\Delta\sigma_{\max}$ between carbons 2 and 13, 3 and 12, and nitrogens 22 and 24, which showed strong deviation (Table S8). The disagreement between these three $\Delta\sigma_{\max}$ values can be explained by the presence and influence of solvent molecules situated in a larger cavity. In contrast to the smaller cavity, where only one “lying” guest molecule can be placed, in the larger cavity in addition to the “standing” guest molecule several solvent molecules can be placed as well. However, the continuum solvent model (SND) used represents solvent as a continuous medium and does not count for individual effects of “explicit” molecules, such as H-bonds formation or charge transfer. We suppose that the deviation from the experiment is due to not accounting for the individual solvent molecules’ effects in the larger porphyrin cavity. Between other $\Delta\sigma_{\max}$ calculated using theoretical and experimental data, a good correlation is observed, proving that the main calculated conformation corresponds to the

SUPPORTING INFORMATION

dominant conformation presented in solution, which shows non-equivalency of the carbon and nitrogen atoms. To improve agreement with experimental measurements the conformer **A** of $\alpha_2\beta_2\text{-P}\cdot\text{10CSA(R)}$ with one and two additional acetonitrile molecules was modelled, and its ^{13}C and ^{15}N NMR shielding tensors and chemical shifts, as well as $\Delta\sigma_{\max}$ between the corresponding chemical shifts were calculated. Inclusion of explicit solvent molecules in the model system improved agreement with the experimental data, especially in the case of the $\Delta\sigma_{\max}$ between carbons 2 and 13, 3 and 12, and nitrogens 22 and 24 (Table S8). However, the model system is sensitive to the presence of solvent molecules, especially in the case of peripheral atoms. Thus, to perform accurate NMR calculations, the whole solvent shell should be modelled which is beyond the scope of this study.

Table S8. Calculated shielding tensors and chemical shifts of ^{13}C of conformer **A** of $\alpha_2\beta_2\text{-P}\cdot\text{10CSA(R)}$ with and without solvent molecules.

Number of atom (in xyz)	$\alpha_2\beta_2\text{-P}\cdot\text{10CSA(R)}$		$\alpha_2\beta_2\text{-P}\cdot\text{10CSA(R)} + 1$ acetonitrile		$\alpha_2\beta_2\text{-P}\cdot\text{10CSA(R)} + 2$ acetonitrile	
	Shielding tensor, ppm	Scaled chemical shift, ppm	Shielding tensor, ppm	Scaled chemical shift, ppm	Shielding tensor, ppm	Scaled chemical shift, ppm
1	-60,94	236,3	-62,83	238,1	-62,84	238,1
2	116,32	63,0	115,74	63,5	115,62	63,7
3	134,16	45,5	133,94	45,7	133,87	45,8
4	132,32	47,3	132,12	47,5	132,25	47,4
7	123,17	56,3	122,69	56,7	123,21	56,2
8	151,34	28,7	151,37	28,7	151,04	29,0
12	161,76	18,5	162,02	18,3	160,60	19,7
16	160,08	20,2	159,39	20,9	160,69	19,6
20	120,29	59,1	119,34	60,0	119,56	59,8
22	151,16	28,9	151,74	28,3	151,49	28,6
26	29,40	147,9	26,32	151,0	26,31	151,0
27	25,99	151,3	27,38	149,9	28,09	149,2
28	32,82	144,6	34,39	143,1	34,25	143,2
29	31,22	146,2	29,68	147,7	27,94	149,4
30	32,35	145,1	31,80	145,6	31,94	145,5
31	58,80	119,2	58,84	119,2	59,68	118,3
32	21,06	156,1	24,13	153,1	25,61	151,6
33	19,13	158,0	24,03	153,2	24,98	152,3
34	31,12	146,3	32,41	145,0	33,27	144,2
35	56,16	121,8	57,43	120,5	57,68	120,3
36	32,74	144,7	31,95	145,5	32,89	144,5
37	25,41	151,9	27,73	149,6	28,54	148,8
38	28,52	148,8	32,52	144,9	33,09	144,3
39	34,09	143,4	32,57	144,8	32,93	144,5
40	27,04	150,3	26,72	150,6	25,79	151,5
41	32,40	145,0	30,66	146,7	27,61	149,7
42	65,21	112,9	63,93	114,2	63,58	114,5
43	63,20	114,9	62,58	115,5	63,69	114,4
46	23,15	154,1	22,41	154,8	22,83	154,4
47	156,80	23,4	156,72	23,5	157,14	23,1
56	159,95	20,3	159,97	20,3	160,12	20,1
60	44,40	133,3	43,94	133,7	43,38	134,3

SUPPORTING INFORMATION

61	41,49	136,1	41,21	136,4	41,72	135,9
62	49,57	128,2	50,24	127,6	50,81	127,0
63	39,15	138,4	39,29	138,3	39,90	137,7
64	34,31	143,1	34,90	142,6	33,32	144,1
70	158,23	22,0	158,15	22,1	157,80	22,4
74	160,38	19,9	160,20	20,1	159,79	20,5
78	157,83	22,4	157,57	22,6	157,61	22,6
82	156,63	23,6	156,30	23,9	156,46	23,7
86	42,39	135,2	43,85	133,8	43,94	133,7
88	35,22	142,3	32,81	144,6	32,98	144,4
93	158,68	21,6	158,88	21,4	158,80	21,4
95	156,68	23,5	156,86	23,3	156,81	23,4
99	157,59	22,6	157,99	22,2	158,11	22,1
104	154,57	25,6	156,19	24,0	156,17	24,0
106	163,44	16,9	160,73	19,5	160,98	19,3
110	157,01	23,2	157,18	23,0	157,48	22,7
113	157,94	22,3	157,97	22,2	157,83	22,4
117	42,89	134,8	42,18	135,5	42,12	135,5
118	41,72	135,9	41,60	136,0	41,09	136,5
119	49,74	128,1	50,10	127,7	50,04	127,8
121	36,67	140,8	37,11	140,4	37,42	140,1
123	41,87	135,8	42,22	135,4	42,65	135,0
125	38,12	139,4	39,35	138,2	40,00	137,6
131	162,15	18,2	161,69	18,6	161,30	19,0
135	156,29	23,9	156,36	23,8	156,56	23,6
139	32,97	144,5	31,01	146,4	31,17	146,2
140	42,73	134,9	42,79	134,9	43,29	134,4
141	48,71	129,1	48,55	129,2	48,55	129,2
143	36,11	141,4	36,42	141,1	36,65	140,9
145	40,72	136,9	41,06	136,5	41,14	136,5
148	41,20	136,4	41,82	135,8	41,65	136,0
149	43,16	134,5	43,54	134,1	43,62	134,0
150	35,43	142,0	32,88	144,5	32,89	144,5
151	51,34	126,5	50,74	127,1	51,00	126,8
152	41,03	136,6	40,46	137,1	40,50	137,1
154	37,23	140,3	37,08	140,4	37,42	140,1
160	160,91	19,4	160,84	19,4	160,85	19,4
170	-64,04	239,3	-63,16	238,4	-62,54	237,8
171	114,95	64,3	114,51	64,7	114,34	64,9
172	134,30	45,4	132,65	47,0	133,12	46,5
173	133,26	46,4	134,01	45,7	133,87	45,8
176	121,90	57,5	122,19	57,2	122,56	56,9
177	152,41	27,7	152,34	27,7	152,55	27,5
181	162,30	18,0	161,69	18,6	161,27	19,0
185	159,21	21,0	158,81	21,4	158,71	21,5
189	121,29	58,1	120,40	59,0	120,18	59,2
192	146,85	33,1	146,10	33,8	146,05	33,9
196	36,05	141,4	36,61	140,9	36,86	140,7
202			59,37	118,6	60,19	117,8
203			180,29	0,4	179,90	0,8
208					54,36	123,5
209					180,40	0,3

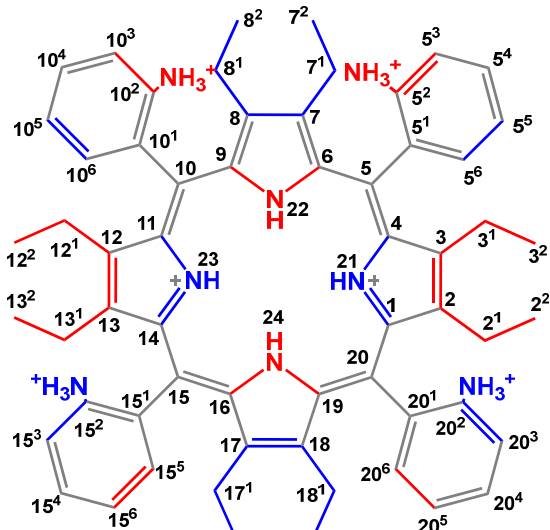
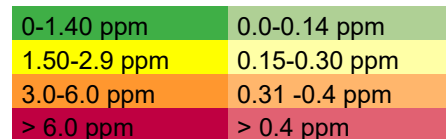
SUPPORTING INFORMATION

Table S9. Calculated shielding tensors of ^{15}N of conformer A of $\alpha_2\beta_2\text{-P}\cdot10\text{CSA(R)}$ with and without solvent molecules.

Number of atom (in xyz)	$\alpha_2\beta_2\text{-P}\cdot10\text{CSA(R)}$		$\alpha_2\beta_2\text{-P}\cdot10\text{CSA(R)} +$ 1 acetonitrile		$\alpha_2\beta_2\text{-P}\cdot10\text{CSA(R)} +$ 2 acetonitrile	
	Shielding tensor, ppm	Scaled chemical shift, ppm	Shielding tensor, ppm	Scaled chemical shift, ppm	Shielding tensor, ppm	Scaled chemical shift, ppm
44	99,30	154,4	87,41	166,3	86,84	166,9
50	99,33	154,4	90,15	163,5	91,46	162,2
52	91,95	161,7	99,64	154,1	100,58	153,1
54	106,38	147,3	101,99	151,7	101,91	151,8
66	180,72	73	180,58	73,1	180,73	73
90	185,44	68,3	184,27	69,4	184,17	69,5
100	173,69	80	173,26	80,4	173,23	80,5
127	178,41	75,3	177,34	76,4	176,61	77,1
			6,94	246,8	2,86	250,8
					-20,51	274,2

Table S10. Calculated and experimentally measured $\Delta\sigma_{\max}$ (ppm) between chemical shifts in ^{13}C of of $\alpha_2\beta_2\text{-P}\cdot10\text{CSA(R)}$ with and without solvent molecules. Right side bottom, illustration of the $\alpha_2\beta_2\text{-P}$ (blue — above and red — below the plane) with corresponding positions.

Positions	Calculated			Exp.
	Conf. A	Conf. A + 1 CH ₃ CN	Conf. A + 2 CH ₃ CN	
1 and 14	1,7	0,0	0,0	0,98
2 and 13	11,5	0,0	0,0	0,59
2 ¹ and 13 ¹	1,2	0,0	0,0	0,26
2 ² and 13 ²	2,4	0,0	0,0	0,22
3 and 12	6,7	0,0	0,0	0,22
3 ¹ and 12 ¹	3,2	0,0	0,0	0,12
3 ² and 12 ²	6,7	0,0	0,0	0,12
4 and 11	1,2	0,0	0,0	0,40
6 and 9	1,3	0,0	0,0	0,35
7 and 8	3,0	0,0	0,0	0,88
7 ¹ and 8 ¹	1,1	0,0	0,0	0,19
7 ² and 8 ²	4,1	0,0	0,0	0,02
10 and 5	2,6	0,0	0,0	0,47
10 ¹ and 5 ¹	1,2	0,0	0,0	0,06
10 ² and 5 ²	0,4	0,0	0,0	0,09
10 ³ and 5 ³	2,6	0,0	0,0	0,14
10 ⁴ and 5 ⁴	1,1	0,0	0,0	0,00
10 ⁵ and 5 ⁵	0,3	0,0	0,0	0,00
10 ⁶ and 5 ⁶	0,2	0,0	0,0	0,04
15 and 20	2,0	0,0	0,0	0,19
15 ¹ and 20 ¹	1,5	0,0	0,0	0,00
15 ² and 20 ²	0,2	0,0	0,0	0,30
15 ³ and 20 ³	0,2	0,0	0,0	0,00
15 ⁴ and 20 ⁴	0,6	0,0	0,0	0,00
15 ⁵ and 20 ⁵	2,7	0,0	0,0	0,00
15 ⁶ and 20 ⁶	3,7	0,0	0,0	1,30
16 and 19	2,9	0,0	0,0	0,52
17 and 18	3,8	0,0	0,0	0,20



SUPPORTING INFORMATION

17 ¹ and 18 ¹	0,5	0,0	0,0	0,12
17 ² and 18 ²	2,2	0,0	0,0	1,18
21 and 23	7,0	-12,2	-13,7	1,67
22 and 24	7,4	-11,8	-10,4	0,00

NBO partial charges calculations and analysis

In order to clarify the source of $\Delta\sigma$ in ¹³C and ¹⁵N NMR, the NBO partial charges were calculated for the following complexes: two porphyrin cations 4+ (differing by the position of protons), porphyrin cation 6+, optimized $[\alpha_2\beta_2\text{-P}(\text{H}_2\text{SO}_4)_2]^{4+}$ and $[\alpha_2\beta_2\text{-P}(\text{H}_2\text{SO}_4 \cdot \text{H}_2\text{O})_2]^{4+}$ complexes (corresponding to the crystal structure and achiral environment), and conformer A of $\alpha_2\beta_2\text{-P}\cdot\text{10CSA(R)}$ without inclusion of solvent molecules and with addition of one and two acetonitrile molecules (Figure S15 and Table S9). The presence or absence of protons change the N(21) – N(24) NBO partial charges in the porphyrin cations 4+ by 0.019–0.043, wherein in the porphyrin cation 6+ where all N(21) – N(24) are protonated the partial charges are very similar and differ only by 0.001. In the achiral $[\alpha_2\beta_2\text{-P}(\text{H}_2\text{SO}_4)_2]^{4+}$ complex one of oxygen atoms of each H_2SO_4 is situated symmetrically in respect to the core protons that result in the similar partial charges of N(21) – N(24). However, addition of two water molecules leads to the difference by 0.008–0.015 in the N(21) – N(24) NBO partial charges. This increased difference in partial charges can be explained by the non-symmetric position of oxygens of H_2SO_4 with respect to the porphyrin's core protons and as a result of the H-bonds' formation of different strength. That is in good agreement with the observation that protonation or deprotonation has a stronger influence on the N(21) – N(24) NBO partial charges, than the H-bonds formation. In the more asymmetric $\alpha_2\beta_2\text{-P}\cdot\text{10CSA(R)}$ complex, the NBO partial charges split up to 0.056 for N(21) – N(24) following the above noticed trend. Addition of acetonitrile molecules results in decrease of the difference between the NBO partial charges of N(21)–N(24), herein the difference between the NBO partial charges of N(22) and N(24) is much more sensitive to the presence of solvent molecules in the cavity. This agrees well with our NMR calculations.

The *ortho*-carbons in the porphyrin cations 4+ and 6+ have similar partial charges (differing up to 0.006) (Figure S15 and Table S9). However, in the $[\alpha_2\beta_2\text{-P}(\text{H}_2\text{SO}_4)_2]^{4+}$ complex, due to the small size of the guest molecule only one H-bond (instead of two) can be formed between the NH_3^+ groups of porphyrin and oxygens of each H_2SO_4 guest molecule. This leads to differences between the NBO partial charges of *ortho*-carbons of up to 0.021 for phenyls with the H-bonded and non-bonded NH_3^+ groups. Addition of two water molecules allows the H-bond formation with all four NH_3^+ groups of porphyrin, although these bonds are not equal; this is proved by difference in the NBO partial charges of *ortho*-carbons of up to 0.12 between phenyls with the H-bonded NH_3^+ groups. In $\alpha_2\beta_2\text{-P}\cdot\text{10CSA(R)}$, the larger size of camphorsulfonic acid allows the H-bond formation with all four NH_3^+ groups of porphyrin; however non-equality of the formed bonds results in differences between the NBO partial charges of *ortho*-carbons of up to 0.13. Wherein, the tilt of phenyl rings varied less than 5.0° in the porphyrin cation 6+,

SUPPORTING INFORMATION

$[\alpha_2\beta_2\text{-P}(\text{H}_2\text{SO}_4)_2]^{4+}$, $[\alpha_2\beta_2\text{-P}(\text{H}_2\text{SO}_4 \cdot \text{H}_2\text{O})_2]^{4+}$ and $\alpha_2\beta_2\text{-P}\cdot\text{10CSA(R)}$ complexes, which allowed us to exclude this factor from consideration. Inclusion of acetonitrile molecules into the model also had a minor effect on *ortho*-carbons.

Summarizing, based on the six model complexes and their NBO partial charges it was shown that $\Delta\sigma$ values rely on the interactions with the chiral guests of certain size and chirality transfer effect.

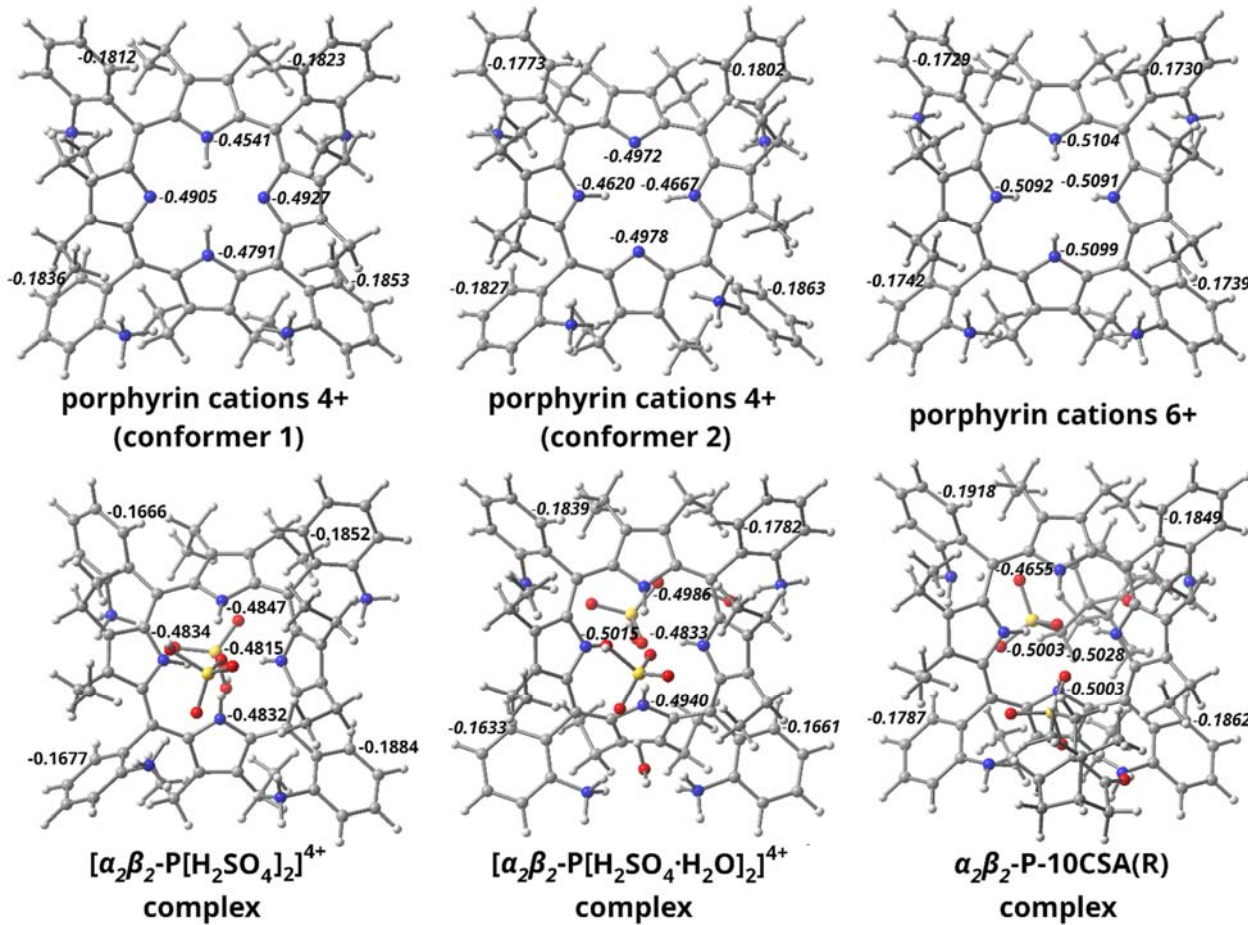


Figure S15. NBO partial charges in variety of calculated complexes.

Table S9: Partial charges for core N atoms and *ortho*-carbons in different porphyrin complexes.

Atom positions	$[\alpha_2\beta_2\text{-P}]^{4+}$ conf. 1	$[\alpha_2\beta_2\text{-P}]^{4+}$ conf. 2	$[\alpha_2\beta_2\text{-P}]^{6+}$	$\alpha_2\beta_2\text{-P}(\text{H}_2\text{SO}_4)_2]^{4+}$	$\alpha_2\beta_2\text{-P}(\text{H}_2\text{SO}_4 \cdot \text{H}_2\text{O})_2]^{4+}$	$\alpha_2\beta_2\text{-P}\cdot\text{10CSA(R)}$	$\alpha_2\beta_2\text{-P}\cdot\text{10CSA(R)} + 1 \text{CH}_3\text{CN}$	$\alpha_2\beta_2\text{-P}\cdot\text{10CSA(R)} + 2 \text{CH}_3\text{CN}$
N(22)	-0.47909	-0.49783	-0.50992	-0.4832	-0.49395	-0.50025	-0.49708	-0.49635
N(23)	-0.49272	-0.46670	-0.50905	-0.4815	-0.48329	-0.50283	-0.49102	-0.49120
N(24)	-0.45405	-0.49720	-0.51043	-0.4847	-0.49861	-0.46549	-0.49102	-0.50509
N(21)	-0.49051	-0.46203	-0.50923	-0.4934	-0.50147	-0.52167	-0.50010	-0.49921
C(5 ⁶)	-0.18363	-0.18273	-0.17424	-0.1677	-0.16333	-0.17866	-0.17550	-0.17476
C(10 ⁶)	-0.18532	-0.18629	-0.17385	-0.1884	-0.16609	-0.18624	-0.18431	-0.18450
C(15 ⁶)	-0.18225	-0.18021	-0.17303	-0.1852	-0.17821	-0.18491	-0.18454	-0.18664
C(20 ⁶)	-0.18124	-0.17726	-0.17285	-0.1666	-0.18393	-0.19176	-0.19280	-0.19389

SUPPORTING INFORMATION

O	0.01306842	0.06551625	-1.44272740	C	-2.05506677	4.19637747	0.96984684	H	5.51588630	-5.33302999	-2.38732088
C	3.87029451	-4.21289823	-1.52302585	C	-3.15165491	4.33213760	0.09254471	H	0.78370588	-6.60371490	0.67614530
H	4.23220227	-3.24236672	-1.89138948	C	-3.96533596	5.46997261	0.08585461	C	-3.92141348	-2.40029210	0.72238596
N	0.91005982	-5.62821941	0.35372848	H	-4.80858862	5.55898784	-0.61675982	C	-4.05950649	-3.76859417	1.06219164
H	0.71593376	-4.98765254	1.19561051	C	-3.68969554	6.50746001	0.99152783	C	-5.11745078	-1.69049683	0.45651911
H	0.13347921	-5.39834876	-0.30676630	H	-4.32681797	7.40372105	0.99807872	C	-5.30964762	-4.38668636	1.17153680
C	0.16012661	-4.24145854	-2.82967942	C	-2.60166972	6.40094380	1.87450786	C	-6.37538395	-2.29737879	0.54739328
H	-0.69791020	-4.74352231	-3.31886385	H	-2.38250488	7.21694471	2.57861040	H	-5.03939255	-0.63290127	0.16874273
C	0.79186430	-3.22139773	-3.97953829	C	-1.78545244	5.26140725	1.85427361	C	-6.47645792	-3.64634994	0.92125459
H	0.08118581	-2.40809337	-4.04372197	H	-0.92359791	5.18497235	2.53219584	H	-5.38597362	-5.45031765	1.44824840
H	1.09459774	-3.71863790	-4.73970998	N	-3.44483285	3.23576975	-0.85807406	H	-7.28211425	-1.71590762	0.32630052
H	1.69155655	-2.74736485	-3.35417349	H	-4.02697547	3.57684870	-1.64404613	H	-7.45838513	-4.13342288	1.00835174
C	-2.85076219	-3.42932386	-2.09397483	H	-3.97453449	2.47060311	-0.39817463	H	-3.71621769	-3.80529000	-1.50978579
N	-2.86902551	-4.62893652	1.23493381	H	-2.57545993	2.77420927	-1.29192359	H	-2.62989587	-4.21192541	-2.84645677
H	-2.05582150	-4.29334638	1.85488747	C	0.13905823	5.40164623	-0.84495569	C	-3.25820773	-2.12467052	-2.80566838
H	-2.41741820	-4.77512307	0.30557635	C	-0.47573568	5.15730819	-2.23471949	H	-2.42395323	-1.72059297	-3.41208243
H	-3.16108588	-5.55473217	1.59548989	H	-0.93505594	6.08824939	-2.62100438	H	-4.12466002	-2.29999557	-3.47272420
C	-4.18625345	-0.45527132	3.27537486	H	-1.25038343	4.36713659	-2.20995692	H	-3.54211251	-1.34066235	-2.07442093
H	-5.10468467	0.14880276	3.43113285	H	0.28660332	4.81920526	-2.96285607	H	-4.53031723	-1.43439939	2.89935893
C	-3.46452332	-0.66937459	4.62090180	H	0.92122907	6.18192028	-0.93068525	S	0.55433729	-0.87053973	3.37431097
H	-3.20092512	0.29230937	5.10178769	H	-0.622218878	5.82772153	-0.17030106	O	1.71926909	-1.20852454	4.20740659
H	-2.53206297	-1.24920463	4.47842858	O	-0.21189523	0.42679742	4.04374851	O	-0.50723048	-1.95145771	3.26532936
H	-4.12380759	-1.22141156	5.31955861	H	-0.07929483	0.37341989	5.01782999	O	0.85768858	-0.34994342	1.97985224
C	-3.46259669	2.60913448	3.24346262	C	-1.86506090	1.75180592	1.31974454	O	-0.39088717	-4.31962910	2.40123476
H	-4.37535171	2.21237534	3.73081052	C	2.20453064	-5.50384851	-0.34997415	H	-0.29516664	-4.81708706	3.24215141
H	-3.78858165	3.51848531	2.69959178	C	2.91398491	-6.68023609	-0.60735668	H	-0.31183851	-3.32973591	2.72463185
C	-2.43640218	3.00368740	4.32073919	H	2.53953896	-7.65239659	-0.24905315	H	0.90021050	-5.04205168	-2.61951618
H	-1.48118598	3.34426350	3.87610698	C	4.11564912	-6.62039493	-1.33361272	S	-0.27906186	1.13535521	-2.46787809
H	-2.19970337	2.14679959	4.98002921	H	4.67302262	-7.54610719	-1.53711672				
H	-2.83450052	3.82116369	4.95322973	C	4.58636341	-5.38376402	-1.80195630				

SUPPORTING INFORMATION

Experimental NMR Data

$\alpha_2\beta_2\text{-P}\cdot\text{10CSA(S)}$

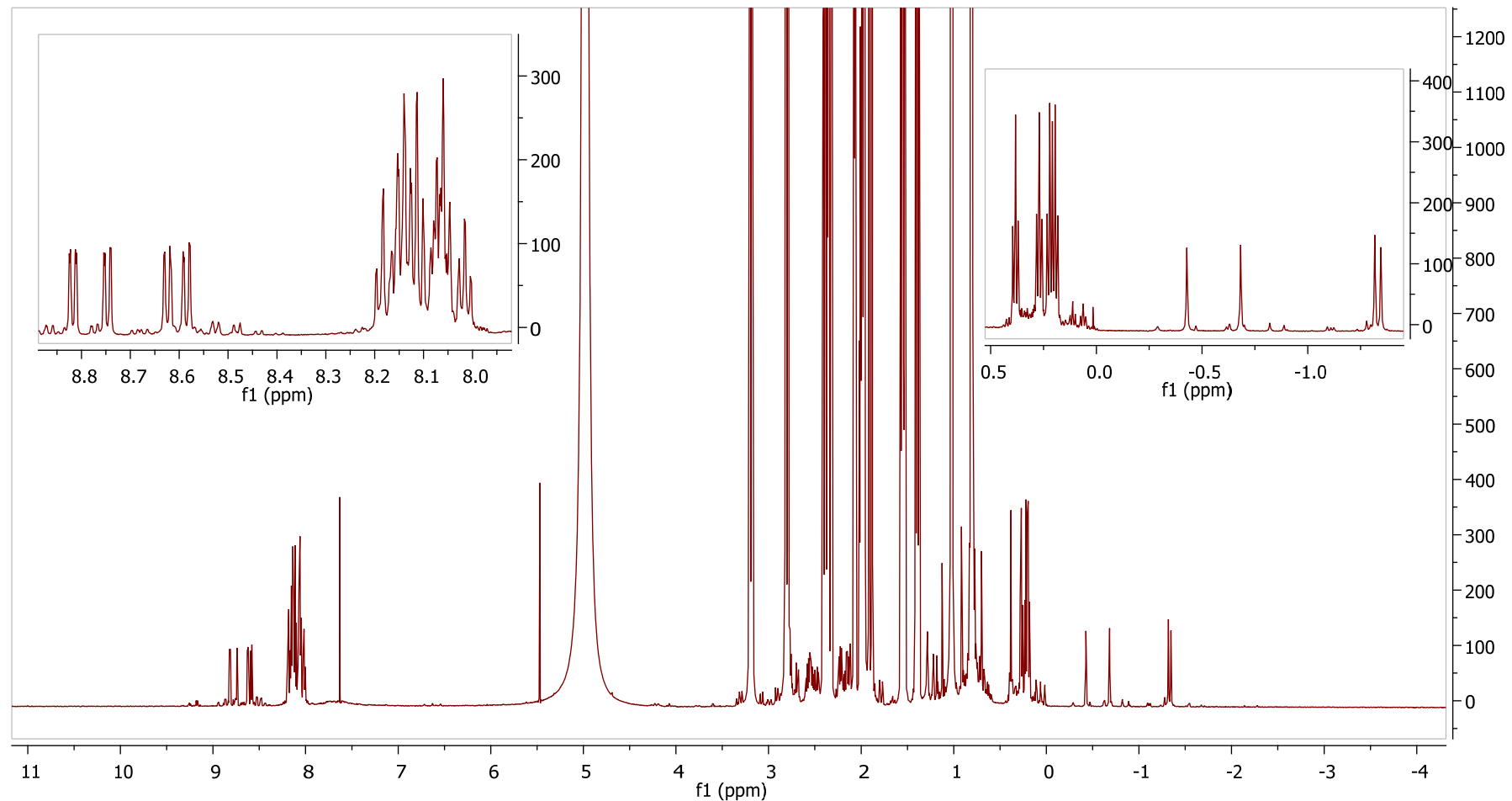


Figure S16. ¹H NMR spectrum of $\alpha_2\beta_2\text{-P}\cdot\text{10CSA(S)}$ with the expansion of areas of interest (600 MHz, acetonitrile-*d*₃, 20 eq. of 10CSA(S), 25 °C).

SUPPORTING INFORMATION

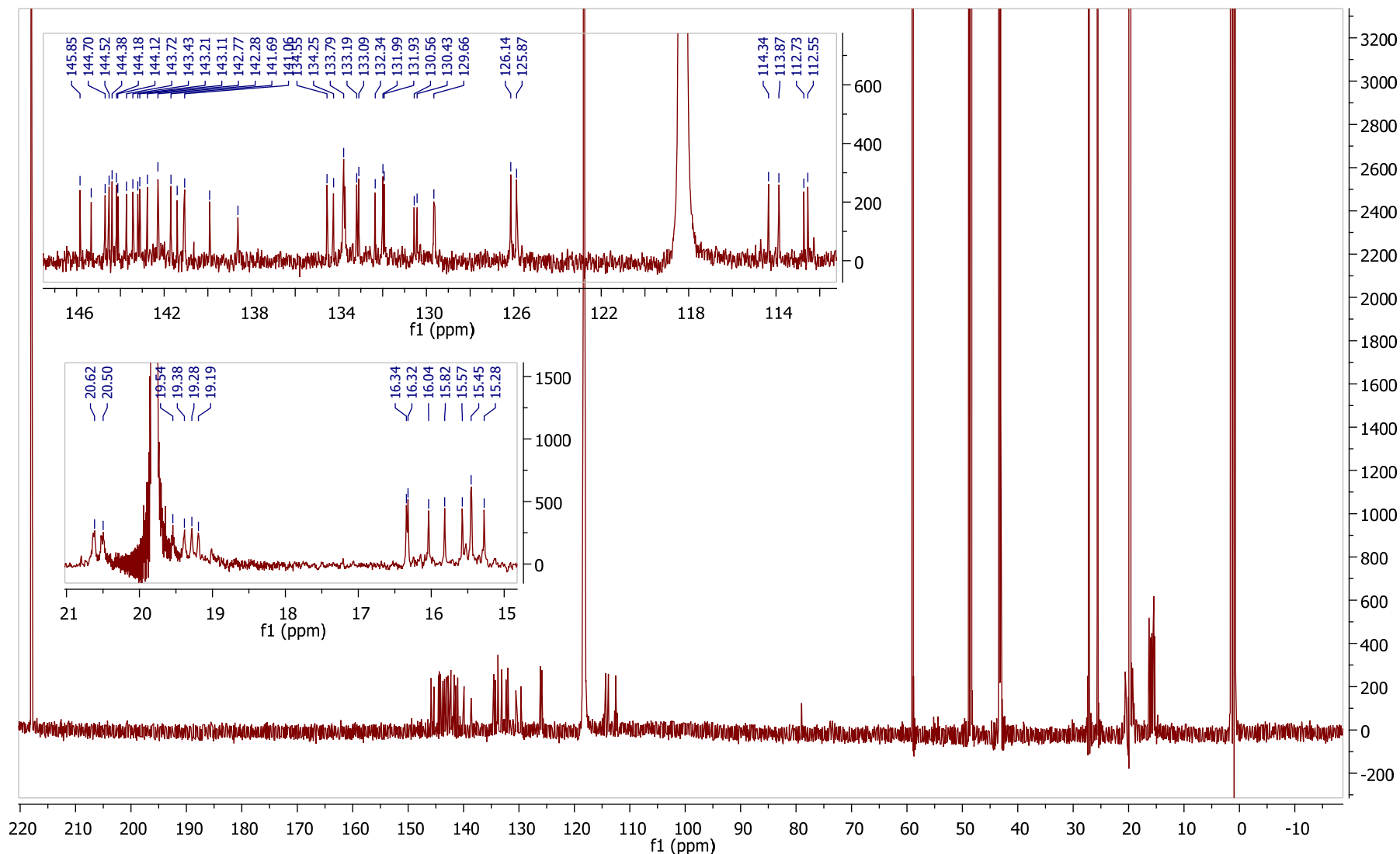


Figure S17. ^{13}C NMR spectrum of $\alpha_2\beta_2\text{-P}\cdot\text{10CSA(S)}$ with expansion of areas of interest (151 MHz, acetonitrile- d_3 , 20 eq. of 10CSA(S), 25 °C).

SUPPORTING INFORMATION

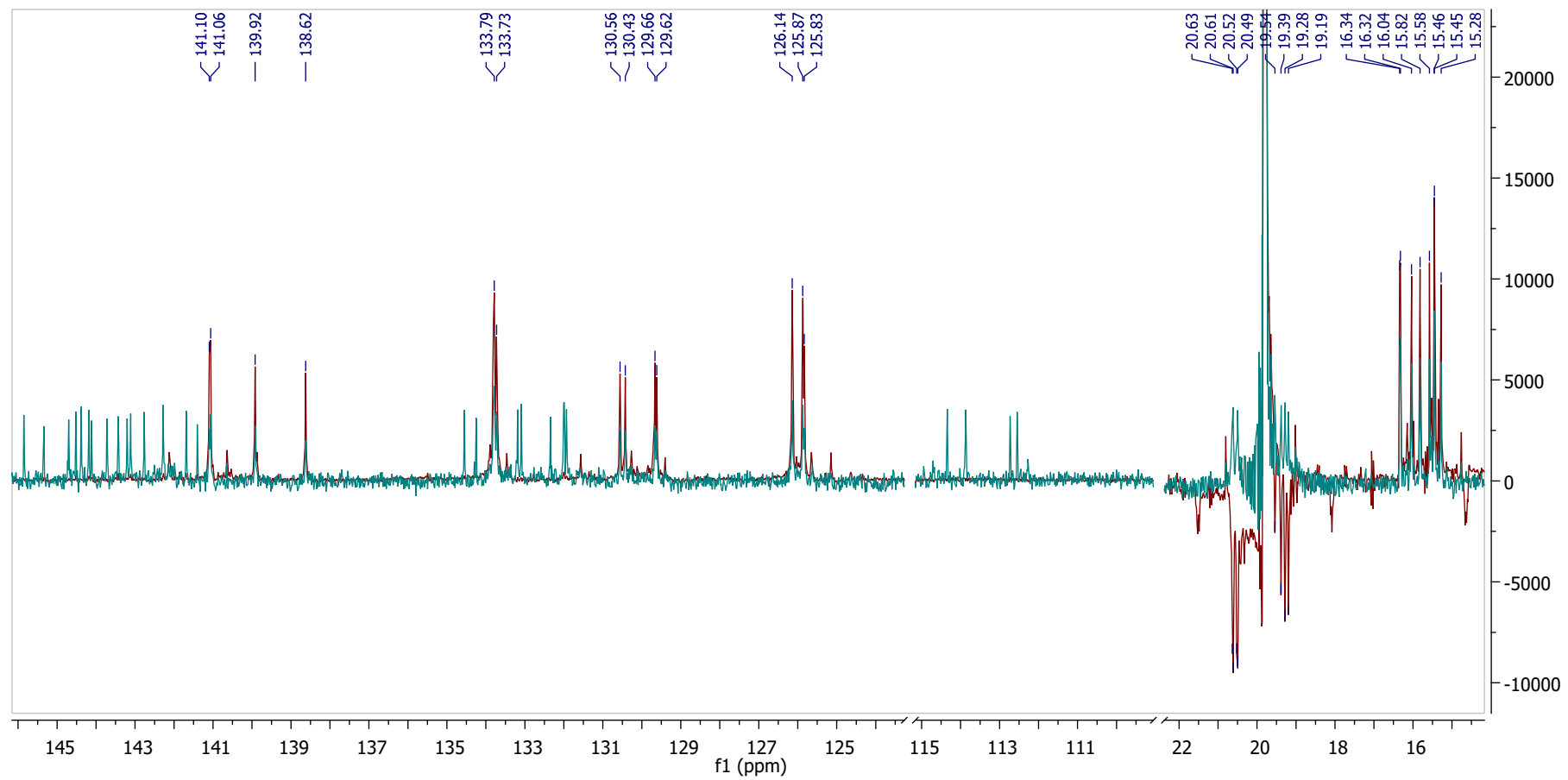


Figure S18. ¹³C NMR (magenta) and DEPT-135 (red) overlay spectra of $\alpha_2,\beta_2\text{-P}\cdot\text{10CSA(S)}$ (151 MHz, acetonitrile-*d*₃, 20 eq. of 10CSA(S), 25 °C).

SUPPORTING INFORMATION

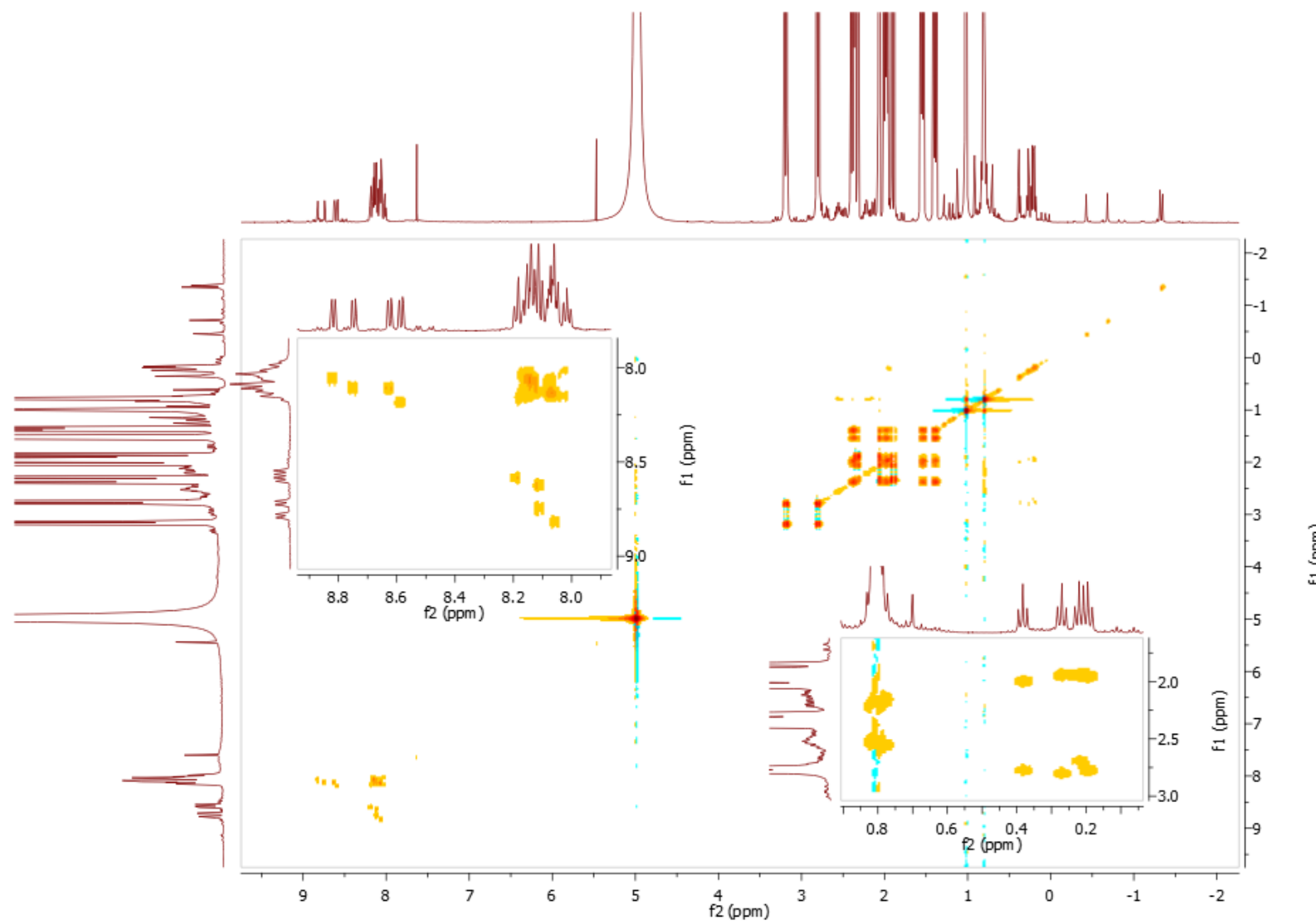


Figure S19. ^1H - ^1H TOCSY spectrum of $\alpha_2,\beta_2\text{-P}\cdot 10\text{CSA(S)}$ with expansion of areas of interest (acetonitrile- d_3 , 20 eq. of 10CSA(S), 25 °C).

SUPPORTING INFORMATION

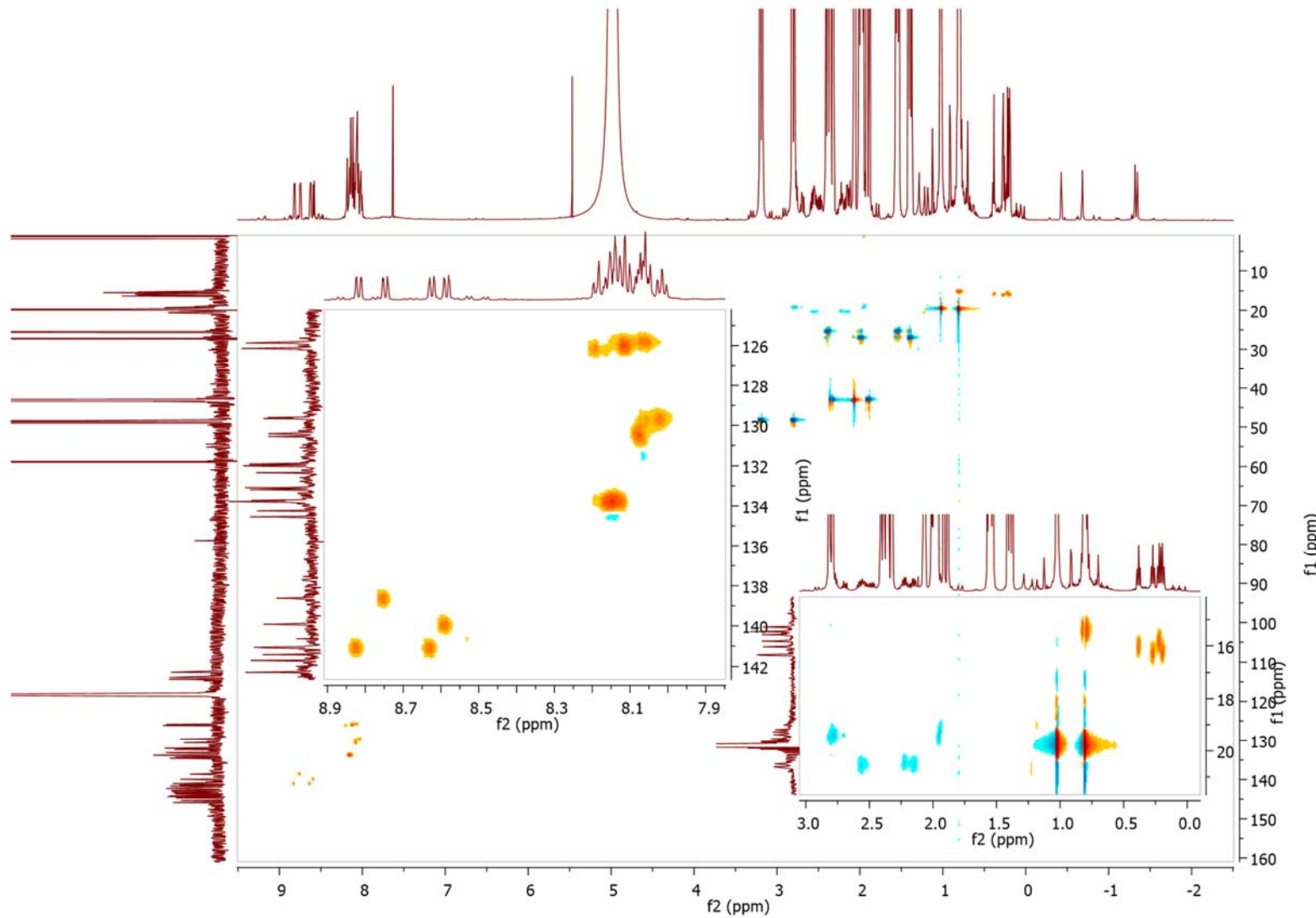
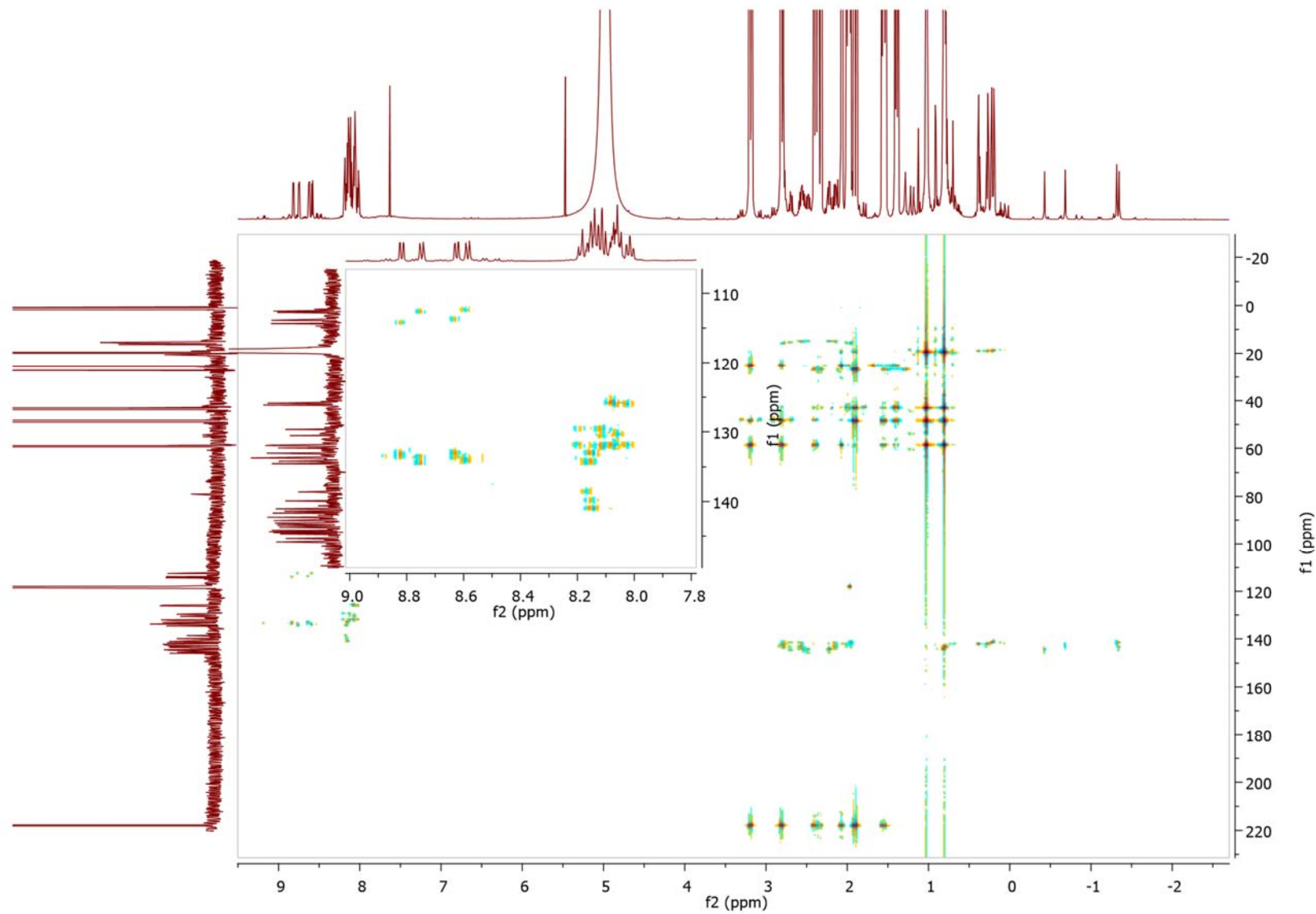


Figure S20. ^1H - ^{13}C HSQC spectrum of $\alpha_2,\beta_2\text{-P}\cdot 10\text{CSA(S)}$ with expansion of areas of interest (acetonitrile- d_3 , 20 eq. of 10CSA(S), 25 °C).

SUPPORTING INFORMATION



SUPPORTING INFORMATION

Figure S21. ^1H - ^{13}C HMBC spectrum of $\alpha_2\beta_2\text{-P}\cdot\text{10CSA(S)}$ with expansion of areas of interest (acetonitrile- d_3 , 20 eq. of 10CSA(S), 25 °C).

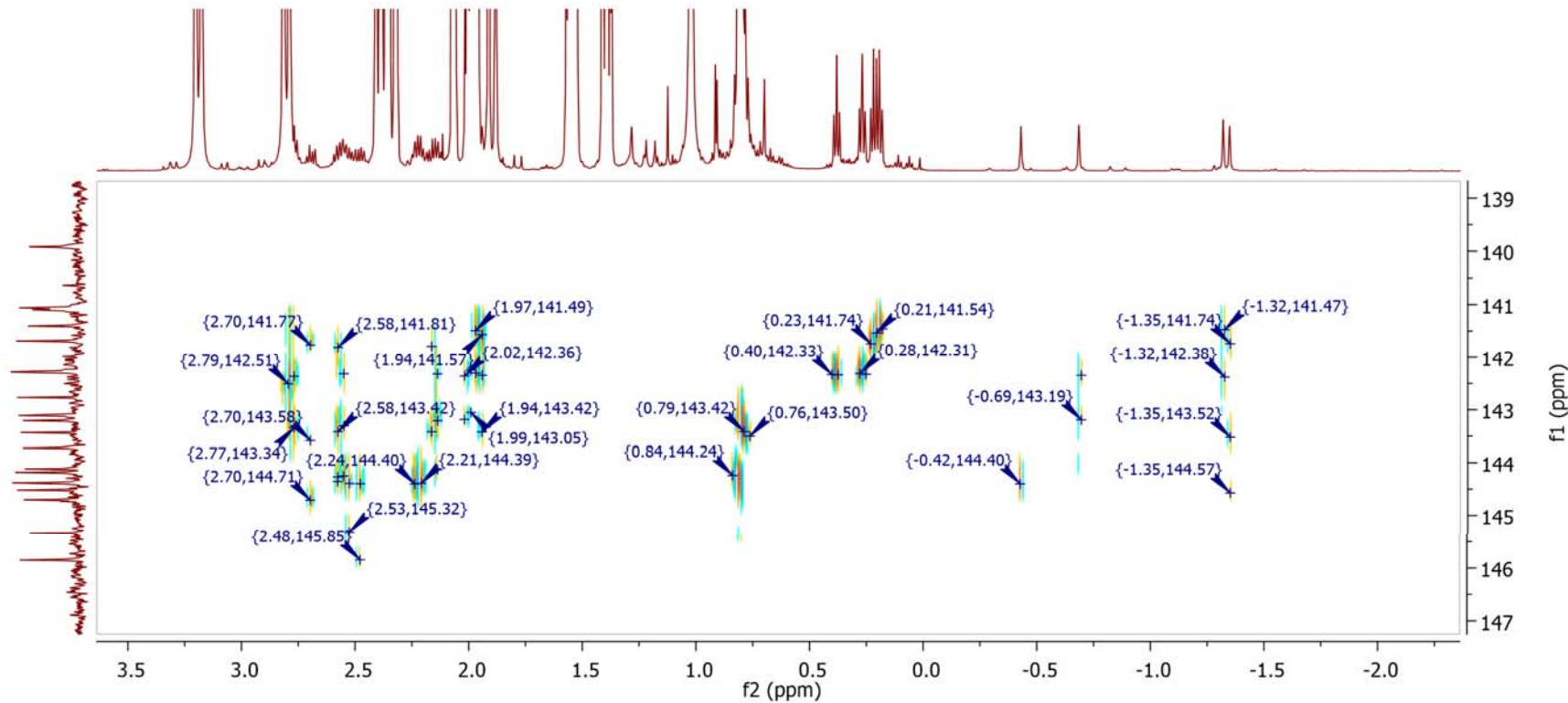


Figure S22. ^1H - ^{13}C HMBC spectrum, expansion of area of interest of $\alpha_2\beta_2\text{-P}\cdot\text{10CSA(S)}$ (acetonitrile- d_3 , 20 eq. of 10CSA(S), 25 °C).

SUPPORTING INFORMATION

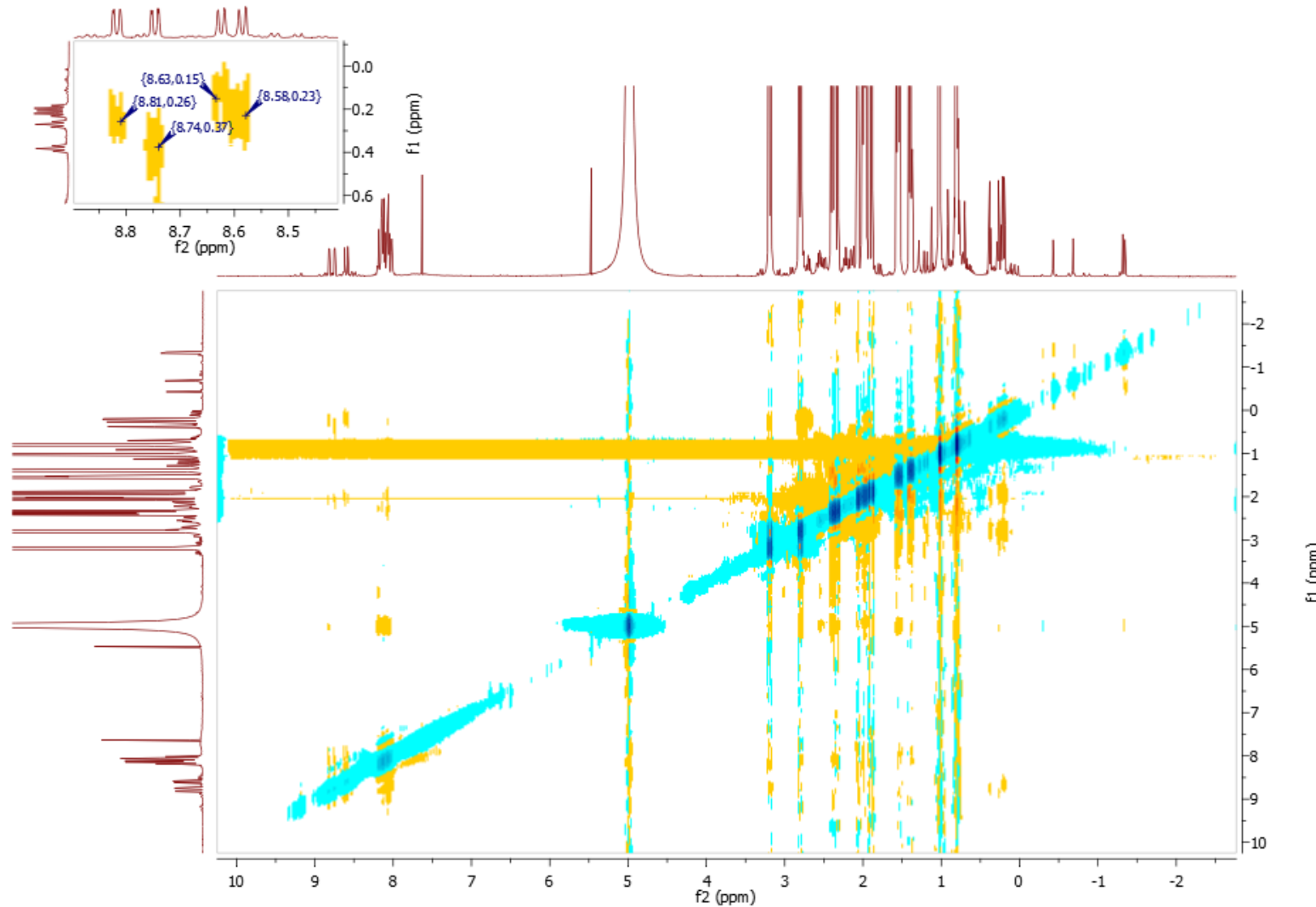


Figure S23. ¹H-¹H ROESY spectrum of $\alpha_2,\beta_2\text{-P}\cdot\text{10CSA(S)}$ with expansion of areas of interest (acetonitrile-*d*₃, 20 eq. of 10CSA(S), 25 °C).

SUPPORTING INFORMATION

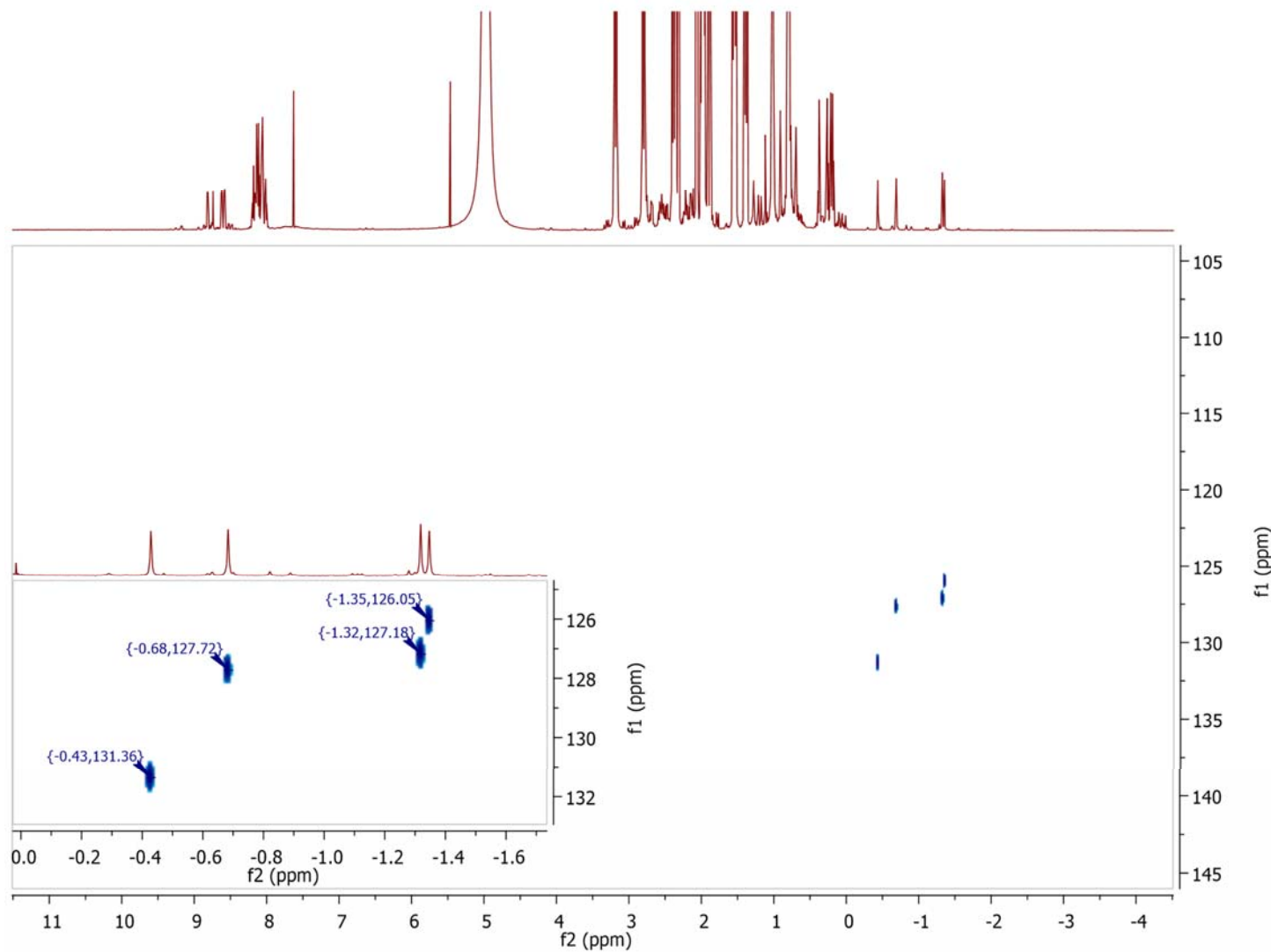
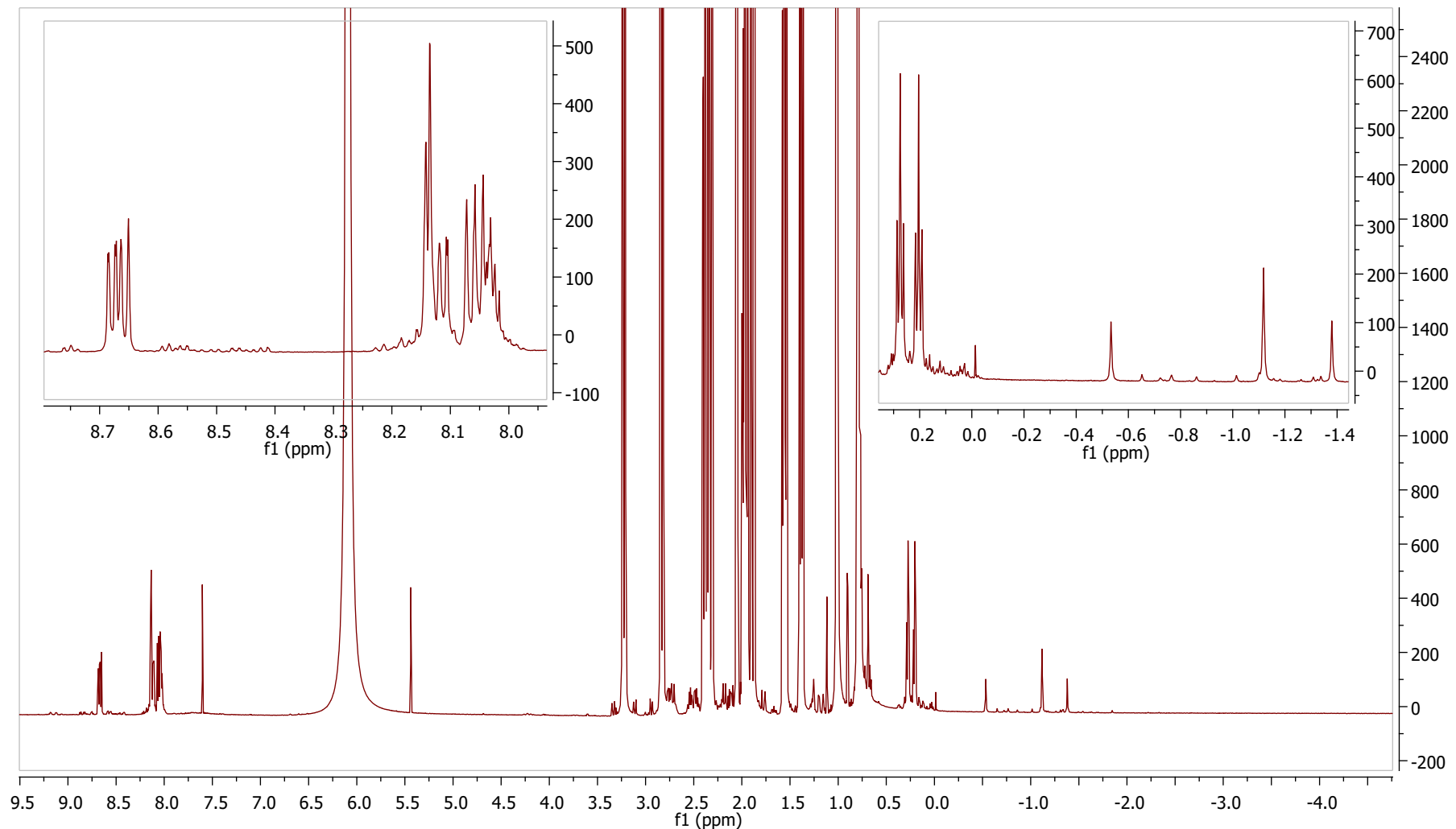


Figure S24. ^1H - ^{15}N HSQC spectrum of $\alpha_2,\beta_2\text{-P}\cdot\text{10CSA(S)}$ with expansion of areas of interest (acetonitrile- d_3 , 20 eq. of 10CSA(S), 25 °C).

SUPPORTING INFORMATION

$\alpha_2\beta_2$ -P-10CSA(SR)



SUPPORTING INFORMATION

Figure S25. ^1H NMR spectrum of $\alpha_2\beta_2\text{-P}\cdot\text{10CSA(SR)}$ with expansion of areas of interest (600 MHz, acetonitrile- d_3 , 20 eq. of 10CSA(S) and 10CSA(R), 25 °C).

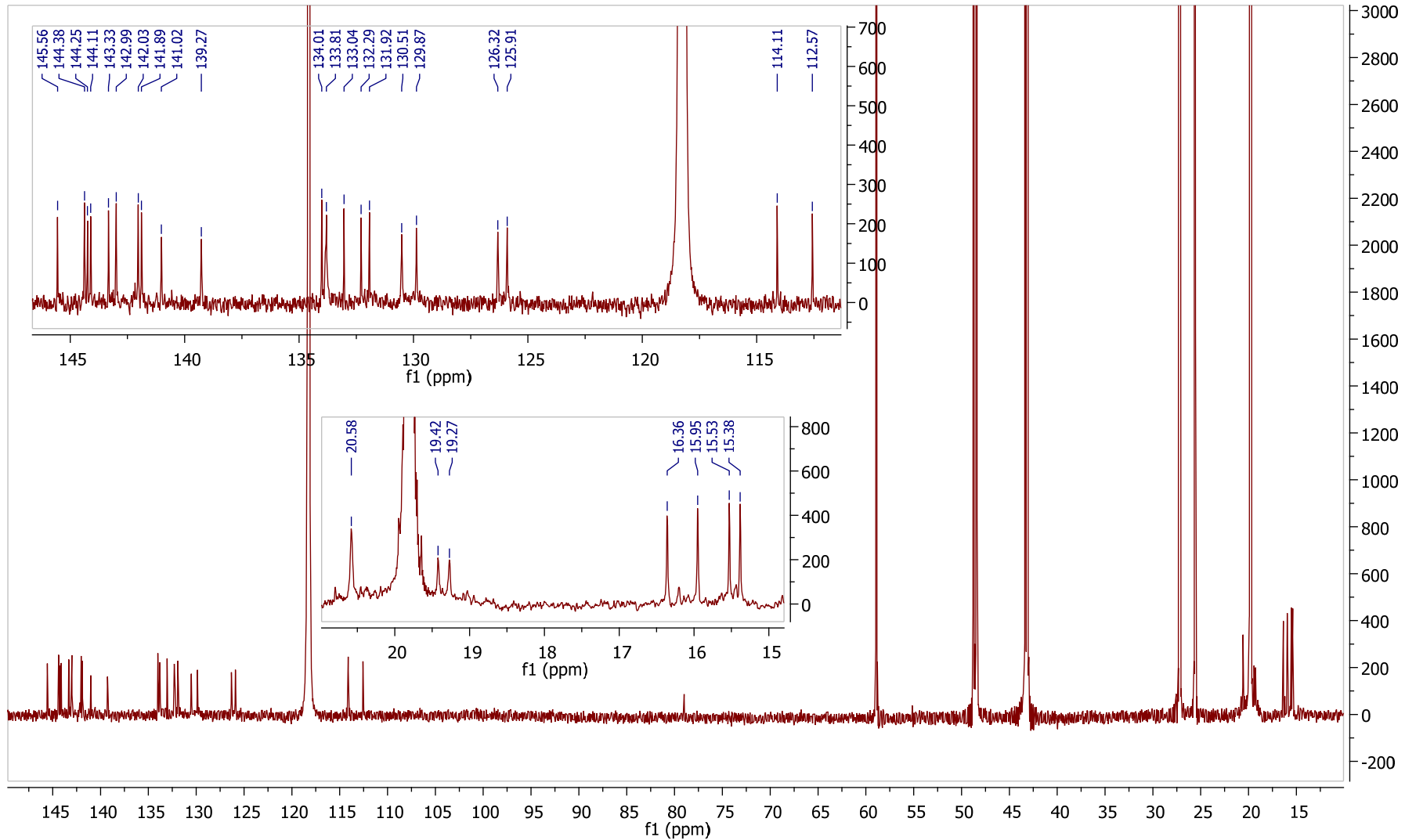
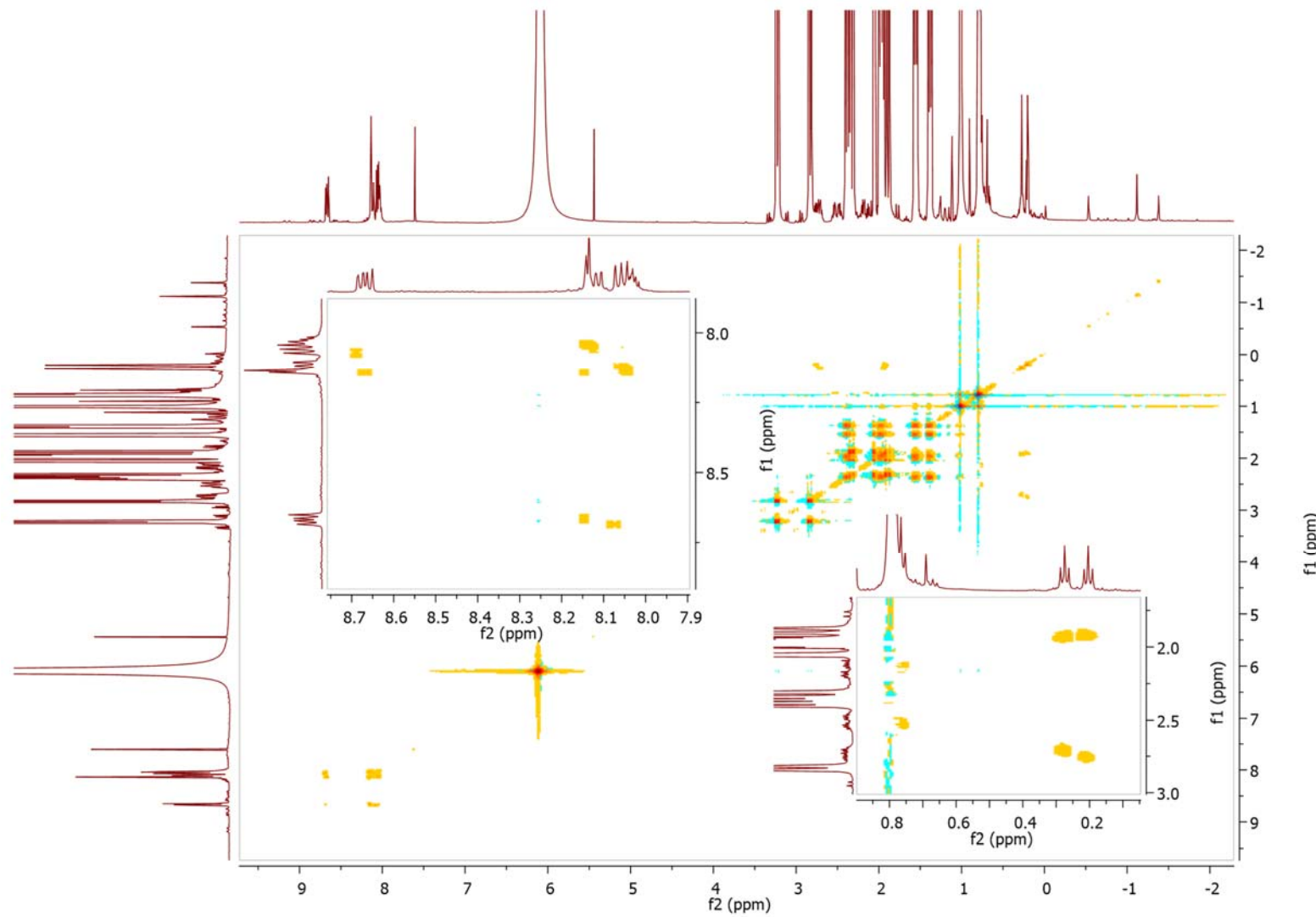


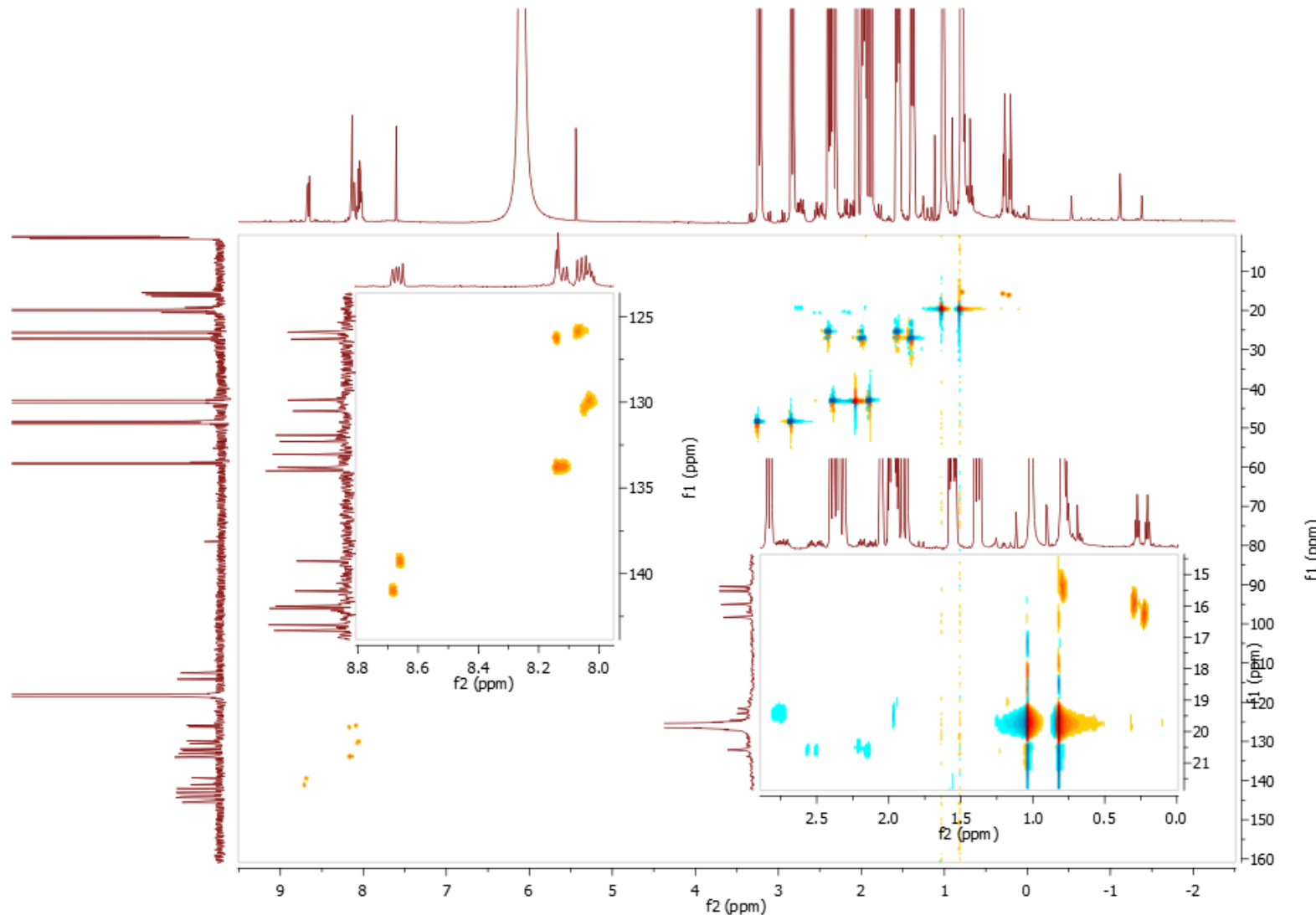
Figure S26. ^{13}C NMR spectrum of $\alpha_2\beta_2\text{-P}\cdot\text{10CSA(SR)}$ with expansion of areas of interest (151 MHz, acetonitrile- d_3 , 20 eq. of 10CSA(S) and 10CSA(R), 25 °C).

SUPPORTING INFORMATION



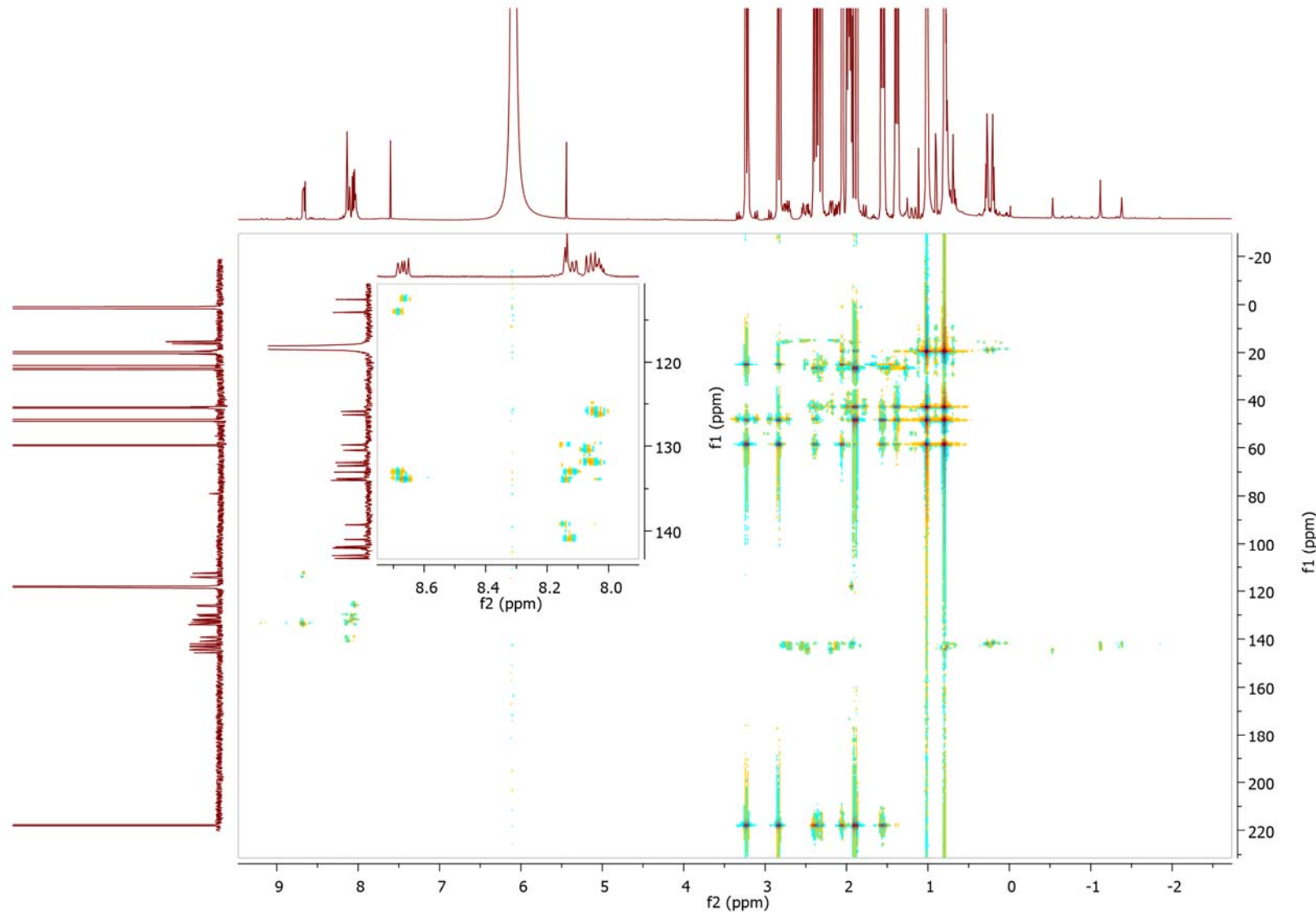
SUPPORTING INFORMATION

Figure S27. ^1H - ^1H TOCSY spectrum of $\alpha_2\beta_2\text{-P}\cdot\text{10CSA(SR)}$ with expansion of areas of interest (acetonitrile- d_3 , 20 eq. of 10CSA(S) and 10CSA(R), 25 °C).



SUPPORTING INFORMATION

Figure S28. ^1H - ^{13}C HSQC spectrum of $\alpha_2,\beta_2\text{-P}\cdot\text{10CSA(SR)}$ with expansion of areas of interest (acetonitrile- d_3 , 20 eq. of 10CSA(S) and 10CSA(R), 25 °C).



SUPPORTING INFORMATION

Figure S29. ^1H - ^{13}C HMBC spectrum of $\alpha_2\beta_2\text{-P}\cdot\text{10CSA(SR)}$ with expansion of areas of interest (acetonitrile- d_3 , 20 eq. of 10CSA(S) and 10CSA(R), 25 °C).

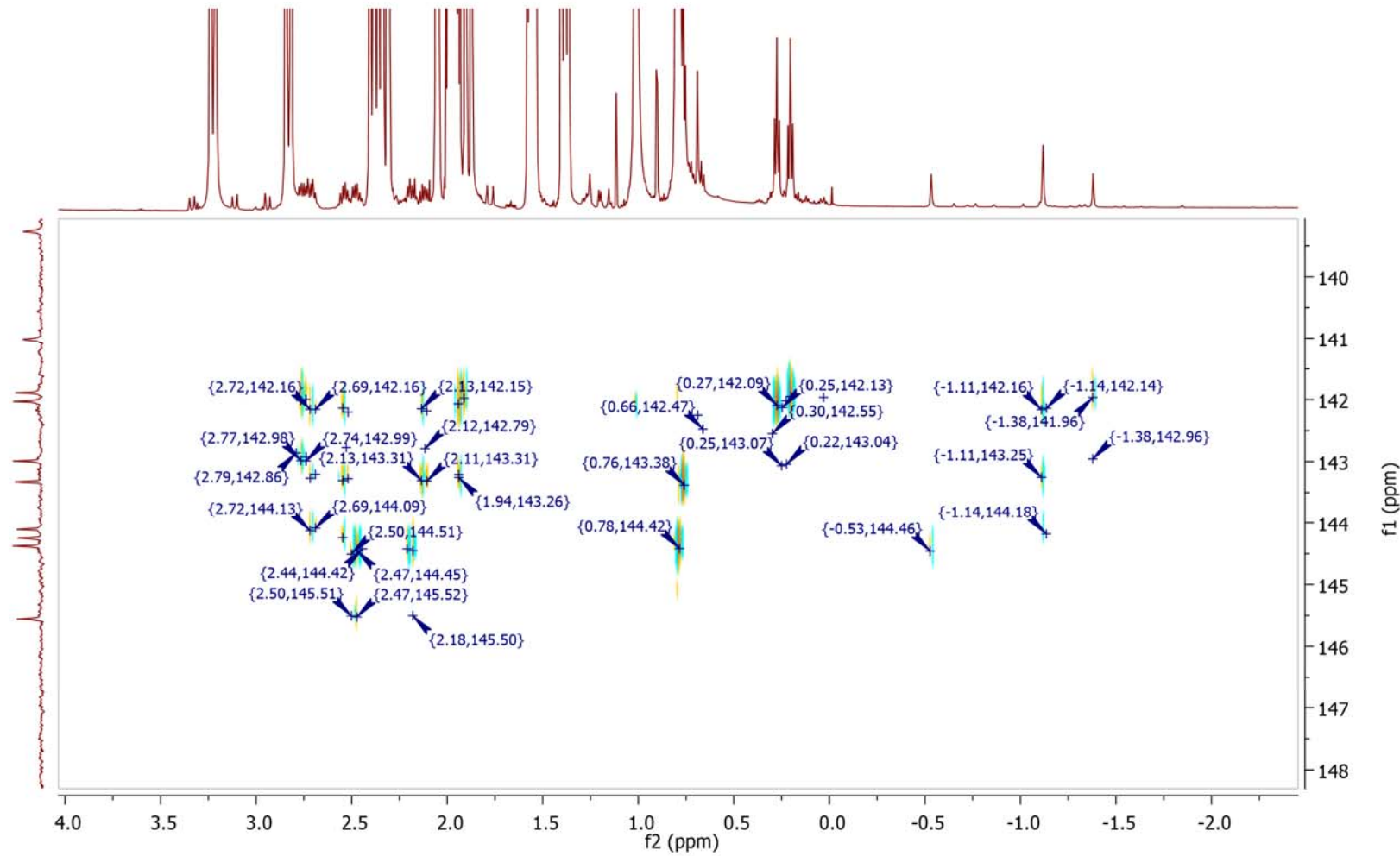


Figure S30. ^1H - ^{13}C HMBC spectrum, expansion of area of interest of $\alpha_2\beta_2\text{-P}\cdot\text{10CSA(SR)}$ (acetonitrile- d_3 , 20 eq. of 10CSA(S) and 10CSA(R), 25 °C).

SUPPORTING INFORMATION

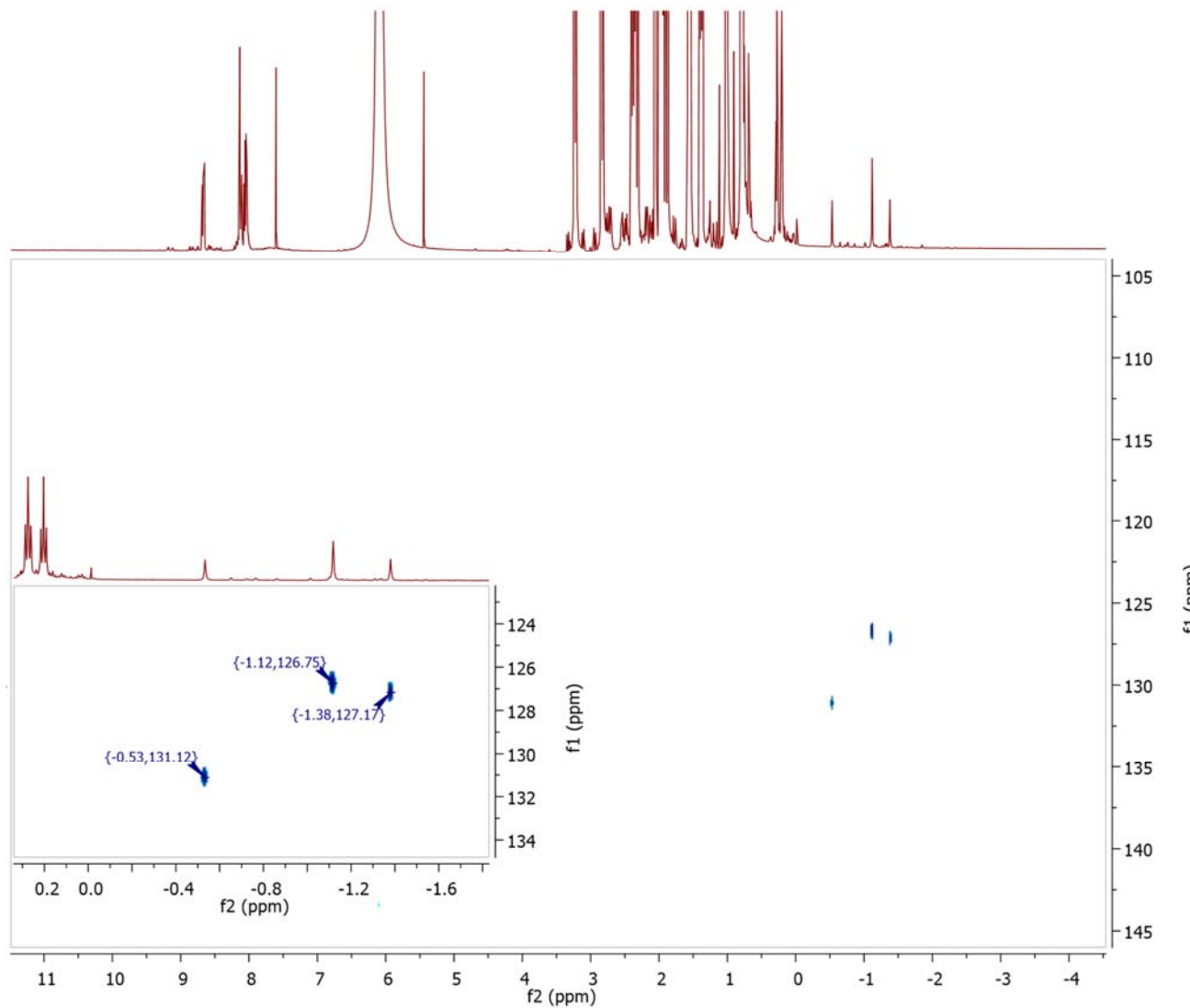


Figure S31. ¹H-¹⁵N HSQC spectrum of $\alpha_2,\beta_2\text{-P}\cdot\text{10CSA(SR)}$ with expansion of areas of interest (acetonitrile-*d*₃, 20 eq. of 10CSA(S) and 10CSA(R), 25 °C)

SUPPORTING INFORMATION

$\alpha_4\text{-P}\cdot\text{10CSA(S)}$

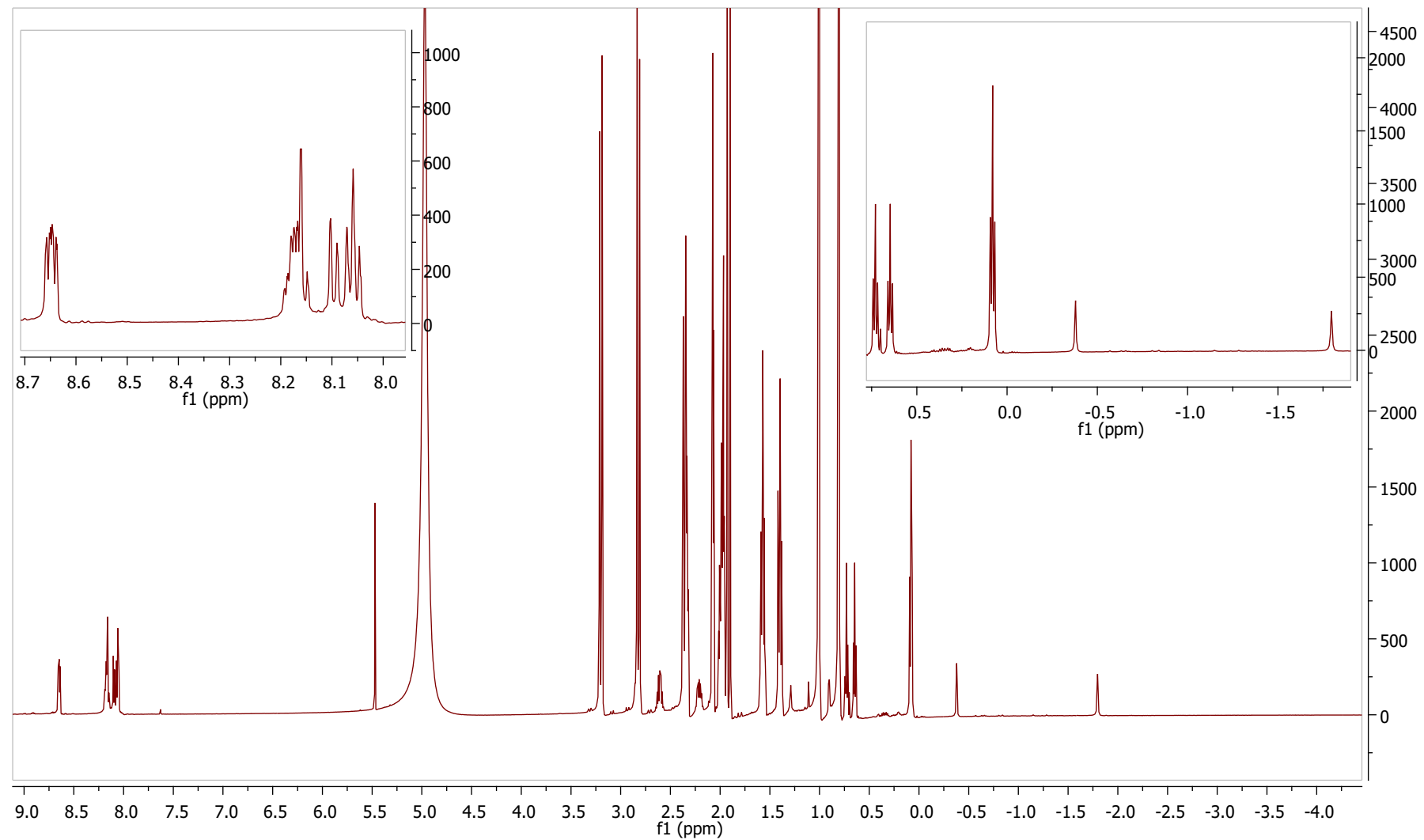


Figure S32. ^1H NMR spectrum of $\alpha_4\text{-P}\cdot\text{10CSA(S)}$ with the expansion of areas of interest (600 MHz, acetonitrile- d_3 , 20 eq. of 10CSA(S), 25 °C).

SUPPORTING INFORMATION

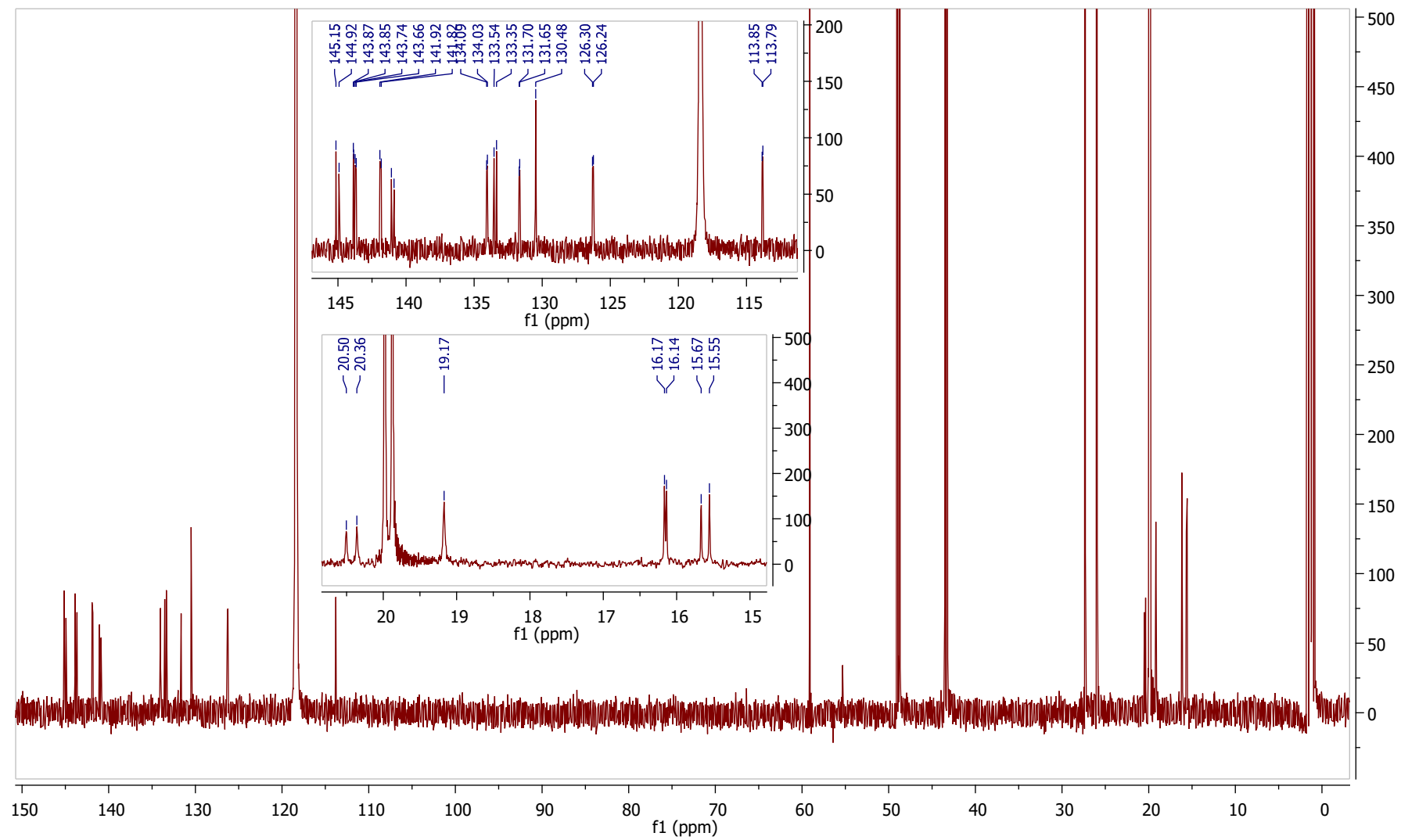


Figure S33. ^{13}C NMR spectrum of $\alpha\text{-P}\cdot\text{10CSA(S)}$ with expansion of areas of interest (151 MHz, acetonitrile- d_3 , 20 eq. of 10CSA(S), 25 °C).

SUPPORTING INFORMATION

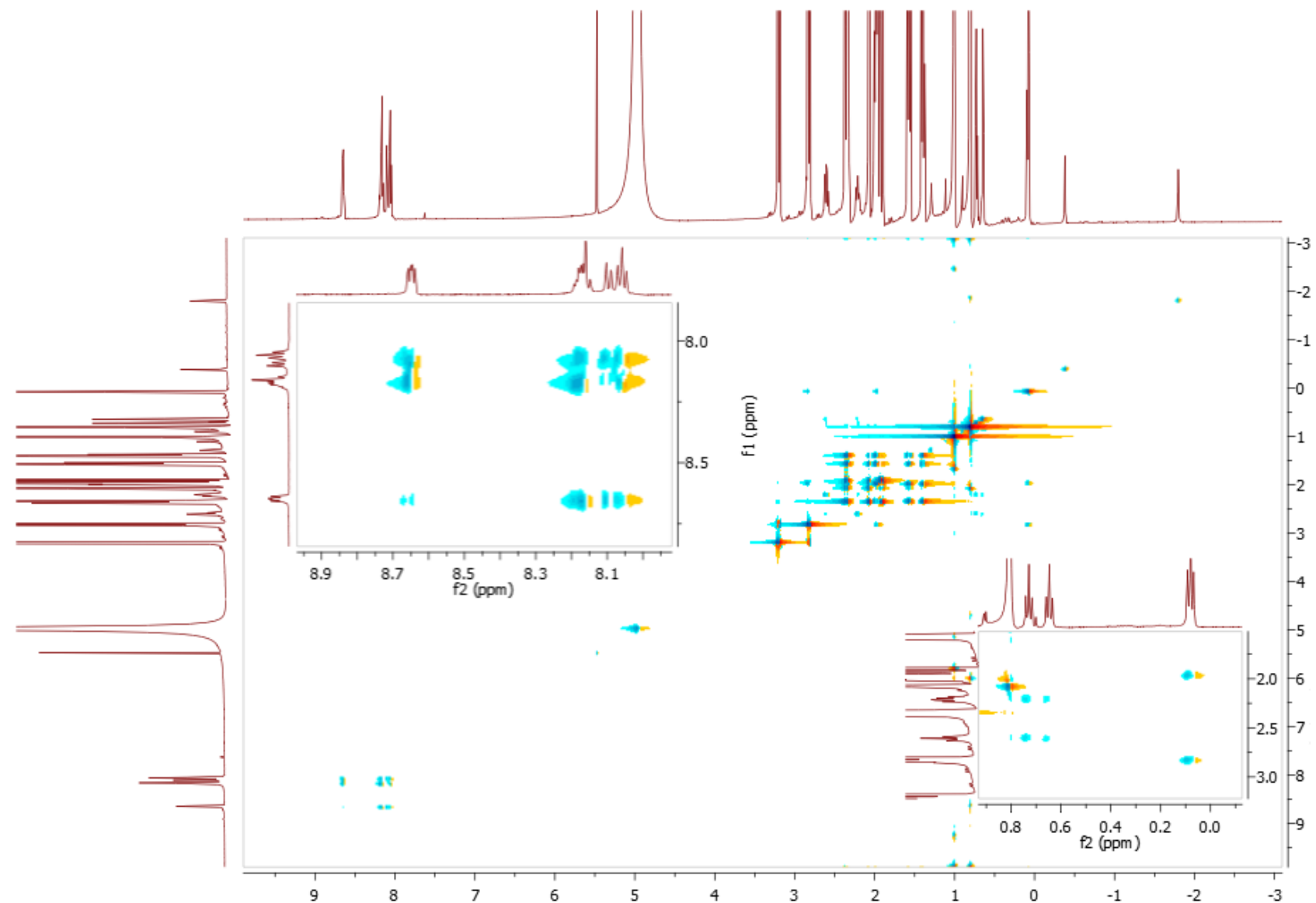


Figure S34. ^1H - ^1H TOCSY spectrum of $\alpha_4\text{-P}\cdot\text{10CSA(S)}$ with expansion of areas of interest (acetonitrile- d_3 , 20 eq. of 10CSA(S), 25 °C).

SUPPORTING INFORMATION

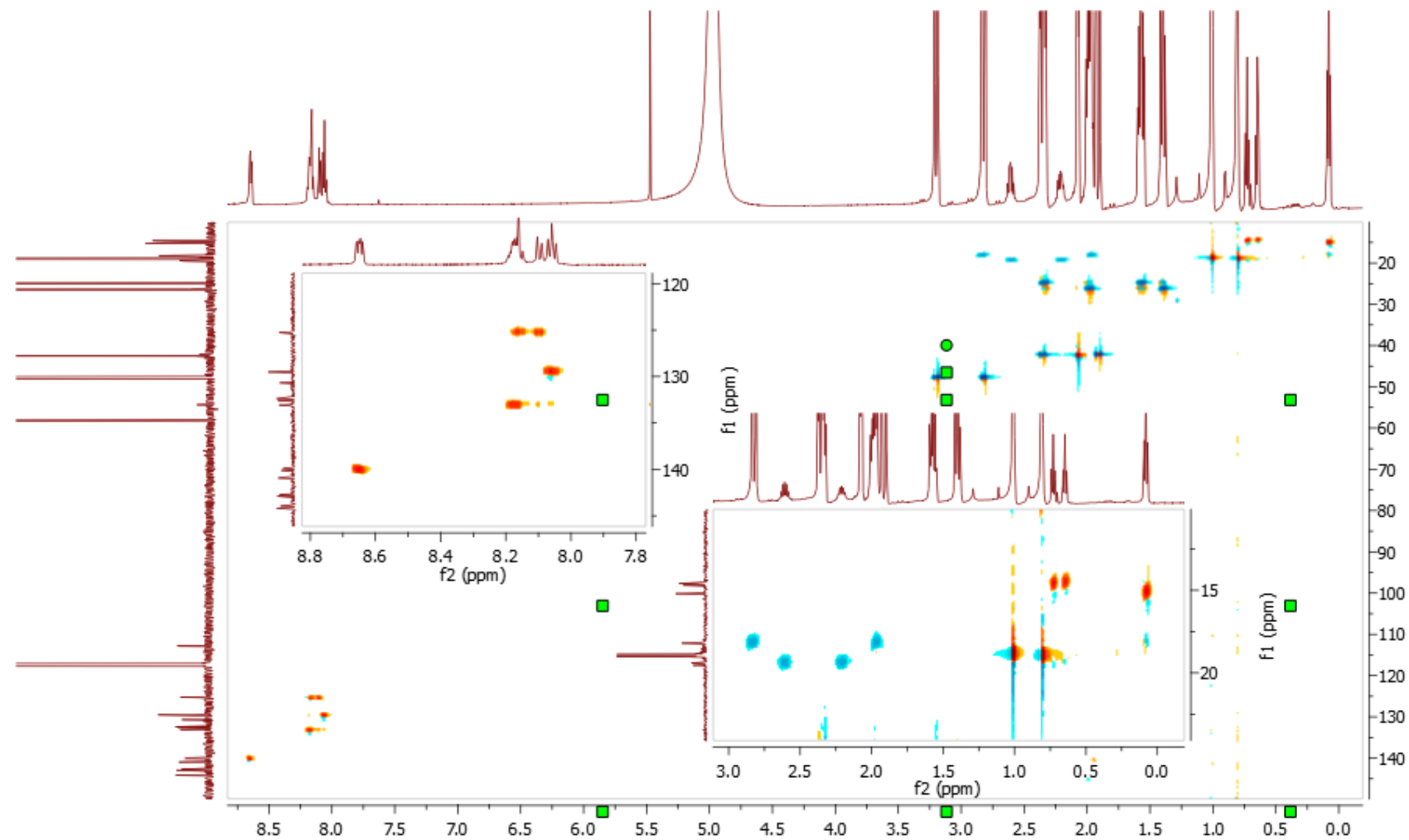


Figure S35. ^1H - ^{13}C HSQC spectrum of $\alpha_4\text{-P}\cdot 10\text{CSA(S)}$ with expansion of areas of interest (acetonitrile- d_3 , 20 eq. of 10CSA(S), 25 °C).

SUPPORTING INFORMATION

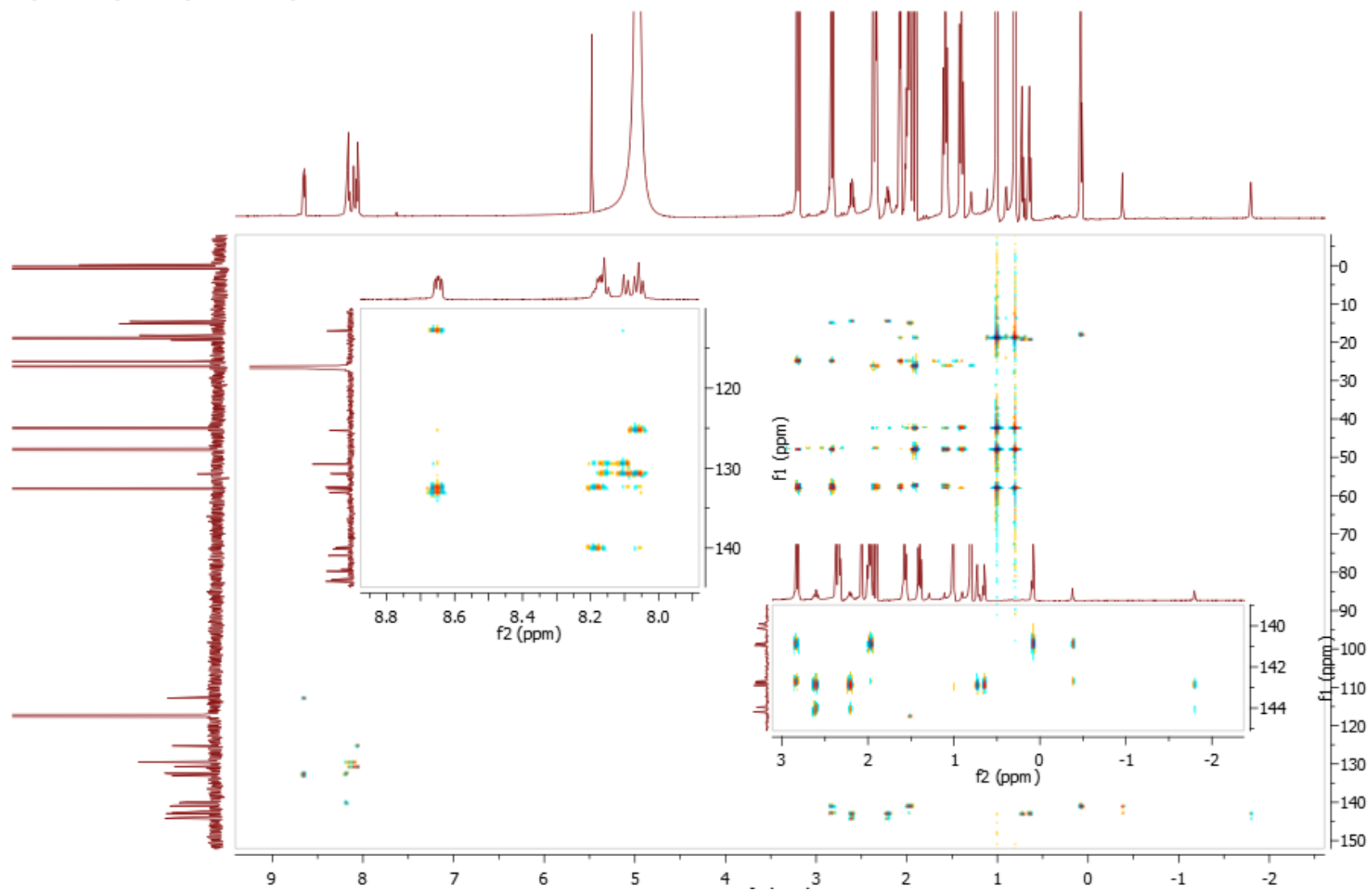
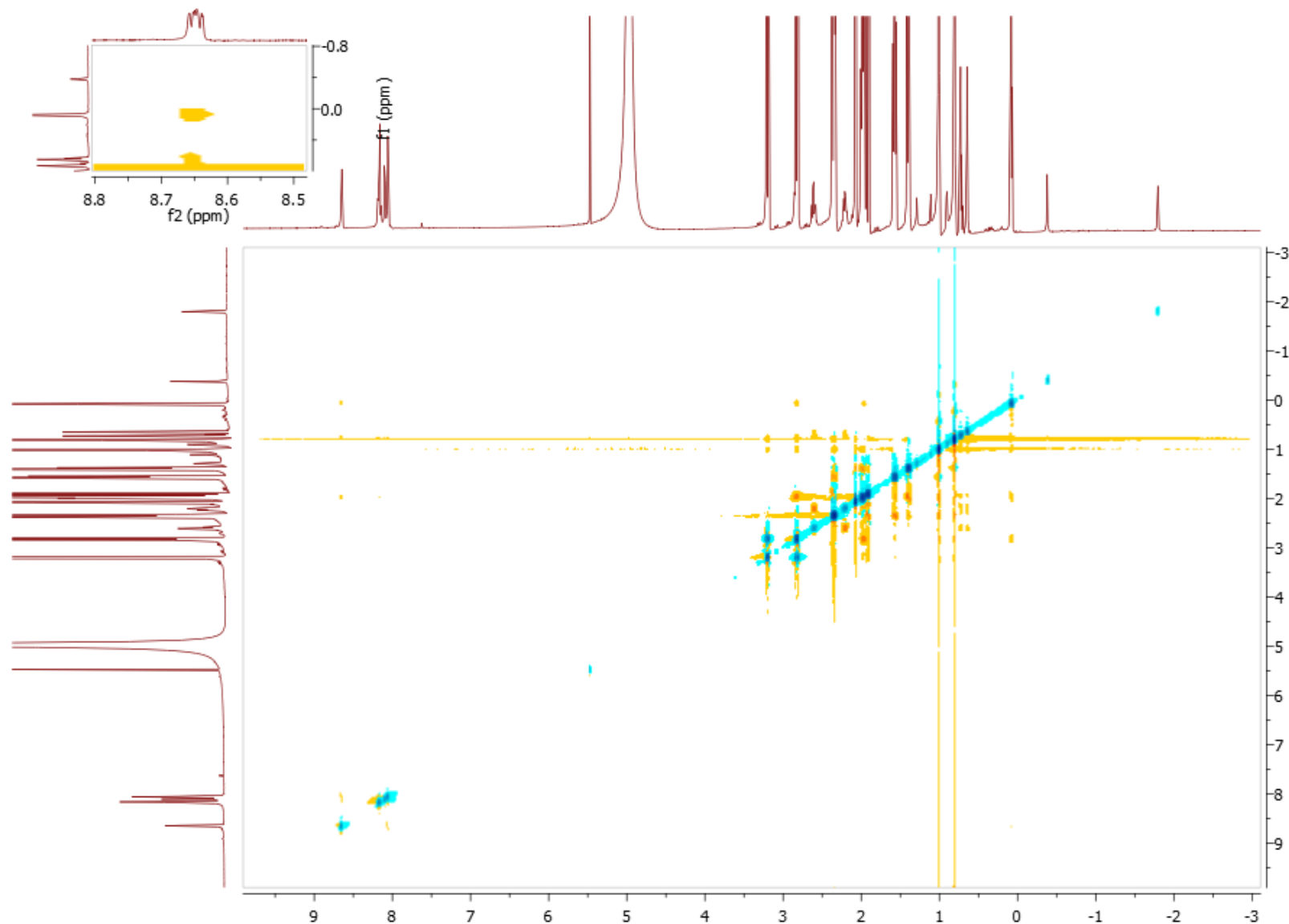


Figure S36. ^1H - ^{13}C HMBC spectrum of $\alpha_4\text{-P}\cdot\text{10CSA(S)}$ with expansion of areas of interest (acetonitrile- d_3 , 20 eq. of 10CSA(S), 25 °C).

SUPPORTING INFORMATION



SUPPORTING INFORMATION

Figure S37. ^1H - ^1H ROESY spectrum of $\alpha_4\text{-P}\cdot\text{10CSA(S)}$ with expansion of areas of interest (acetonitrile- d_3 , 20 eq. of 10CSA(S), 25 °C).

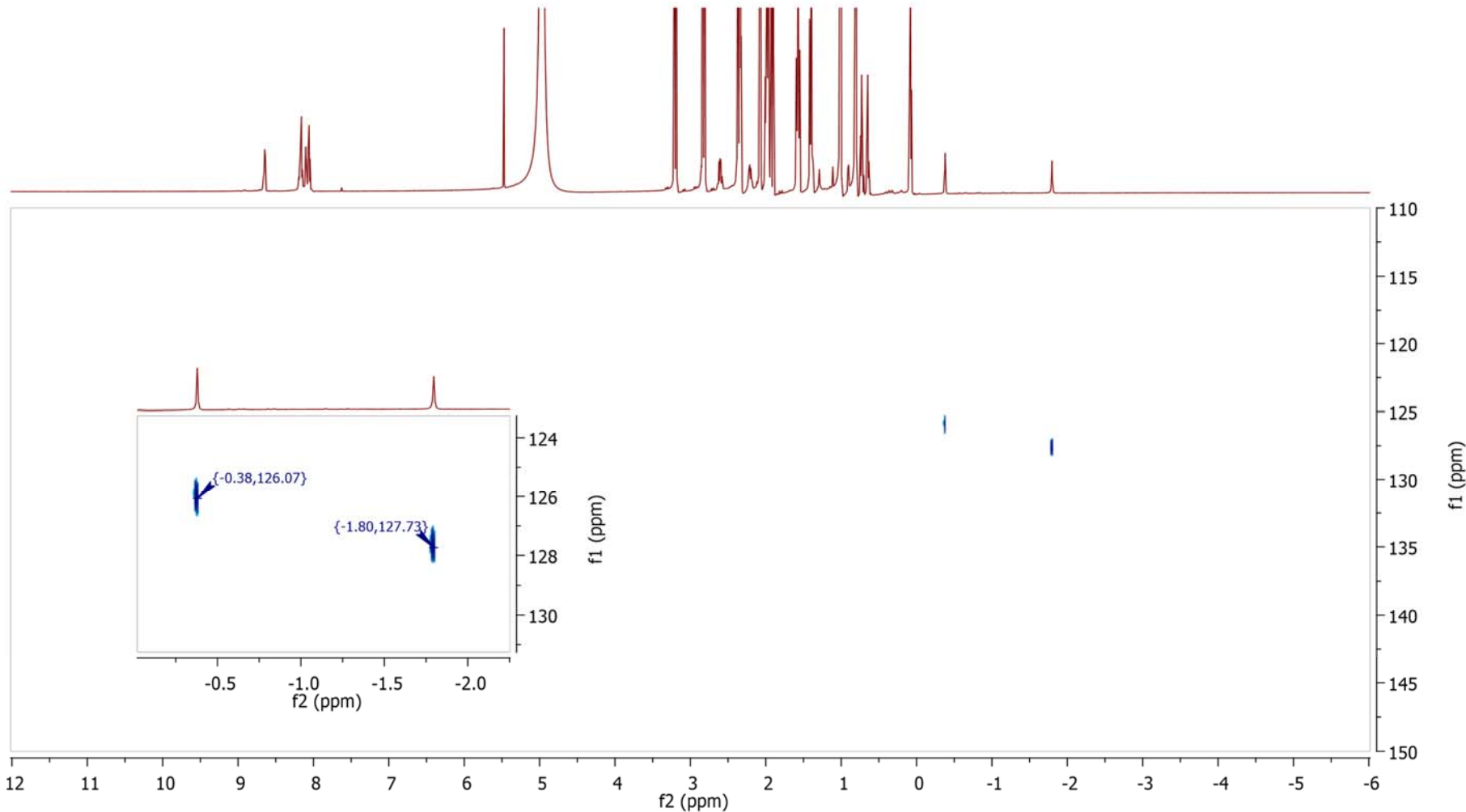


Figure S38. ^1H - ^{15}N HSQC spectrum of $\alpha_4\text{-P}\cdot\text{10CSA(S)}$ with expansion of areas of interest (acetonitrile- d_3 , 20 eq. of 10CSA(S), 25 °C).

SUPPORTING INFORMATION

$\alpha_4\text{-P}\cdot\text{10CSA(SR)}$

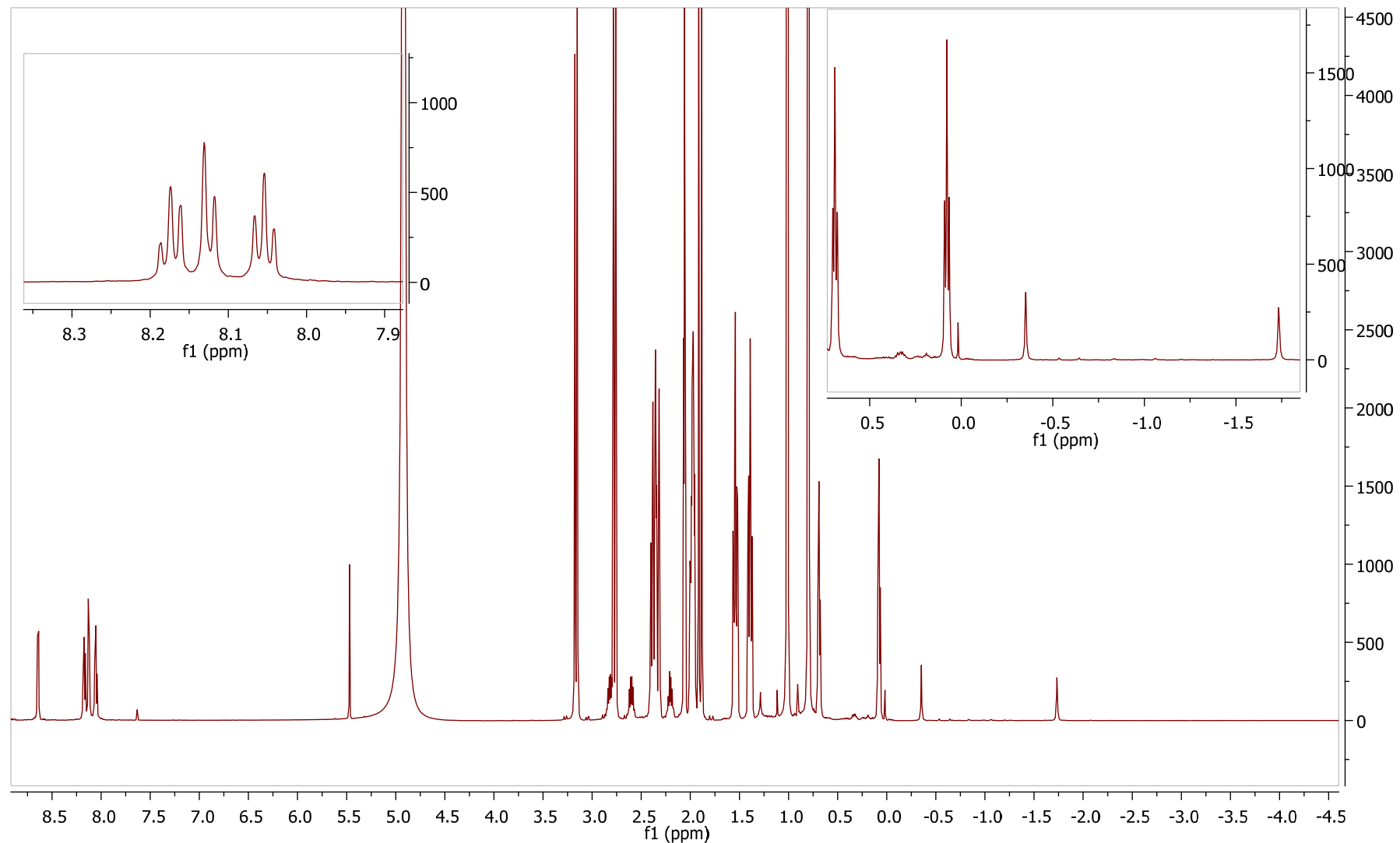


Figure S39. ^1H NMR spectrum of $\alpha_4\text{-P}\cdot\text{10CSA(SR)}$ with expansion of areas of interest (600 MHz, acetonitrile- d_3 , 20 eq. of 10CSA(S) and 10CSA(R), 25 °C).

SUPPORTING INFORMATION

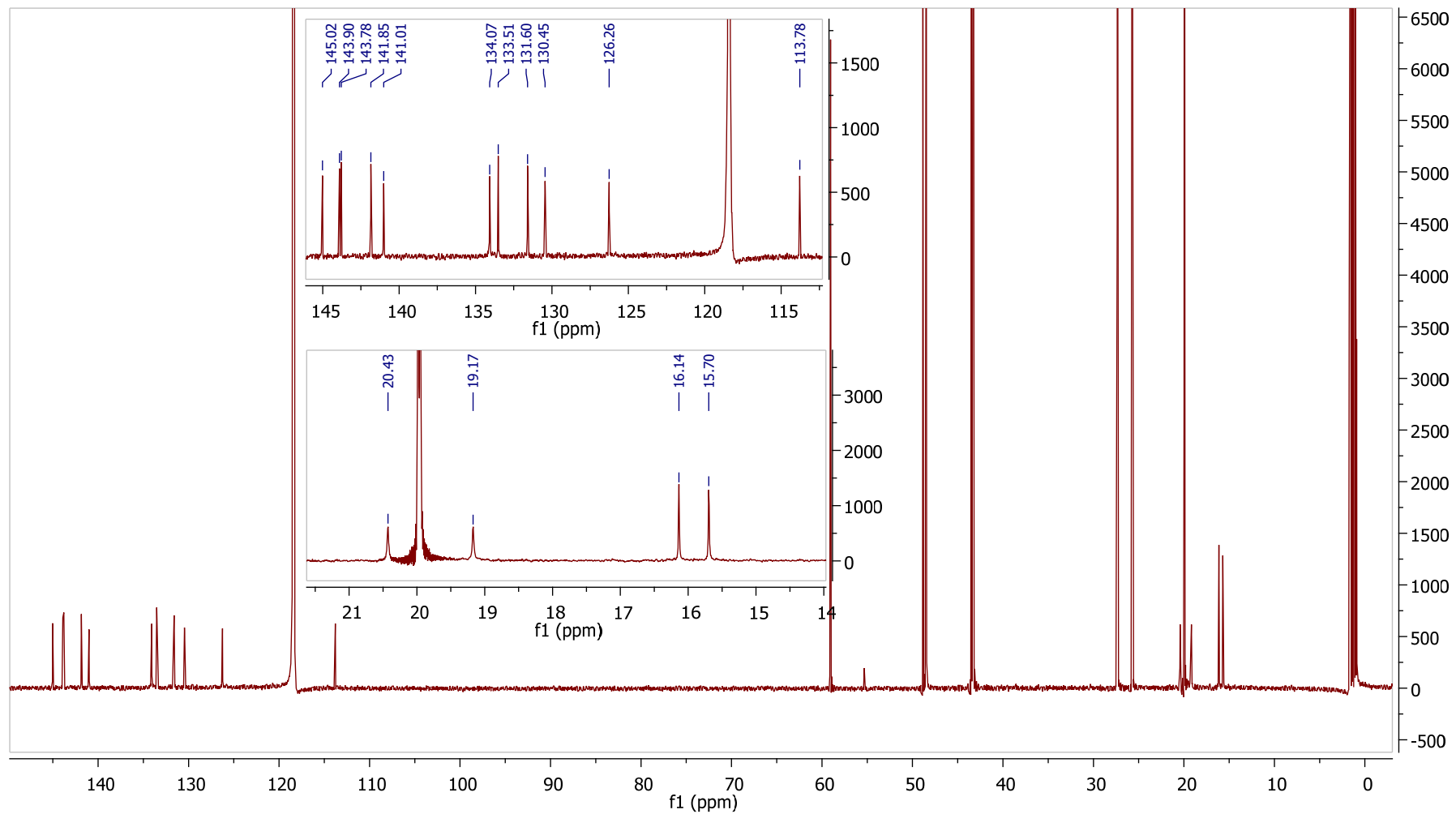


Figure S40. ^{13}C NMR spectrum of $\alpha_4\text{-P}\cdot 10\text{CSA(SR)}$ with expansion of areas of interest (151 MHz, acetonitrile- d_3 , 20 eq. of 10CSA(S) and 10CSA(R), 25 °C).

SUPPORTING INFORMATION

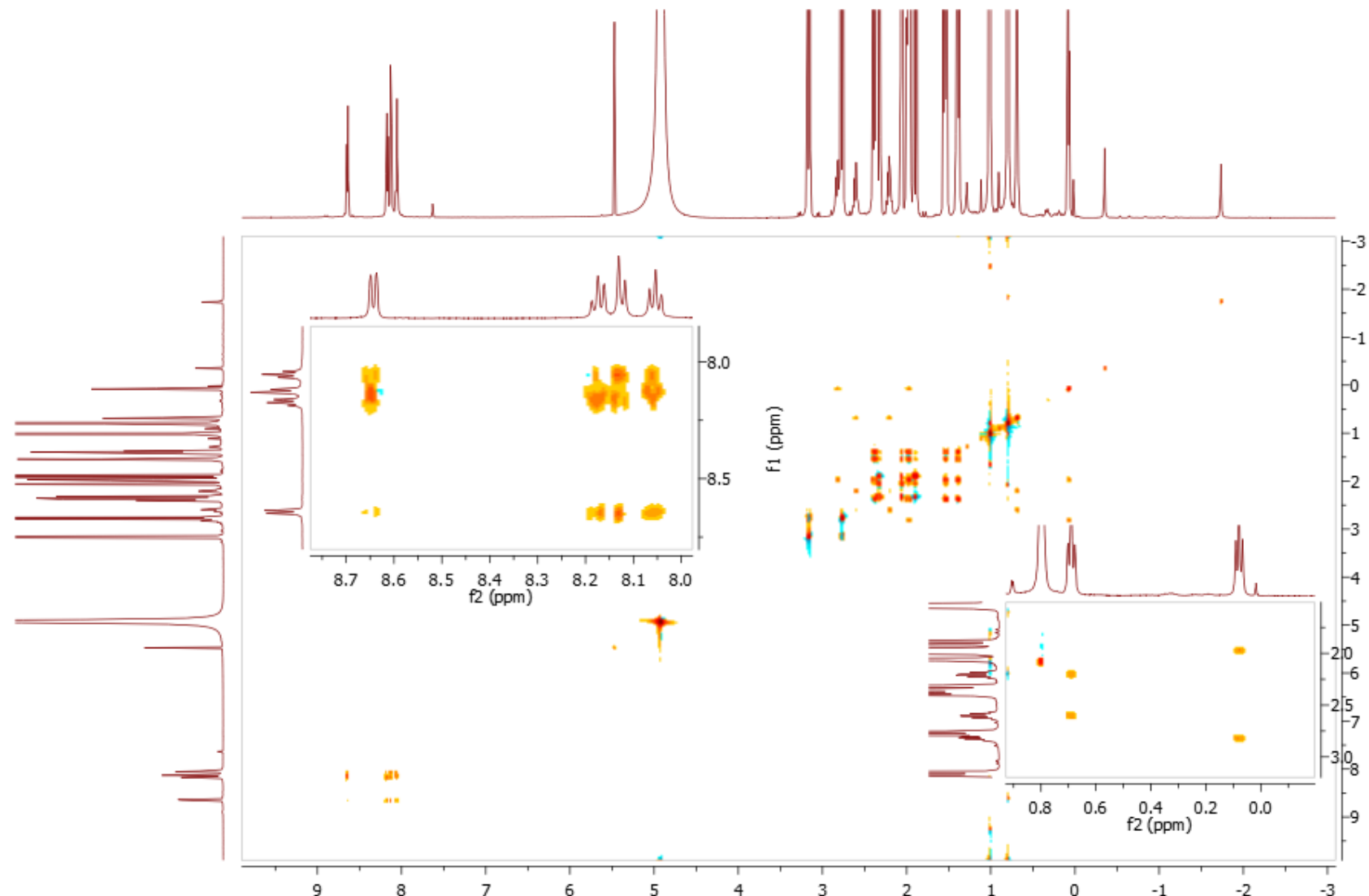


Figure S41. ^1H - ^1H TOCSY spectrum of $\alpha_4\text{-P}\cdot 10\text{CSA(SR)}$ with expansion of areas of interest (acetonitrile- d_3 , 20 eq. of 10CSA(S) and 10CSA(R), 25 °C).

SUPPORTING INFORMATION

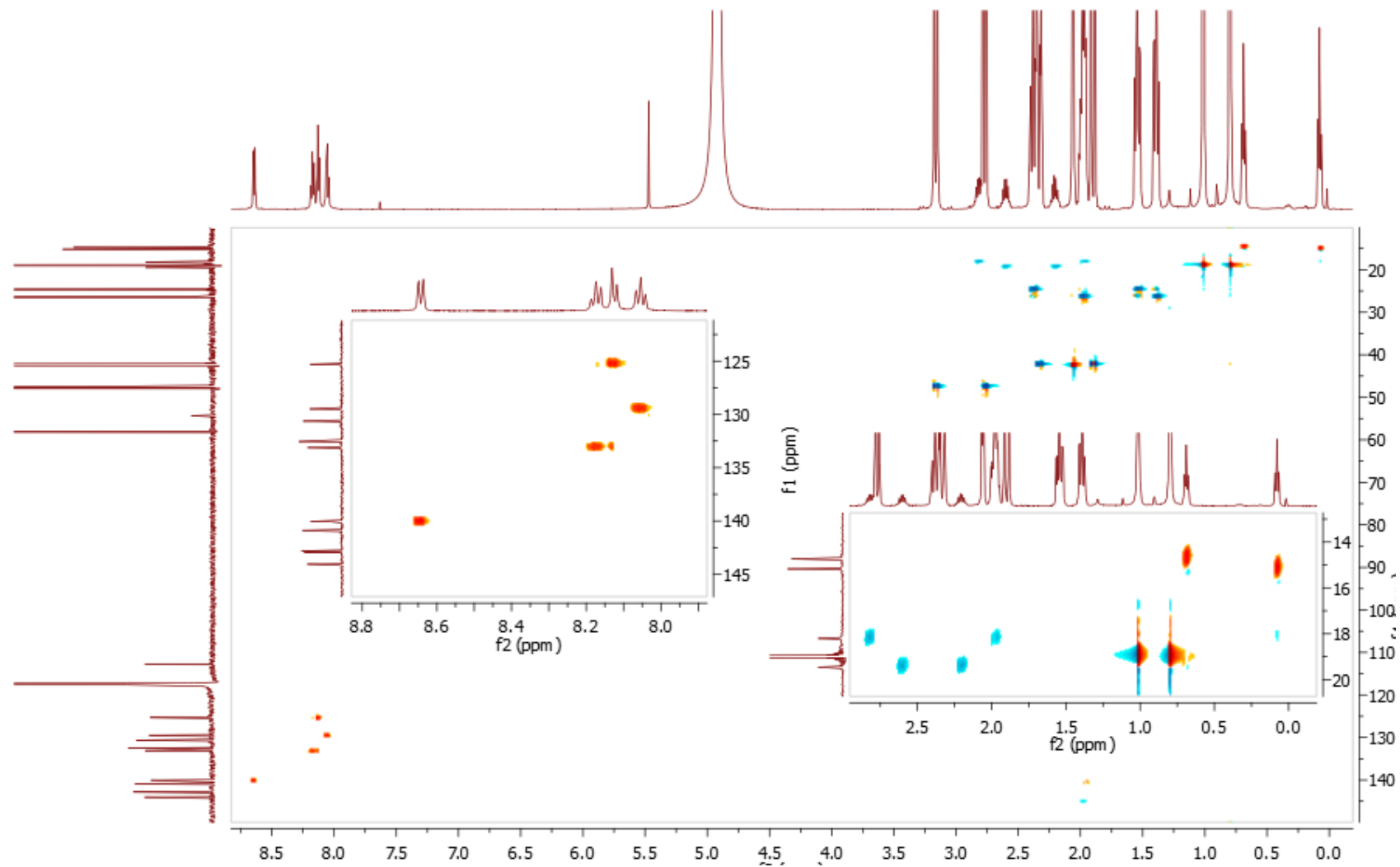


Figure S42. ^1H - ^{13}C HSQC spectrum of $\alpha_4\text{-P}\cdot\text{10CSA(SR)}$ with expansion of areas of interest (acetonitrile- d_3 , 20 eq. of 10CSA(S) and 10CSA(R), 25 °C).

SUPPORTING INFORMATION

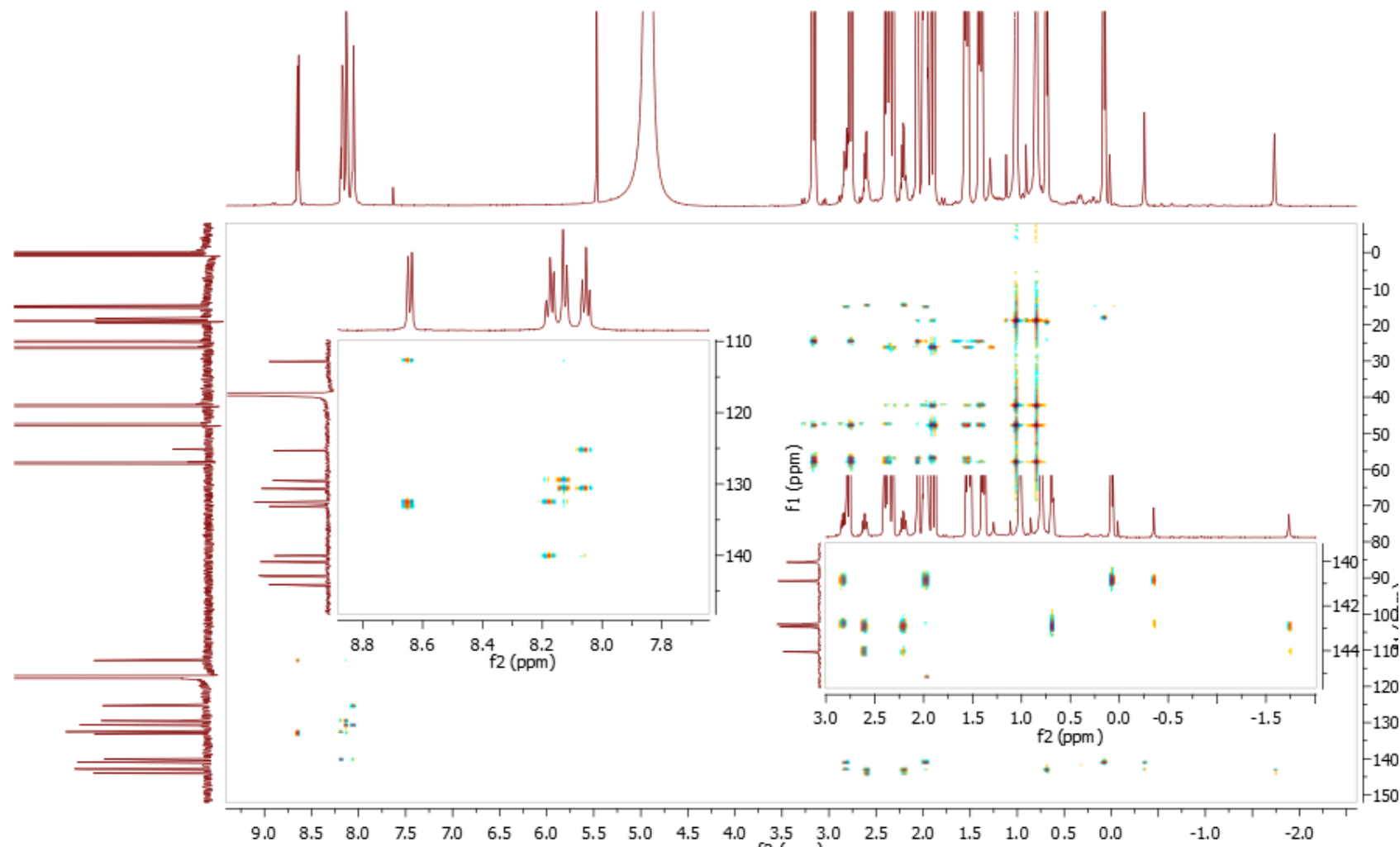


Figure S43. ^1H - ^{13}C HMBC spectrum of $\alpha\text{-P}\cdot 10\text{CSA(SR)}$ with expansion of areas of interest (acetonitrile- d_3 , 20 eq. of 10CSA(S) and 10CSA(R), 25 °C).

SUPPORTING INFORMATION

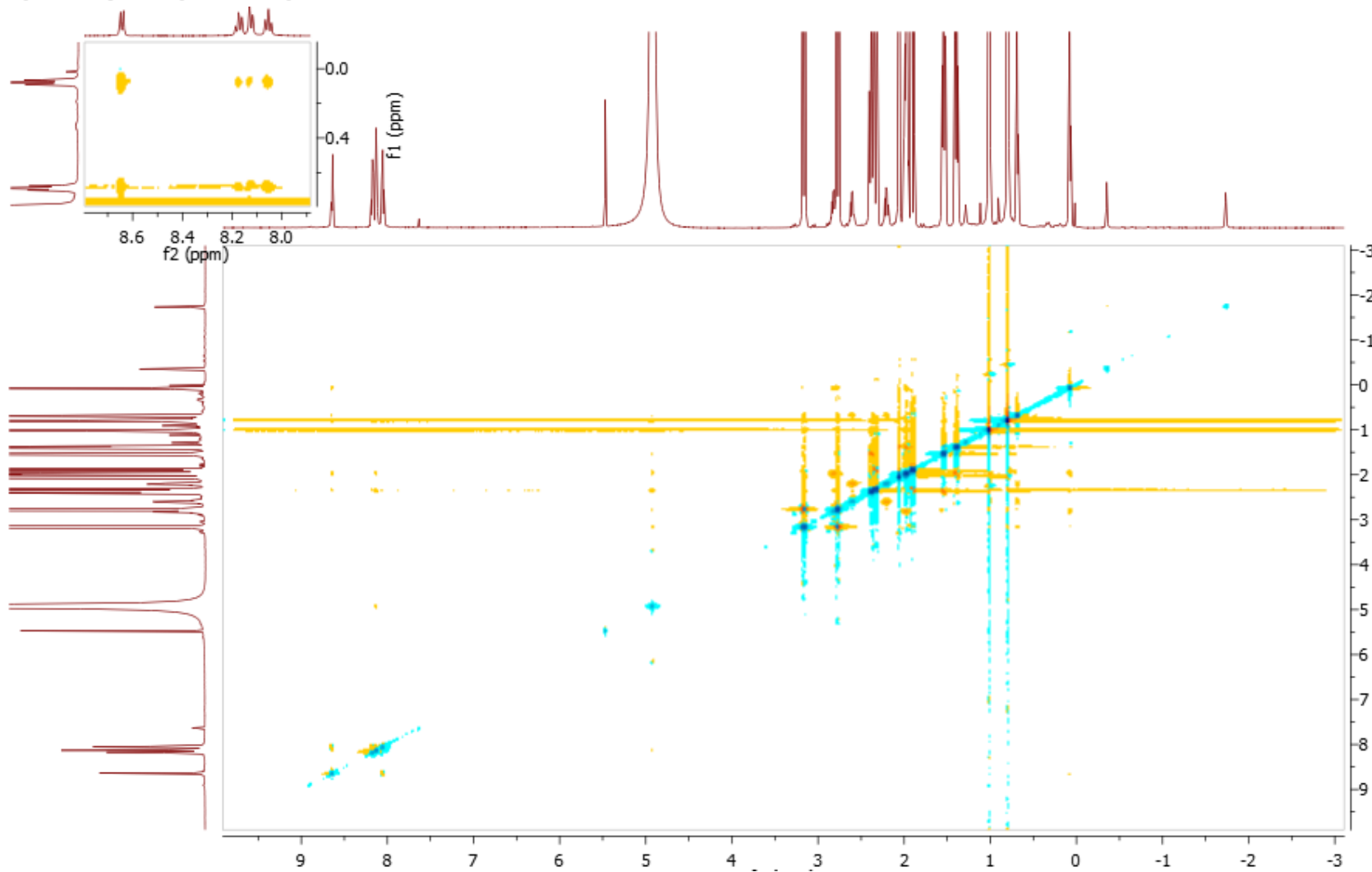


Figure S44. ¹H-¹H ROESY spectrum of $\alpha_4\text{-P}\cdot\text{10CSA(SR)}$ with expansion of areas of interest (acetonitrile-*d*₃, 20 eq. of 10CSA(S) and 10CSA(R), 25 °C).

SUPPORTING INFORMATION

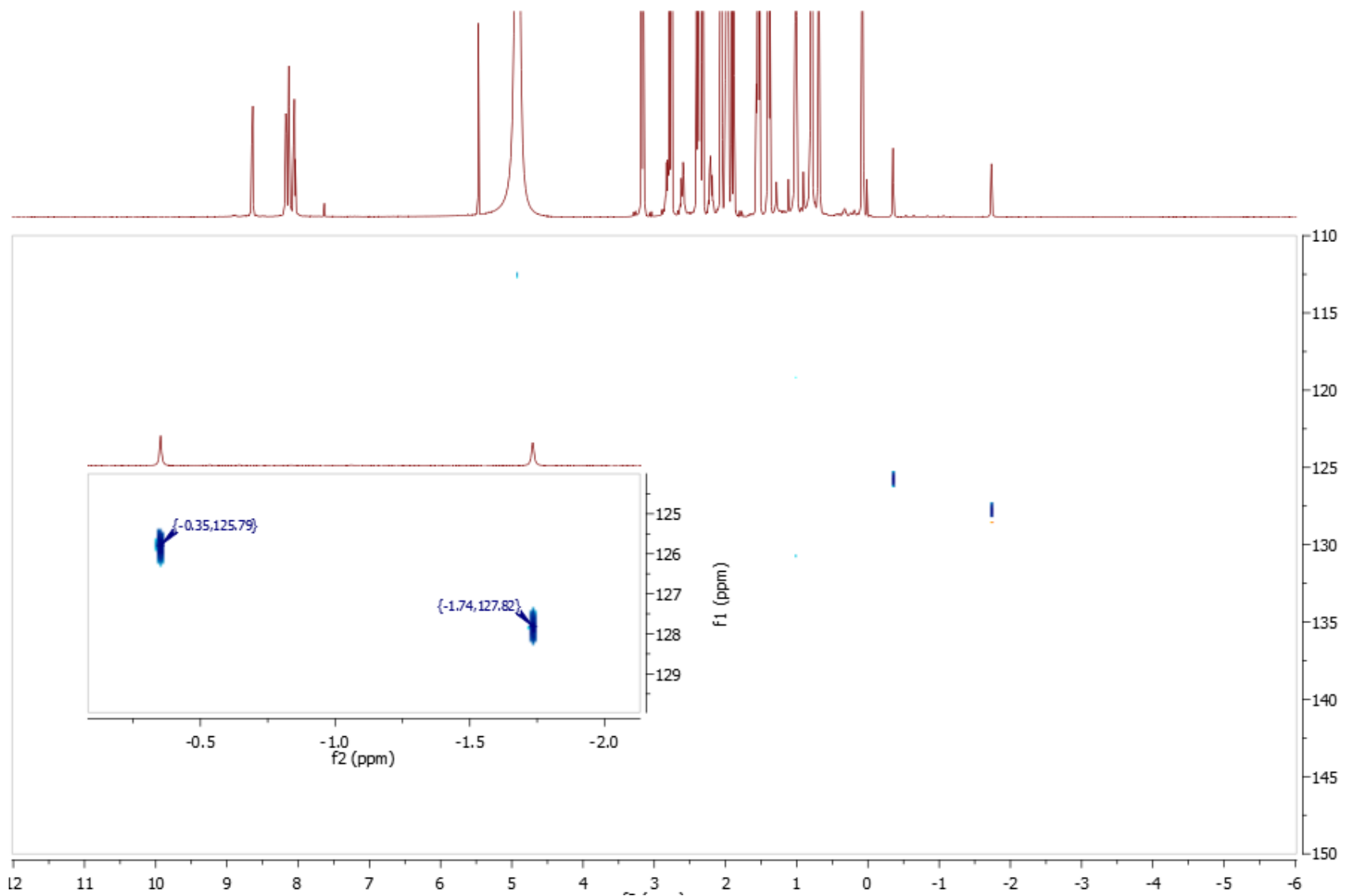


Figure S45. ^1H - ^{15}N HSQC spectrum of $\alpha_4\text{-P}\cdot\text{10CSA(SR)}$ with expansion of areas of interest (acetonitrile- d_3 , 20 eq. of 10CSA(S) and 10CSA(R), 25 °C)

SUPPORTING INFORMATION

$\alpha\beta\alpha\beta\text{-P}\cdot\text{10CSA(S)}$

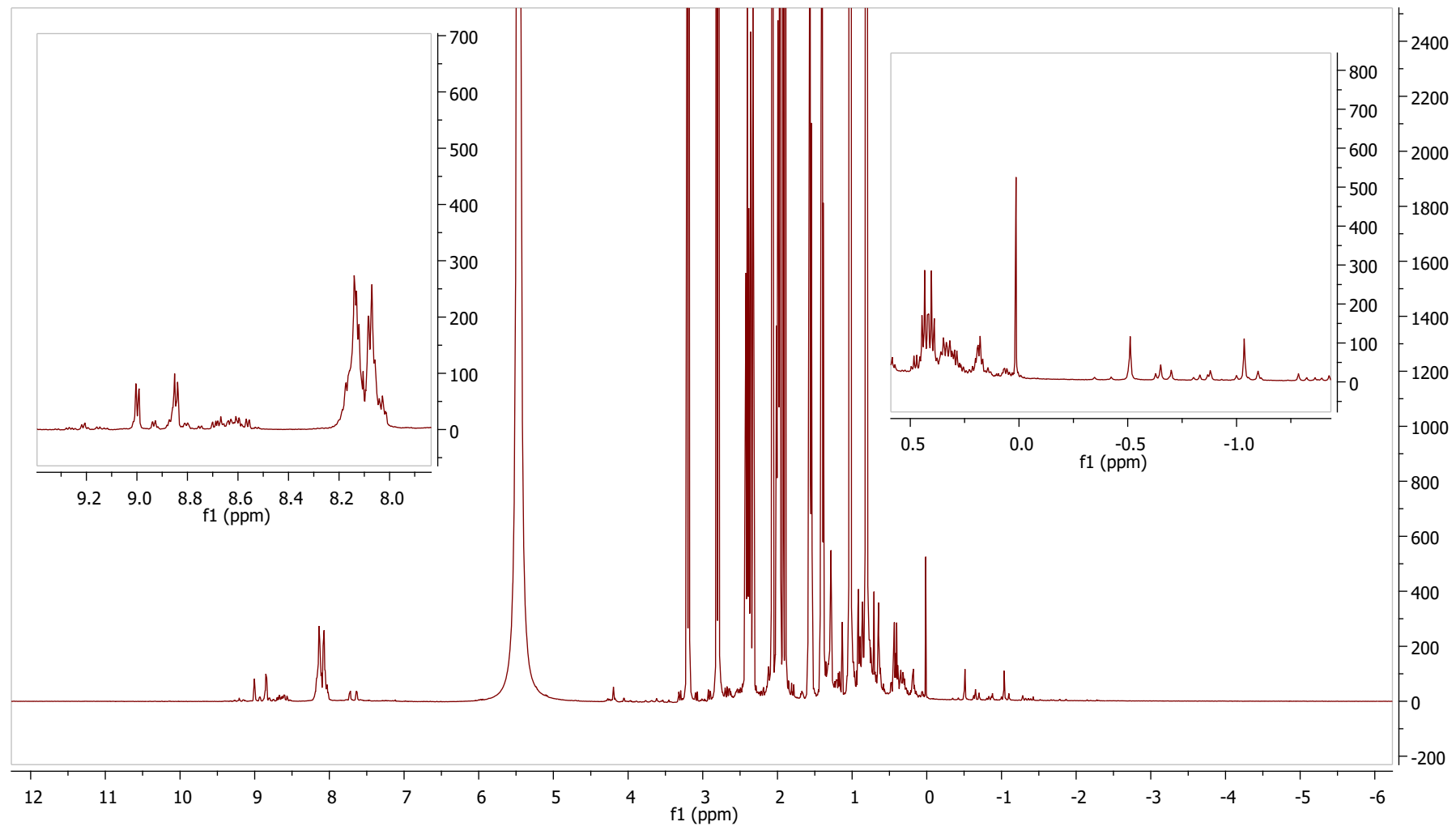


Figure S46. ^1H NMR spectrum of $\alpha\beta\alpha\beta\text{-P}\cdot\text{10CSA(S)}$ with the expansion of areas of interest (600 MHz, acetonitrile- d_3 , 20 eq. of 10CSA(S), 25 °C).

SUPPORTING INFORMATION

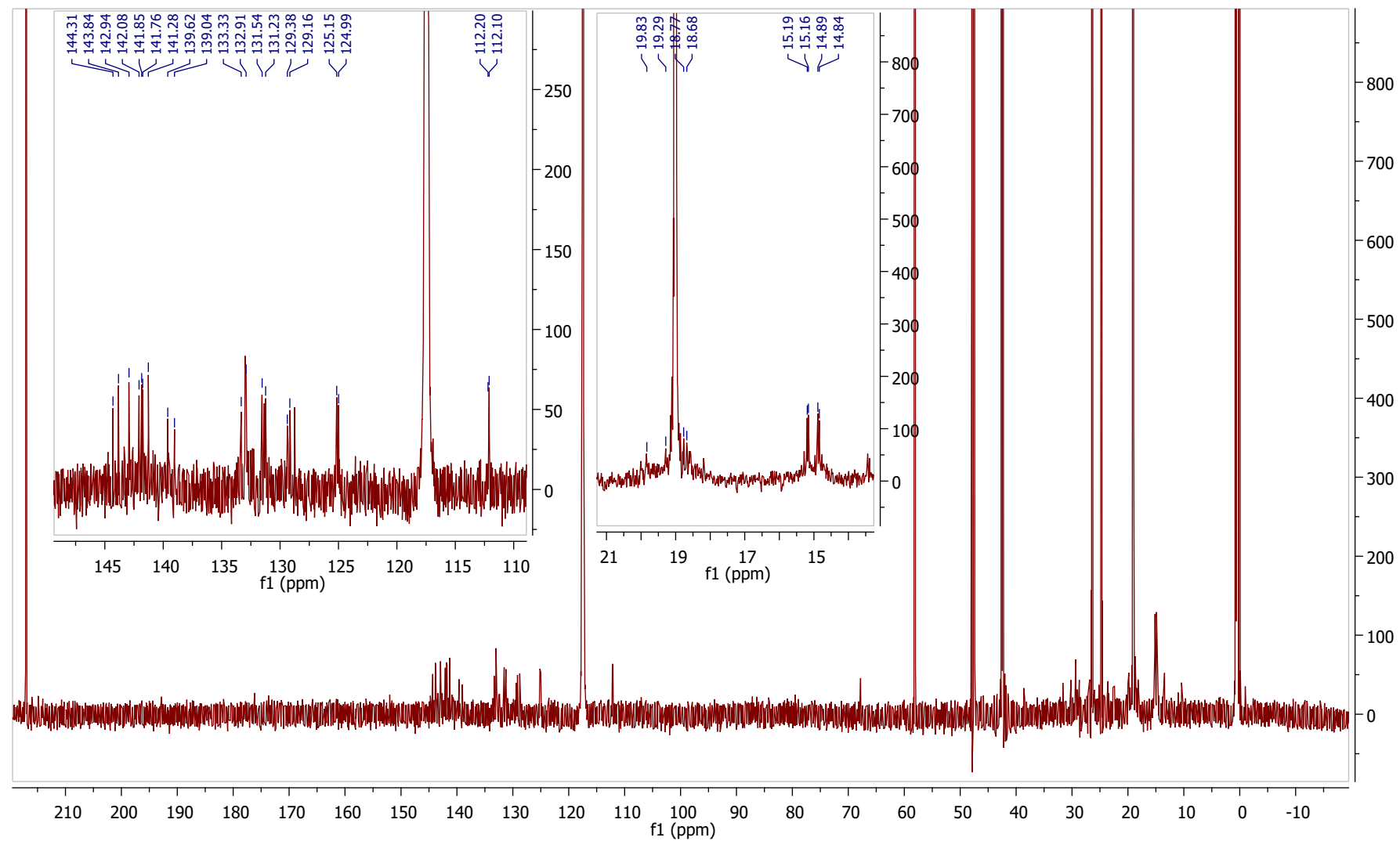


Figure S47. ^{13}C NMR spectrum of $\alpha\beta\alpha\beta\text{-P}\cdot\text{10CSA(S)}$ with expansion of areas of interest (151 MHz, acetonitrile- d_3 , 20 eq. of 10CSA(S), 25 °C).

SUPPORTING INFORMATION

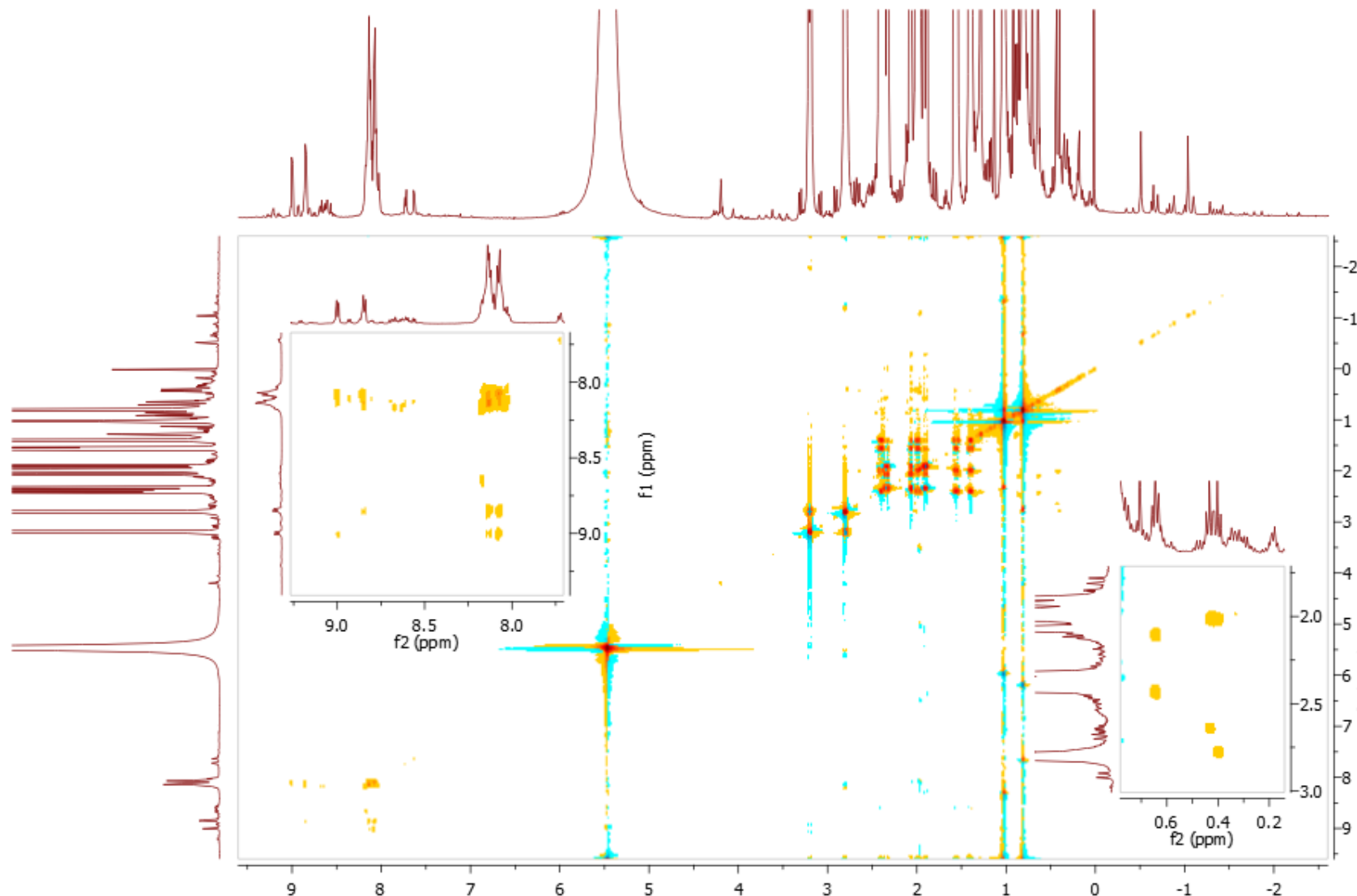


Figure S48. ^1H - ^1H TOCSY spectrum of $\alpha\beta\alpha\beta\text{-P}\cdot 10\text{CSA(S)}$ with expansion of areas of interest (acetonitrile- d_3 , 20 eq. of 10CSA(S), 25 °C).

SUPPORTING INFORMATION

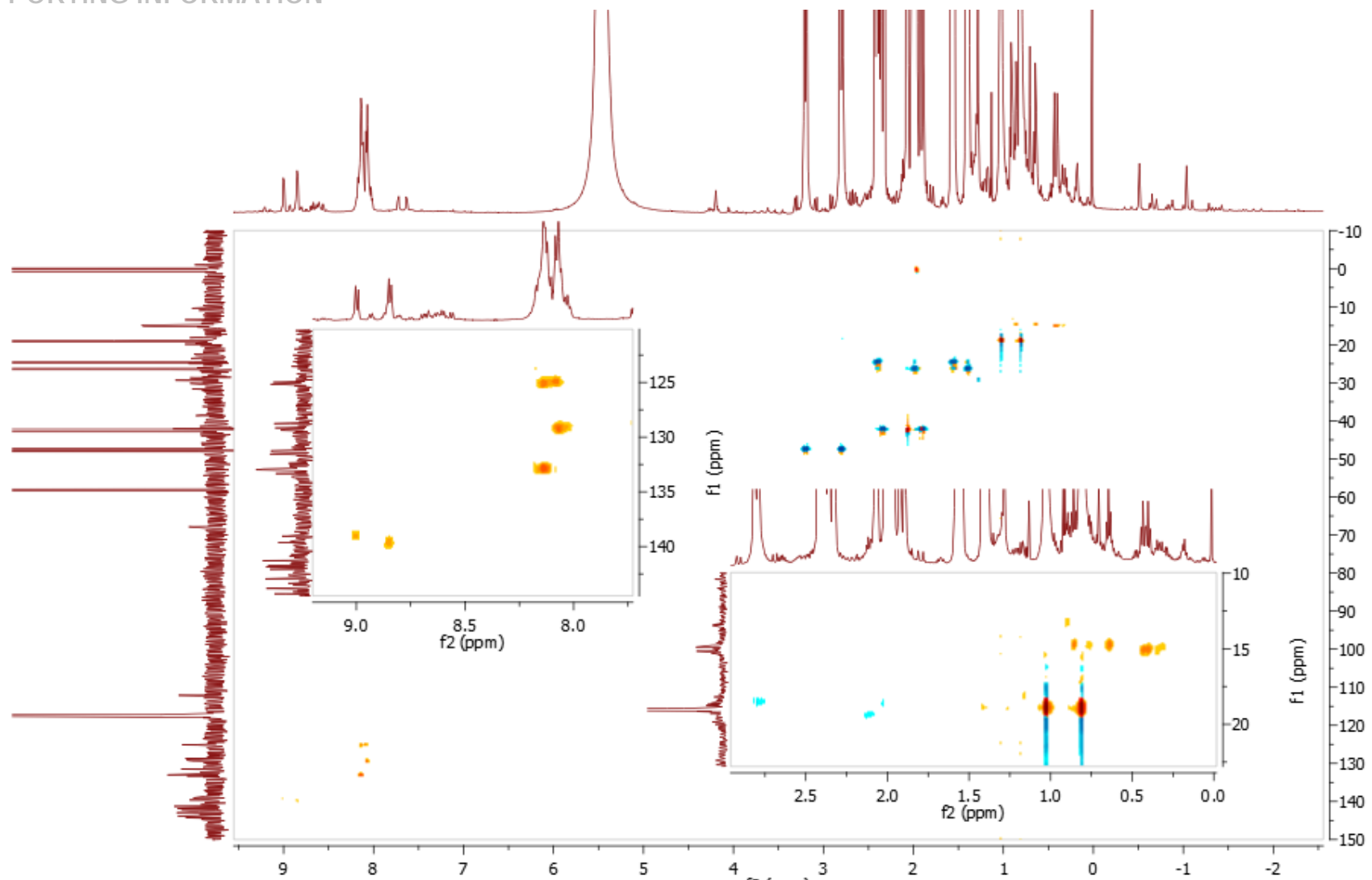


Figure S49. ¹H-¹³C HSQC spectrum of $\alpha\beta\alpha\beta\text{-P}\cdot 10\text{CSA}(\text{S})$ with expansion of areas of interest (acetonitrile-*d*₃, 20 eq. of 10CSA(S), 25 °C).

SUPPORTING INFORMATION

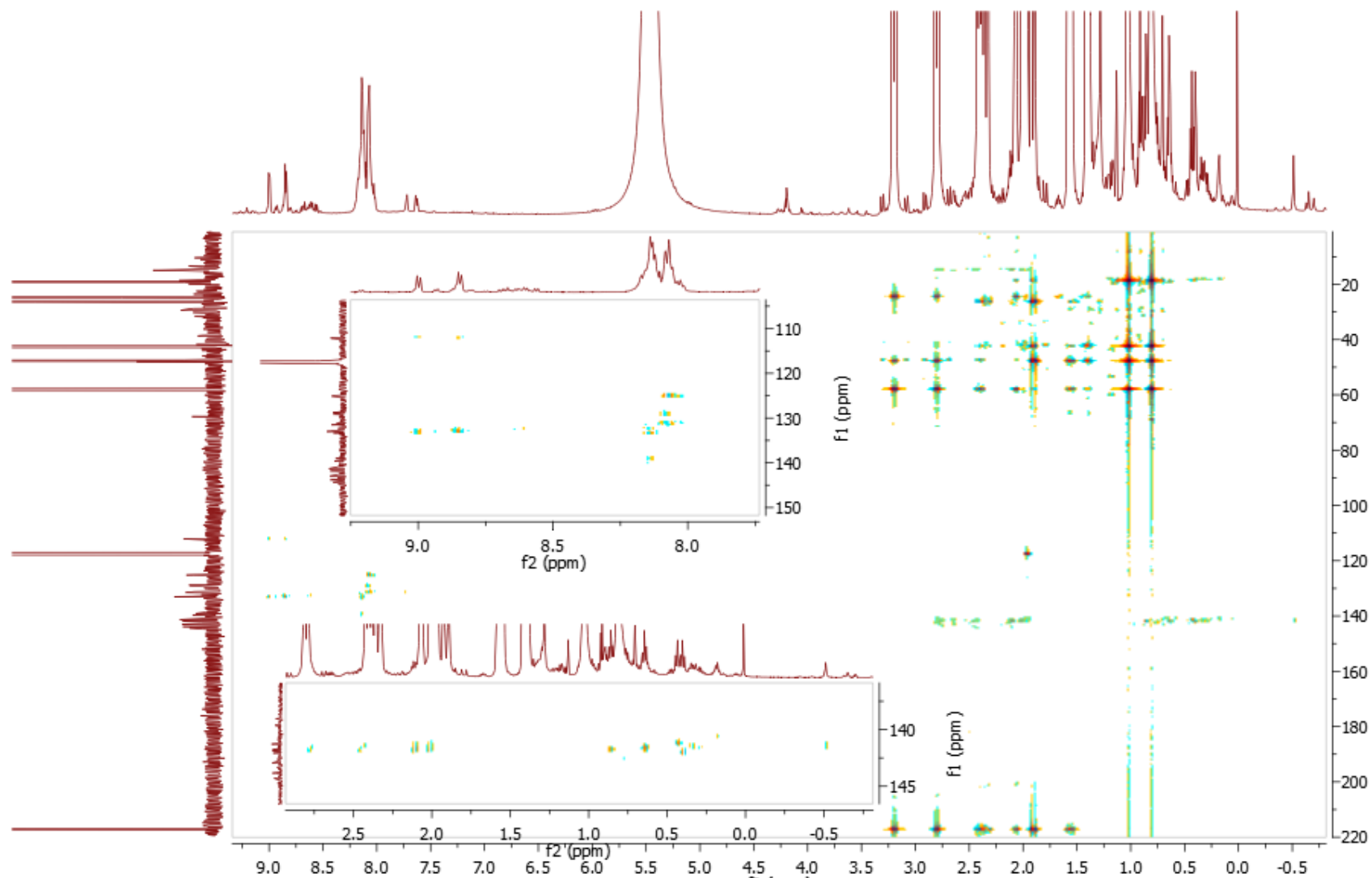


Figure S50. ^1H - ^{13}C HMBC spectrum of $\alpha\beta\alpha\beta\text{-P}\cdot 10\text{CSA(S)}$ with expansion of areas of interest (acetonitrile- d_3 , 20 eq. of 10CSA(S), 25 °C).

SUPPORTING INFORMATION

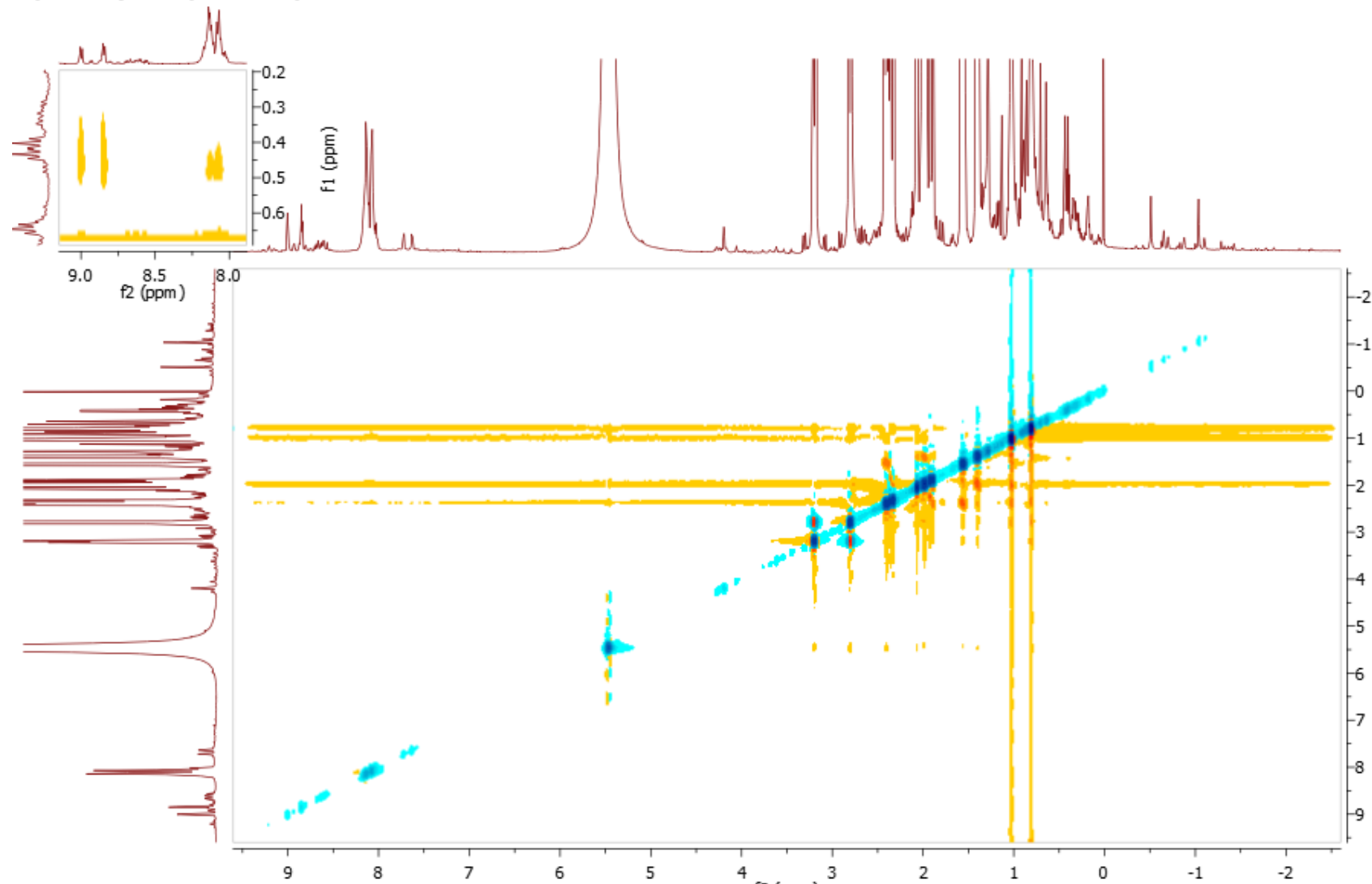


Figure S51. ¹H-¹H ROESY spectrum of $\alpha\beta\alpha\beta\text{-P}\cdot\text{10CSA(S)}$ with expansion of areas of interest (acetonitrile-*d*₃, 20 eq. of 10CSA(S), 25 °C).

SUPPORTING INFORMATION

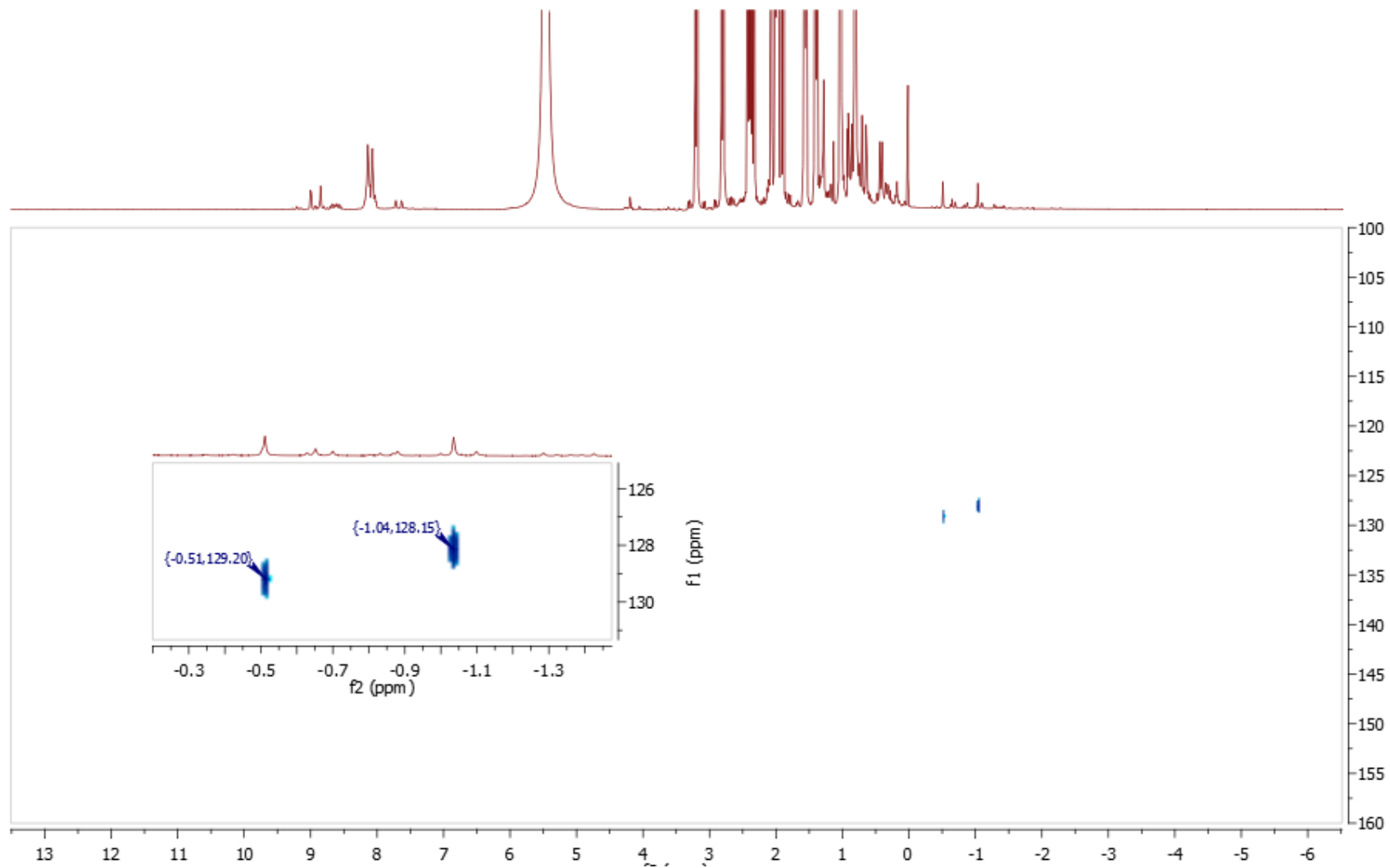


Figure S52. ^1H - ^{15}N HSQC spectrum of $\alpha\beta\alpha\beta\text{-P}\cdot 10\text{CSA(S)}$ with expansion of areas of interest (acetonitrile- d_3 , 20 eq. of 10CSA(S), 25 °C).

SUPPORTING INFORMATION

$\alpha\beta\alpha\beta\text{-P}\cdot\text{10CSA(SR)}$

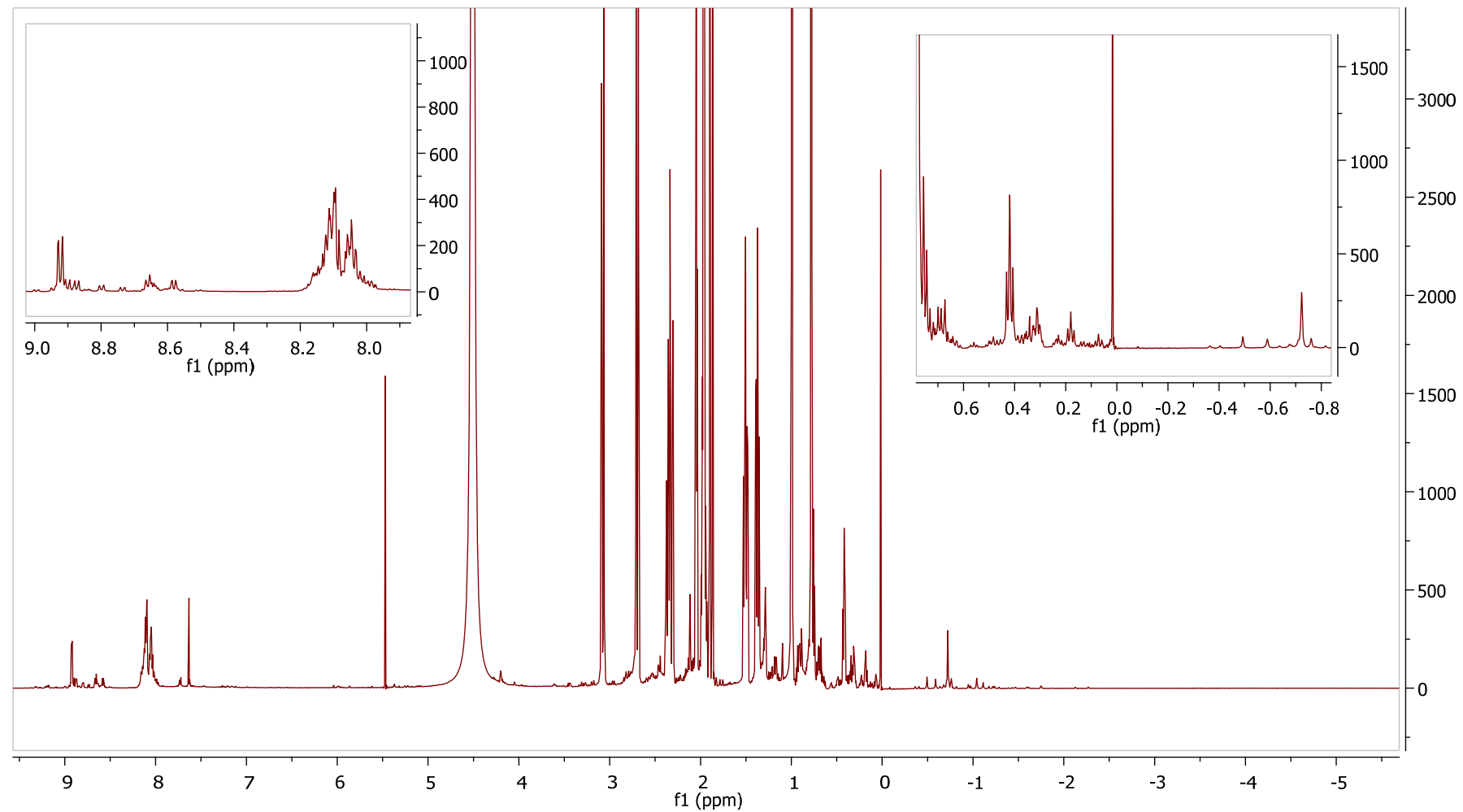


Figure S53. ^1H NMR spectrum of $\alpha\beta\alpha\beta\text{-P}\cdot\text{10CSA(SR)}$ with expansion of areas of interest (600 MHz, acetonitrile- d_3 , 20 eq. of 10CSA(S) and 10CSA(R), 25 °C).

SUPPORTING INFORMATION

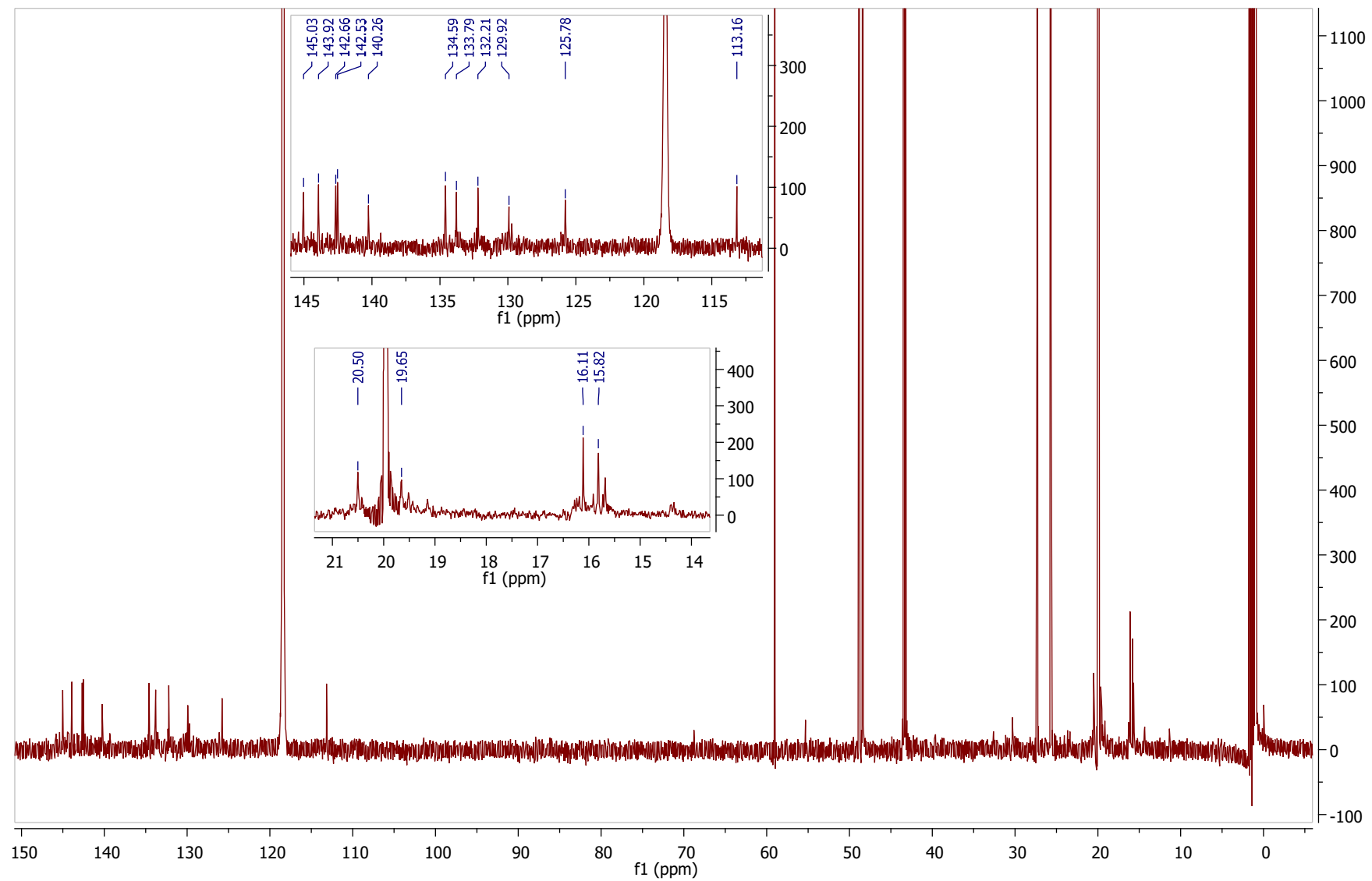


Figure S54. ^{13}C NMR spectrum of $\alpha\beta\alpha\beta\text{-P}\cdot\text{10CSA(SR)}$ with expansion of areas of interest (151 MHz, acetonitrile- d_3 , 20 eq. of 10CSA(S) and 10CSA(R), 25 °C).

SUPPORTING INFORMATION

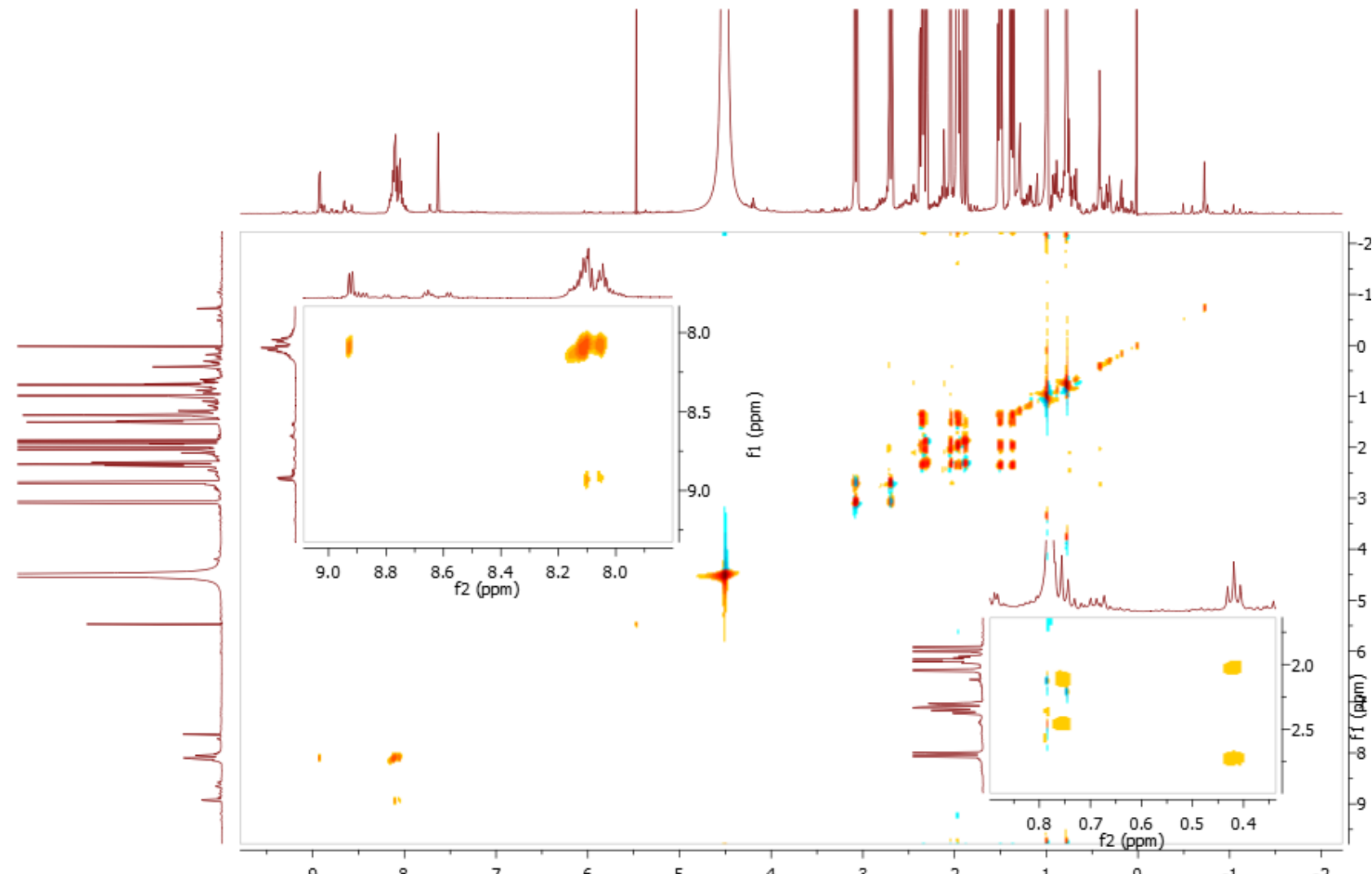


Figure S55. ^1H - ^1H TOCSY spectrum of $\alpha\beta\alpha\beta\text{-P}\cdot 10\text{CSA(SR)}$ with expansion of areas of interest (acetonitrile- d_3 , 20 eq. of 10CSA(S) and 10CSA(R), 25 °C).

SUPPORTING INFORMATION

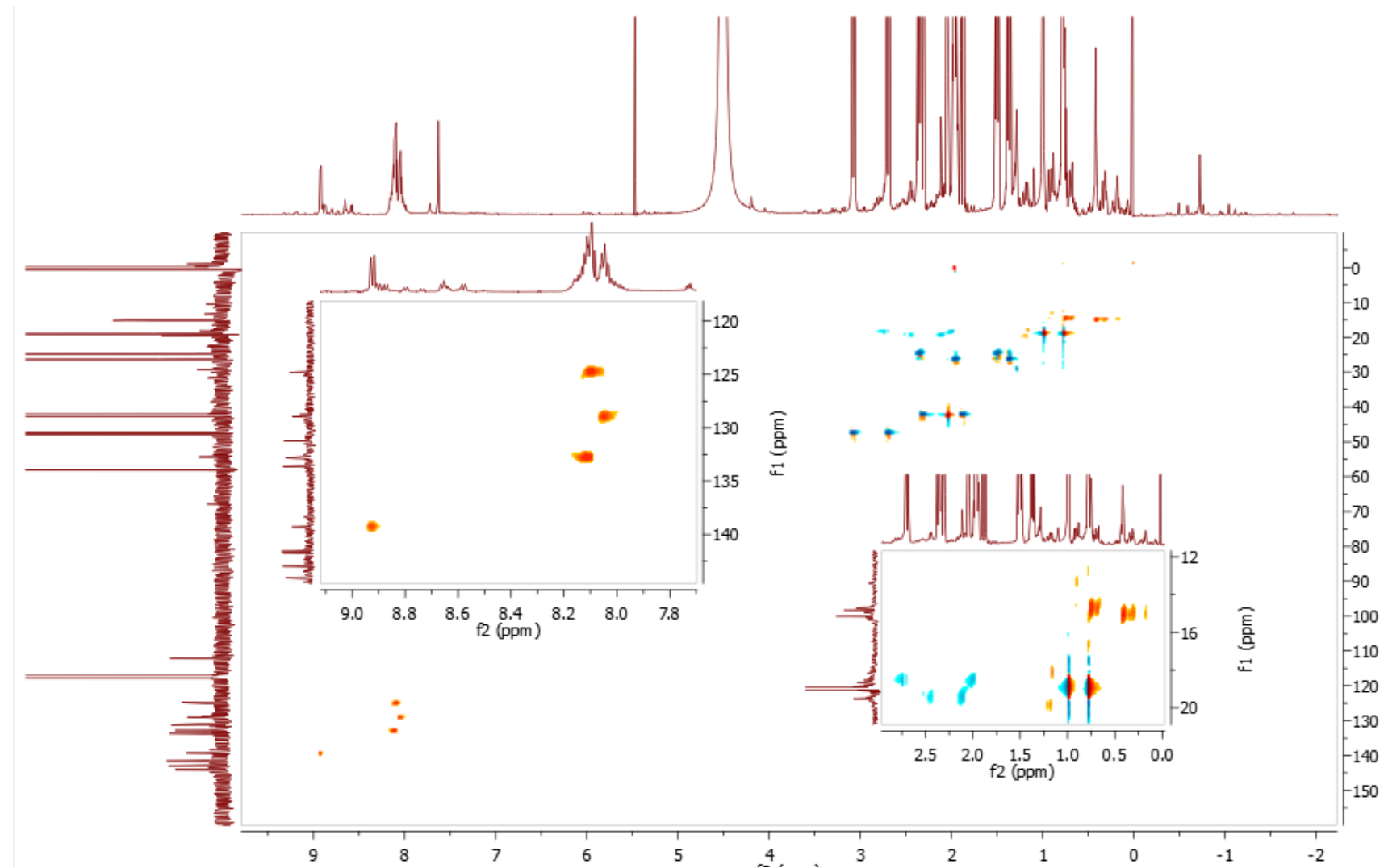


Figure S56. ^1H - ^{13}C HSQC spectrum of $\alpha\beta\alpha\beta\text{-P}\cdot 10\text{CSA(SR)}$ with expansion of areas of interest (acetonitrile- d_3 , 20 eq. of 10CSA(S) and 10CSA(R), 25 °C).

SUPPORTING INFORMATION

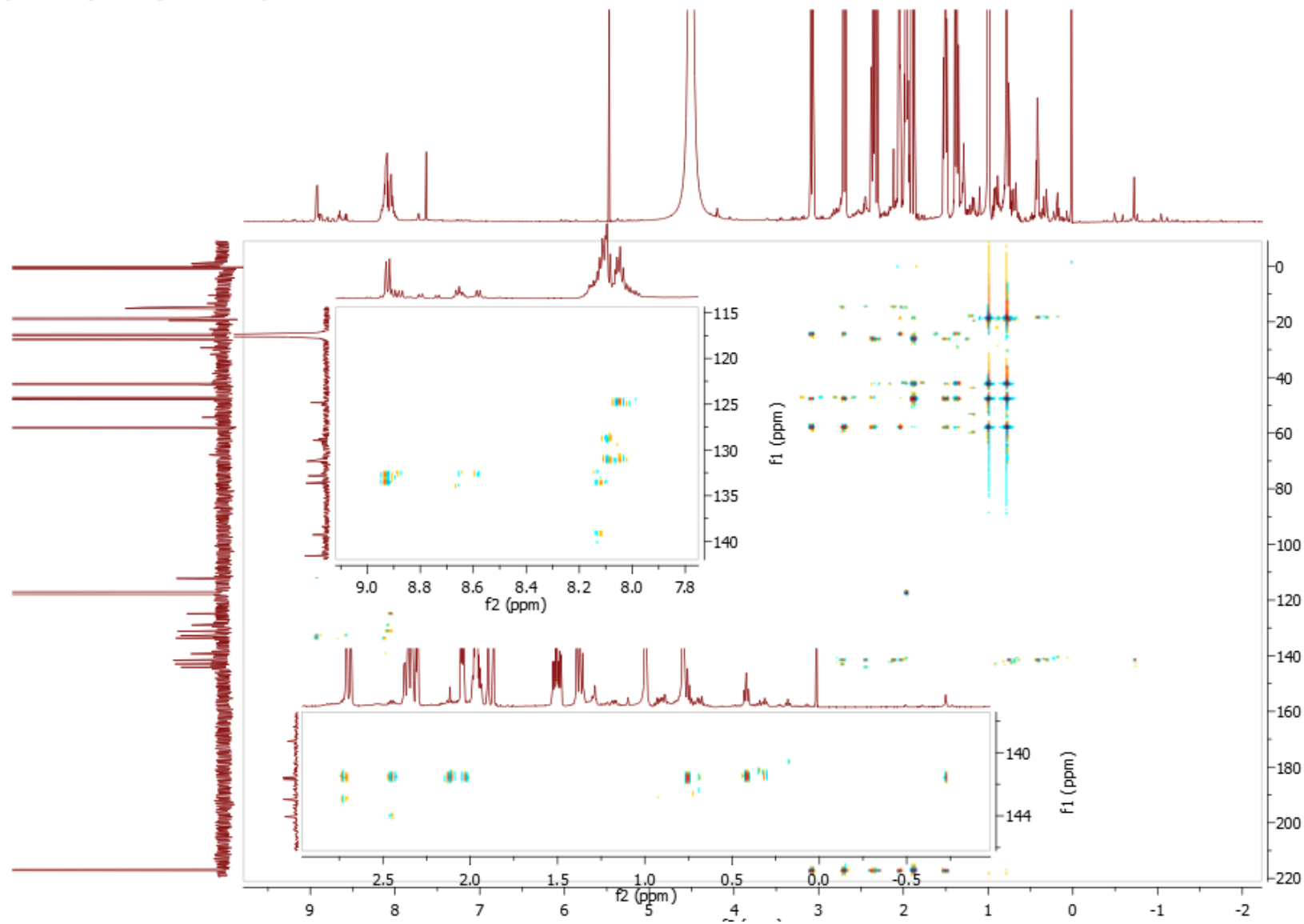


Figure S57. ^1H - ^{13}C HMBC spectrum of $\alpha\beta\alpha\beta\text{-P}\cdot 10\text{CSA(SR)}$ with expansion of areas of interest (acetonitrile- d_3 , 20 eq. of 10CSA(S) and 10CSA(R), 25 °C).

SUPPORTING INFORMATION

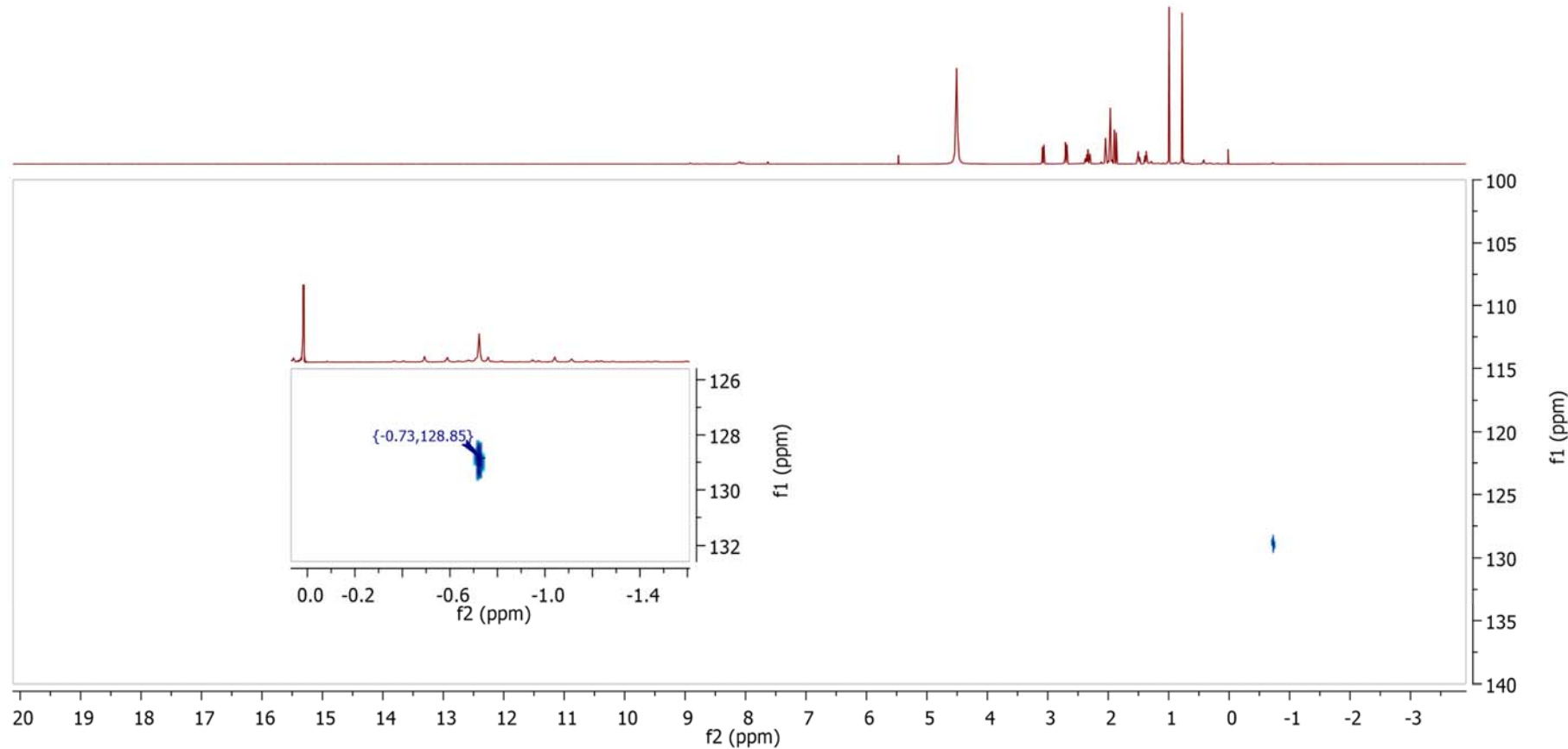


Figure S58. ¹H-¹⁵N HSQC spectrum of *αβαβ-P · 10CSA(SR)* with expansion of areas of interest (acetonitrile-*d*₃, 20 eq. of 10CSA(S) and 10CSA(R), 25 °C)

SUPPORTING INFORMATION

$\alpha_3\beta\text{-P}\cdot\mathbf{10CSA(S)}$

SUPPORTING INFORMATION

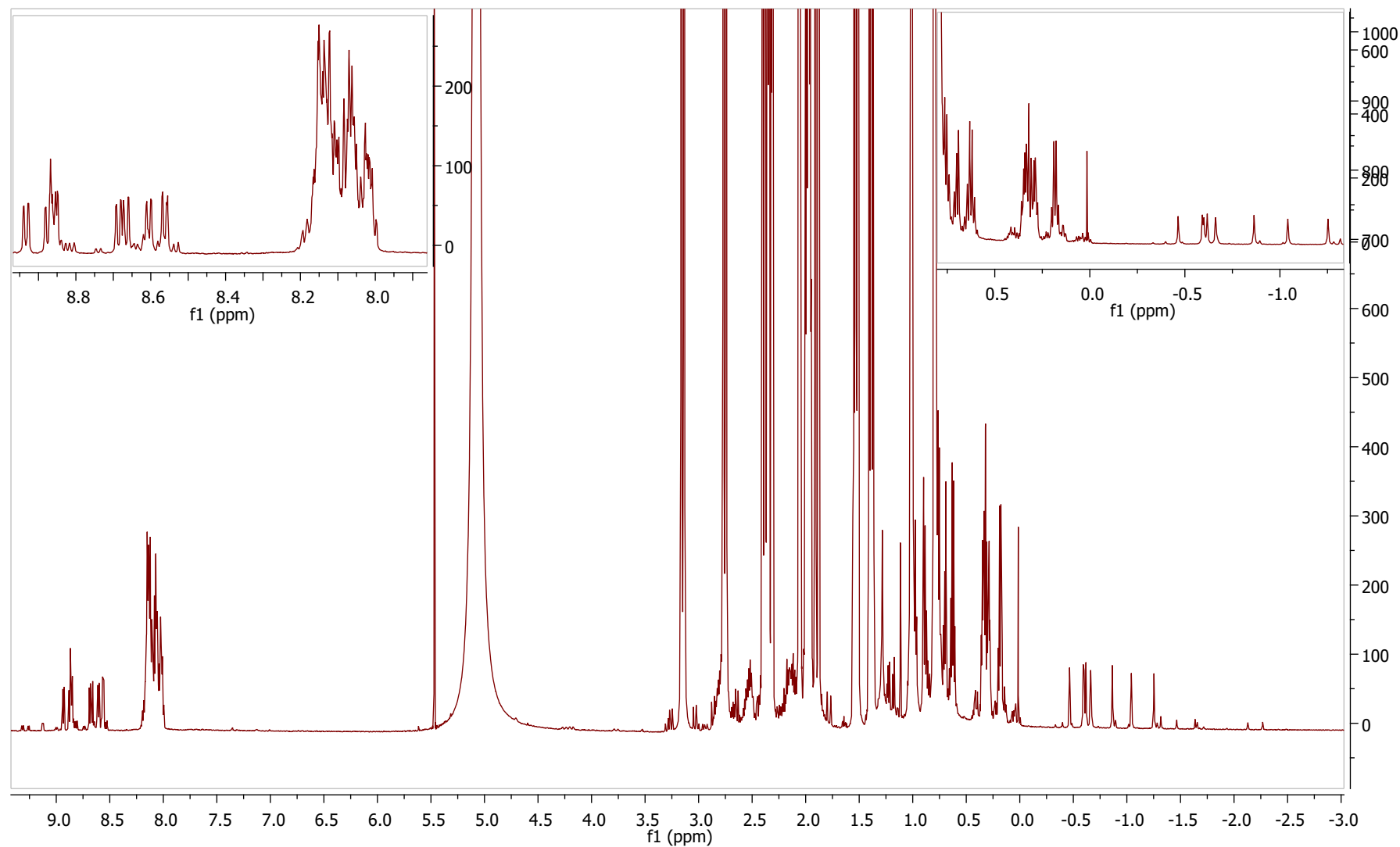


Figure S59. ¹H NMR spectrum of $\alpha_3\beta\text{-P}\cdot\text{10CSA}(\text{S})$ with the expansion of areas of interest (600 MHz, acetonitrile- d_3 , 20 eq. of 10CSA(S), 25 °C).

SUPPORTING INFORMATION

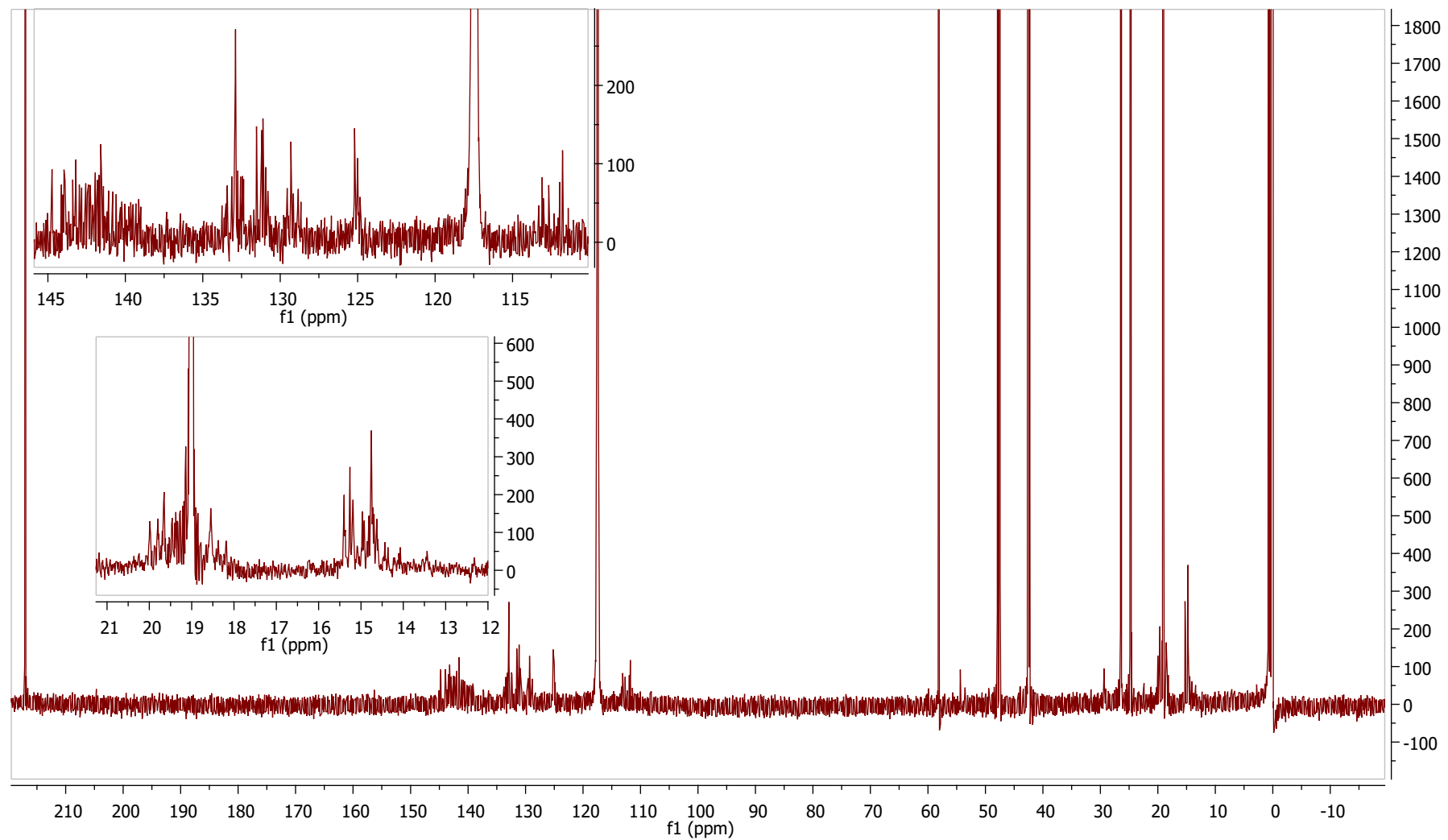


Figure S60. ^{13}C NMR spectrum of $\alpha_3\beta\text{-P}\cdot\text{10CSA(S)}$ with expansion of areas of interest (151 MHz, acetonitrile- d_3 , 20 eq. of 10CSA(S), 25 °C).

SUPPORTING INFORMATION

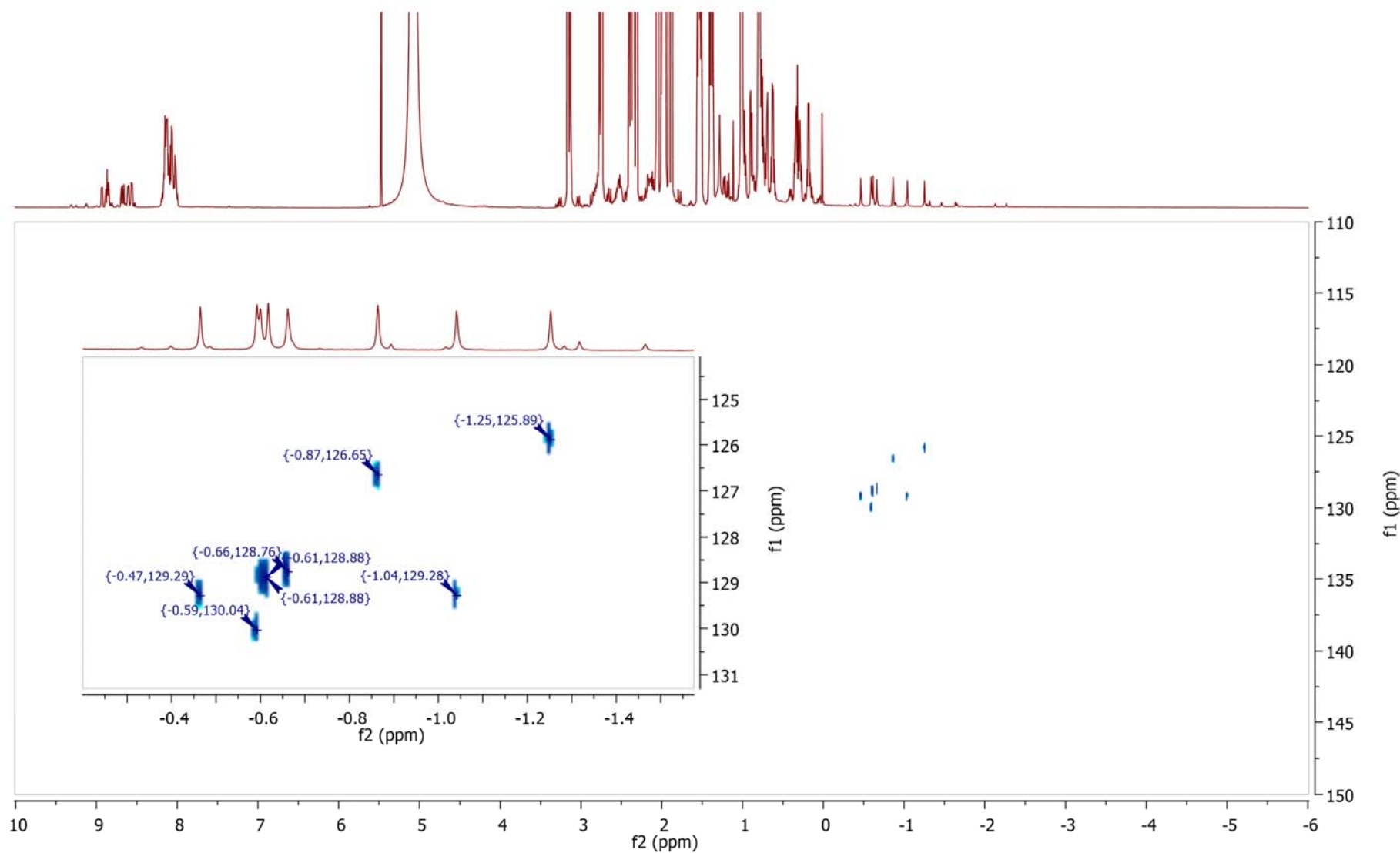


Figure S61. ¹H-¹⁵N HSQC spectrum of $\alpha_3\beta\text{-P}\cdot 10\text{CSA(S)}$ with expansion of areas of interest (acetonitrile-*d*₃, 20 eq. of 10CSA(S), 25 °C).

SUPPORTING INFORMATION

$\alpha_3\beta\text{-P}\cdot\text{10CSA(SR)}$

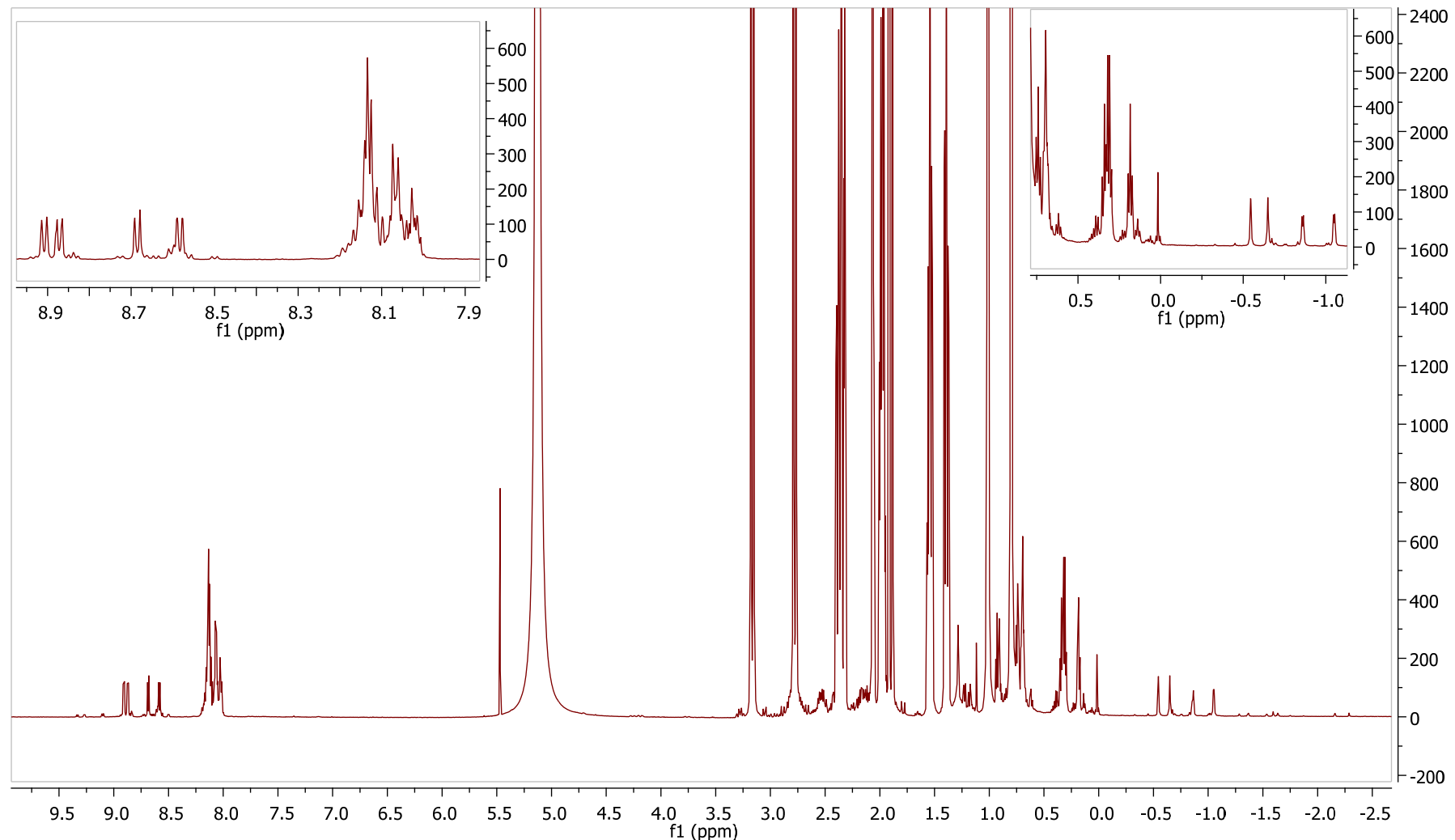


Figure S62. ^1H NMR spectrum of $\alpha_3\beta\text{-P}\cdot\text{10CSA(SR)}$ with expansion of areas of interest (600 MHz, acetonitrile- d_3 , 20 eq. of 10CSA(S) and 10CSA(R), 25 °C).

SUPPORTING INFORMATION

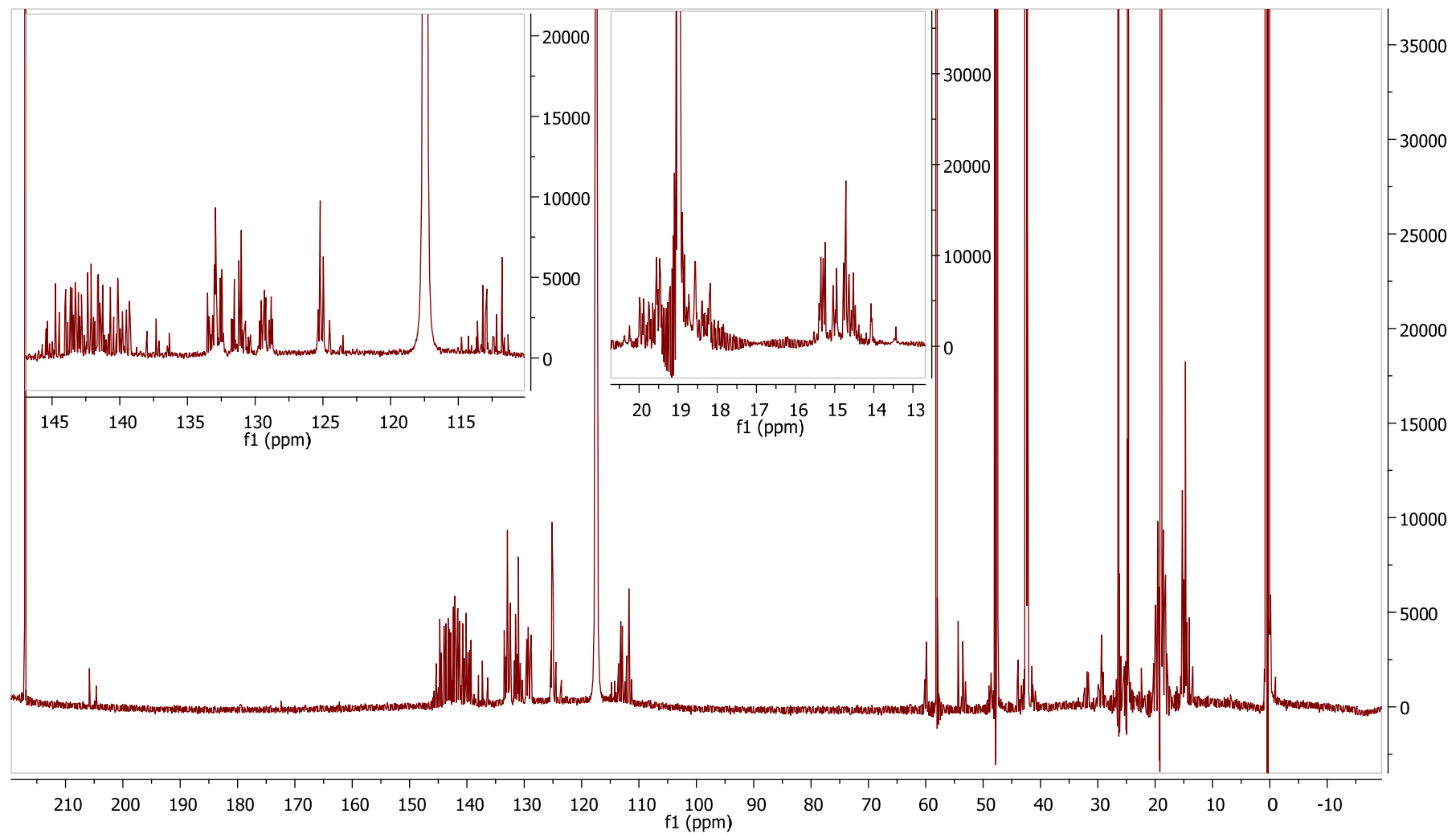


Figure S63. ¹³C NMR spectrum of $\alpha_3\beta$ -P·10CSA(SR) with expansion of areas of interest (151 MHz, acetonitrile-*d*₃, 20 eq. of 10CSA(S) and 10CSA(R), 25 °C).

SUPPORTING INFORMATION

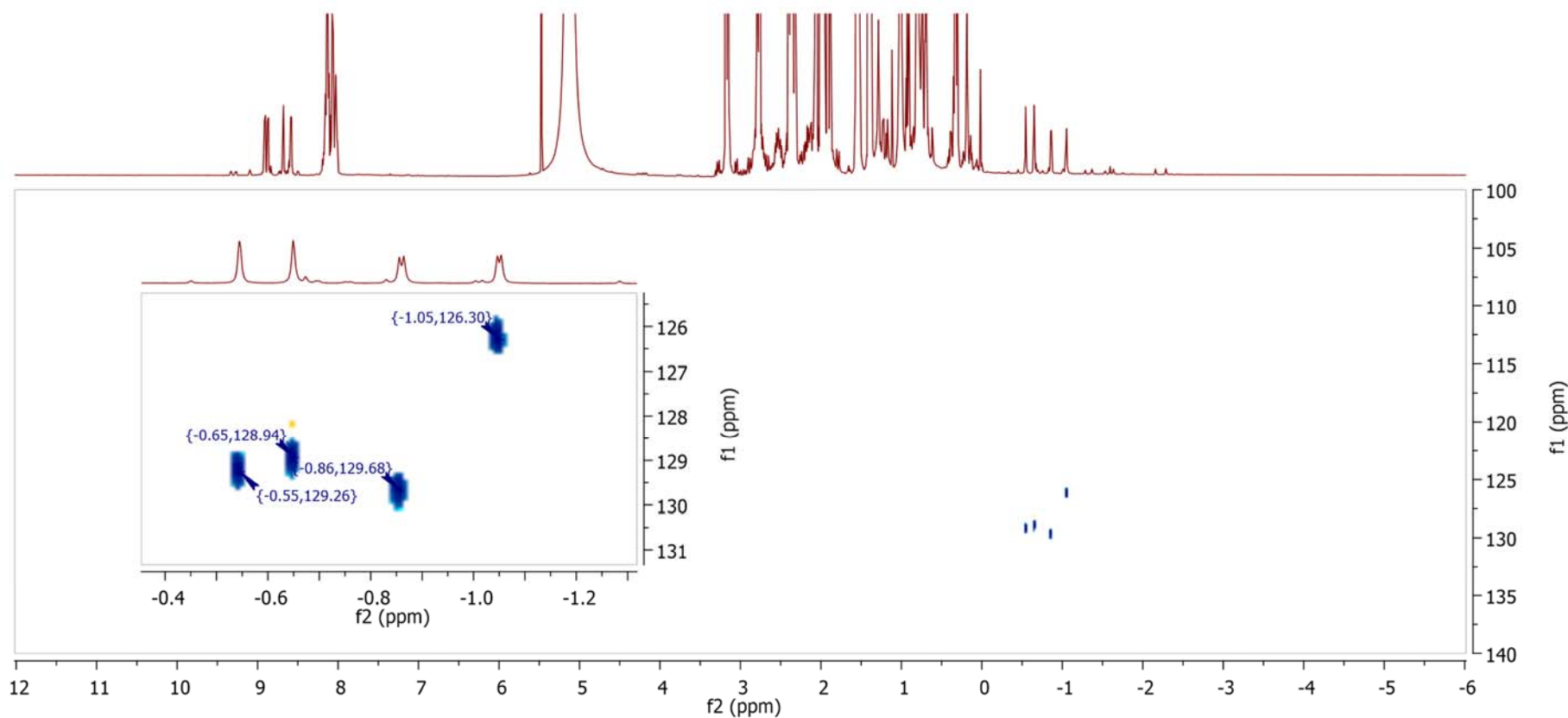


Figure S64. ^1H - ^{15}N HSQC spectrum of $\alpha_3\beta\text{-P}\cdot 10\text{CSA(SR)}$ with expansion of areas of interest (acetonitrile- d_3 , 20 eq. of 10CSA(S) and 10CSA(R), 25 °C)

SUPPORTING INFORMATION

References

- [1] W. Jentzen, X.-Z. Song, J. A. Shelnutt, *J. Phys. Chem. B* **1997**, *101*, 1684–1699.
- [2] C. J. Kingsbury, M. O. Senge, *Coord. Chem. Rev.* **2021**, *431*, 213760–213783.
- [3] H. Hope, *Prog. Inorg. Chem.* **2007**, *41*, 1–19.
- [4] APEX3, Version 2016.9-0, Bruker AXS, Inc., Madison, WI, **2016**.
- [5] SADABS, Version 2016/2, Bruker AXS, Inc., Madison, WI, **2014**.
- [6] a) O. V. Dolomanov, L. J. Bourhis, R. J. Gildea, J. A. K. Howard, H. Puschmann, *J. Appl. Cryst.* **2009**, *42*, 339–341; b) G. Sheldrick, *Acta Crystallogr.* **2015**, *A71*, 3–8.
- [7] M. J. Frisch, G. W. Trucks, H. B. Schlegel, G. E. Scuseria, M. A. Robb, J. R. Cheeseman, G. Scalmani, V. Barone, G. A. Petersson, H. Nakatsuji, X. Li, M. Caricato, A. V. Marenich, J. Bloino, B. G. Janesko, R. Gomperts, B. Mennucci, H. P. Hratchian, J. V. Ortiz, A. F. Izmaylov, J. L. Sonnenberg, Williams, F. Ding, F. Lipparini, F. Egidi, J. Goings, B. Peng, A. Petrone, T. Henderson, D. Ransinghe, V. G. Zakrzewski, J. Gao, N. Rega, G. Zheng, W. Liang, M. Hada, M. Ehara, K. Toyota, R. Fukuda, J. Hasegawa, M. Ishida, T. Nakajima, Y. Honda, O. Kitao, H. Nakai, T. Vreven, K. Throssell, J. A. Montgomery Jr., J. E. Peralta, F. Ogliaro, M. J. Bearpark, J. J. Heyd, E. N. Brothers, K. N. Kudin, V. N. Staroverov, T. A. Keith, R. Kobayashi, J. A. Normand, K. Raghavachari, A. P. Rentell, J. C. Burant, S. S. Iyengar, J. Tomasi, M. Cossi, J. M. Millam, M. Klene, C. Adamo, R. Cammi, J. W. Ochterski, R. L. Martin, K. Morokuma, O. Farkas, J. B. Foresman, D. J. Fox, Wallingford, CT, **2016**.
- [8] a) A. D. Becke, *Physical Review A* **1988**, *38*, 3098–3100; b) J. P. Perdew, *Physical Review B* **1986**, *33*, 8822–8824.
- [9] S. Grimme, S. Ehrlich, L. Goerigk, *J. Comput. Chem.* **2011**, *32*, 1456–1465.
- [10] a) F. Weigend, R. Ahlrichs, *PCCP* **2005**, *7*, 3297–3305; b) F. Weigend, *PCCP* **2006**, *8*, 1057–1065.
- [11] a) I. Osadchuk, V. Borovkov, R. Aav, E. Clot, *PCCP* **2020**, *22*, 11025–11037; b) I. Osadchuk, N. Konrad, K.-N. Truong, K. Rissanen, E. Clot, R. Aav, D. Kananovich, V. Borovkov, *Symmetry* **2021**, *13*, 275–289; c) I. Osadchuk, R. Aav, V. Borovkov, E. Clot, *Chemphyschem* **2021**, *22*, 1817–1833.
- [12] A. V. Marenich, C. J. Cramer, D. G. Truhlar, *J. Phys. Chem. B* **2009**, *113*, 6378–6396.
- [13] a) R. K. Dennington, Todd A.; Millam, John M. Semichem, *GaussView*, Version 6.1, Shawnee Mission, KS, **2016**; b) J. E. Carpenter, F. Weinhold, *J. Mol. Struct. (Theocchem)* **1988**, *169*, 41–62.
- [14] a) A. D. Becke, *J. Chem. Phys.* **1993**, *98*, 5648–5652; b) F. London, *J. Phys. Radium* **1937**, *8*, 397–409; c) R. McWeeny, *Physical Review* **1962**, *126*, 1028–1034; d) R. Ditchfield, *Mol. Phys.* **1974**, *27*, 789–807; e) K. Wolinski, J. F. Hinton, P. Pulay, *J. Am. Chem. Soc.* **1990**, *112*, 8251–8260; f) J. R. Cheeseman, G. W. Trucks, T. A. Keith, M. J. Frisch, *J. Chem. Phys.* **1996**, *104*, 5497–5509.
- [15] A. D. McLean, G. S. Chandler, *J. Chem. Phys.* **1980**, *72*, 5639–5648.
- [16] R. Krishnan, J. S. Binkley, R. Seeger, J. A. Pople, *J. Chem. Phys.* **1980**, *72*, 650–654.
- [17] M. W. Lodewyk, M. R. Siebert, D. J. Tantillo, *Chem. Rev.* **2012**, *112*, 1839–1862.
- [18] a) J. P. Foster, F. Weinhold, *J. Am. Chem. Soc.* **1980**, *102*, 7211–7218; b) A. E. Reed, F. Weinhold, *J. Chem. Phys.* **1983**, *78*, 4066–4073; c) A. E. Reed, R. B. Weinstock, F. Weinhold, *J. Chem. Phys.* **1985**, *83*, 735–746; d) A. E. Reed, F. Weinhold, *J. Chem. Phys.* **1985**, *83*, 1736–1740.
- [19] T. A. Keith, AIMAll; Version 19.10.12; Grismill Software: Overland Park KS, USA, 2019; Available online: aim.tkgrismill.com (accessed on 2028 April 2021).
- [20] K. Norvaiša, J. E. O'Brien, D. J. Gibbons, M. O. Senge, *Chem. Eur. J.* **2020**, *27*, 331–339.
- [21] J. Labuta, S. Ishihara, T. Šíkorský, Z. Futera, A. Shundo, L. Hanyková, J. V. Burda, K. Ariga, J. P. Hill, *Nat. Commun.* **2013**, *4*, 2188–2196.